

Introduction

3. Introduction to Carbon Nanotubes

Carbon nanotubes are among the amazing objects that science sometimes creates by accident, without meaning to, but that will likely revolutionize the technological landscape of the century ahead. Our society stands to be significantly influenced by carbon nanotubes, shaped by nanotube applications in every aspect, just as silicon-based technology still shapes society today. The world already dreams of space-elevators tethered by the strongest of cables, hydrogen-powered vehicles, artificial muscles, and so on – feats that would be made possible by the emerging carbon nanotube science.

Of course, nothing is set in stone yet. We are still at the stage of possibilities and potential. The recent example of fullerenes – molecules closely related to nanotubes, whose importance was so anticipated that their discovery in 1985 brought a Nobel Prize to their finders in 1996 although few related applications have actually yet reached the market – teaches us to play the game of enthusiastic predictions with some caution. But in the case of carbon nanotubes, expectations are high. Taking again the example of electronics, the miniaturization of chips is about to reach its lowest limits. Are we going to accept that our video camera, computers, and cellular phones no longer decrease in size and increase in memory every six months? Surely not. Always going deeper, farther, smaller, higher is a characteristic unique to humankind, and which helps to explain its domination of the living world on earth. Carbon nanotubes can help us fulfill our expectation of constant technological progress as a source of better living.

In this chapter, after the structure, synthesis methods, growth mechanisms, and properties of carbon nanotubes will be described, an entire section will be devoted to nanotube-related nano-objects. Indeed, should pristine nanotubes reach any limitation in some area, their ready and close association to foreign atoms, molecules,

3.1 Structure of Carbon Nanotubes	40
3.1.1 Single-Wall Nanotubes	40
3.1.2 Multiwall Nanotubes	43
3.2 Synthesis of Carbon Nanotubes	45
3.2.1 Solid Carbon Source-Based Production Techniques for Carbon Nanotubes	45
3.2.2 Gaseous Carbon Source-Based Production Techniques for Carbon Nanotubes	52
3.2.3 Miscellaneous Techniques	57
3.2.4 Synthesis of Aligned Carbon Nanotubes	58
3.3 Growth Mechanisms of Carbon Nanotubes	59
3.3.1 Catalyst-Free Growth	59
3.3.2 Catalytically Activated Growth	60
3.4 Properties of Carbon Nanotubes	63
3.4.1 Variability of Carbon Nanotube Properties	63
3.4.2 General Properties	63
3.4.3 SWNT Adsorption Properties	63
3.4.4 Transport Properties	65
3.4.5 Mechanical Properties	67
3.4.6 Reactivity	67
3.5 Carbon Nanotube-Based Nano-Objects ...	68
3.5.1 Hetero-Nanotubes	68
3.5.2 Hybrid Carbon Nanotubes	68
3.5.3 Functionalized Nanotubes	71
3.6 Applications of Carbon Nanotubes	73
3.6.1 Current Applications	73
3.6.2 Expected Applications Related to Adsorption	76
References	86

and compounds offers the prospect of an even magnified set of properties. Finally, we will describe carbon nanotube applications supporting the idea that the future for the science and technology of carbon nanotubes looks very promising.

Carbon nanotubes have been synthesized for a long time as products from the action of a catalyst over the gaseous species originating from the thermal decomposition of hydrocarbons (see Sect. 3.2). Some of the first evidence that the nanofilaments thus produced were actually nanotubes – i. e., exhibiting an inner cavity – can be found in the transmission electron microscope micrographs published by *Hillert et al.* in 1958 [3.1]. This was of course related to and made possible by the progress in transmission electron microscopy. It is then likely that the carbon filaments prepared by *Hughes* and *Chambers* in 1889 [3.2], reported by *Maruyama et al.* [3.3] as probably the first patent ever deposited in the field, and whose preparation method was also based on the catalytically enhanced thermal cracking of hydrocarbons, were already carbon nanotube-related morphologies. The preparation of vapor-grown carbon fibers had actually been reported as early as more than one century ago [3.4, 5]. Since then, the interest in carbon nanofilaments/nanotubes has been recurrent, though within a scientific area almost limited to the carbon material scientist community. The reader is invited to consult the review published by *Baker et al.* [3.6] regarding the early works. The worldwide enthusiasm came unexpectedly in 1991, after the catalyst-free formation of nearly perfect concentric multiwall carbon nanotubes (c-MWNTs, see Sect. 3.1) was reported [3.7] as by-products of the formation of fullerenes by the electric-arc technique. But the real breakthrough occurred two years later, when attempts in situ to fill the nanotubes with various metals

(see Sect. 3.5) led to the discovery – again unexpected – of single-wall carbon nanotubes (SWNTs) simultaneously by *Iijima et al.* [3.8] and *Bethune et al.* [3.9]. Single-wall carbon nanotubes were really new nano-objects many of whose properties and behaviors are quite specific (see Sect. 3.4). They are also beautiful objects for fundamental physics as well as unique molecules for experimental chemistry, still keeping some mystery since their formation mechanisms are a subject of controversy and are still debated (see Sect. 3.3). Potential applications seem countless, although few have reached a marketable status so far (see Sect. 3.6). Consequently, about five papers a day with carbon nanotubes as the main topic are currently published by research teams from around the world, an illustration of how extraordinarily active – and highly competitive – is this field of research. It is a quite unusual situation, similar to that of fullerenes, which, by the way, are again carbon nano-objects structurally closely related to nanotubes.

This is not, however, only about scientific exaltation. Economical aspects are leading the game to a greater and greater extent. According to experts, the world market is predicted to be more than 430 M\$ in 2004 and estimated to grow to several b\$ before 2009. That is serious business, and it will be closely related to how scientists and engineers will be able to deal with the many challenges found on the path from the beautiful, ideal molecule to the reliable – and it is hoped, cheap – manufactured product.

3.1 Structure of Carbon Nanotubes

It is simple to imagine a single-wall carbon nanotube (SWNT). Ideally, it is enough to consider a perfect graphene sheet (a graphene being the same polyaromatic mono-atomic layer made of an hexagonal display of sp^2 hybridized carbon atoms that genuine graphite is built up with), to roll it into a cylinder (Fig. 3.1) paying attention that the hexagonal rings put in contact join coherently, then to close the tips by two caps, each cap being a hemi-fullerene with the appropriate diameter (Fig. 3.2a–c).

3.1.1 Single-Wall Nanotubes

Geometrically, there is no restriction regarding the tube diameter. But calculations have shown that col-

lapsing the single-wall tube into a flattened two-layer ribbon is energetically more favorable than maintaining the tubular morphology beyond a diameter value of ~ 2.5 nm [3.10]. On the other hand, it intuitively comes to mind that the shorter the radius of curvature, the higher the stress and the energetic cost, although SWNTs with diameters as low as 0.4 nm have been successfully synthesized [3.11]. A suitable energetic compromise is thus reached for ~ 1.4 nm, the most frequent diameter encountered regardless of the synthesis techniques (at least those based on solid carbon source) when conditions for high SWNT yields are used. There is no such restriction for nanotube length, which only depends on limitations brought by the preparation method and the specific conditions used for the synthesis (thermal gradients, res-

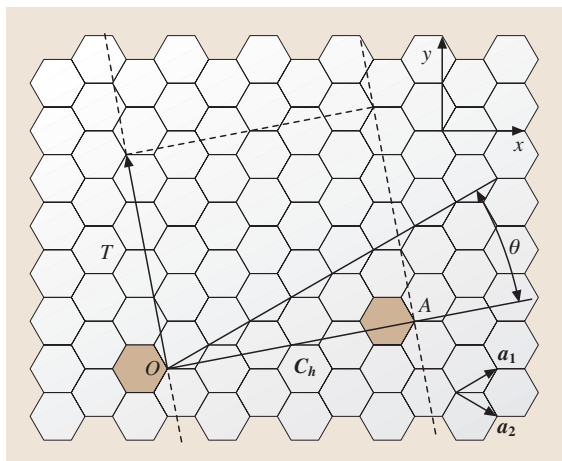


Fig. 3.1 Sketch of the way to make a single-wall carbon nanotube, starting from a graphene sheet (adapted from [3.12])

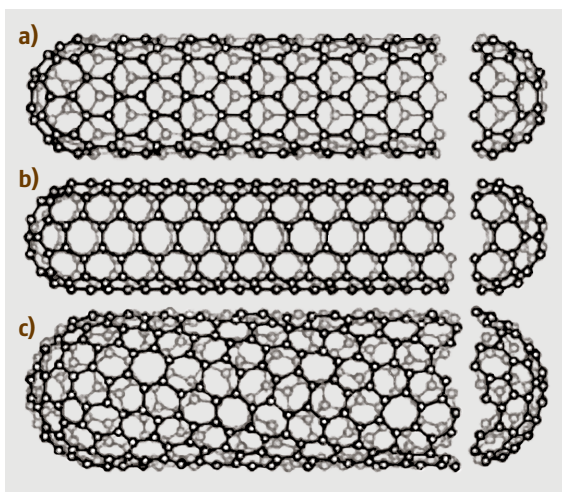


Fig. 3.2a–c Sketch of three different SWNT structures as examples for (a) a zig-zag-type nanotube, (b) an armchair-type nanotube, (c) a helical nanotube (adapted from [3.13])

idence time, etc.). Experimental data are consistent with these statements, since SWNTs wider than 2.5 nm are scarcely reported in literature, whatever the preparation method, while SWNT length can be in the micrometer or the millimeter range. These features make single-wall carbon nanotubes a unique example of single molecules with huge aspect ratios.

Two important consequences derive from the SWNT structure as described above:

1. All carbon atoms are involved in hexagonal aromatic rings only and are therefore in equivalent position, except at the nanotube tips where $6 \times 5 = 30$ atoms at each tip are involved in pentagonal rings (considering that adjacent pentagons are unlikely) – though not more, not less, as a consequence of the Euler’s rule that also governs the fullerene structure. In case SWNTs are ideally perfect, their chemical reactivity will therefore be highly favored at the tube tips, at the very location of the pentagonal rings.
2. Though carbon atoms are involved in aromatic rings, the C=C bond angles are no longer planar as they should ideally be. This means that the hybridization of carbon atoms are no longer pure sp^2 but get some percentage of the sp^3 character, in a proportion that increases as the tube radius of curvature decreases. For example, the effect is the same as for the C_{60} fullerene molecules, whose radius of curvature is 0.35 nm, and the subsequent sp^3 character proportion about 30%. On the one hand, this is supposed to make the SWNT surface (though consisting of aromatic ring faces) a bit more reactive than regular, planar graphene, relatively speaking. On the other hand, this somehow induces a variable overlapping of the bands of density of states, thereby inducing a unique versatile electronic behavior (see Sect. 3.4).

As illustrated by Fig. 3.2, there are many ways to roll a graphene into a single-wall nanotube, some of the resulting nanotubes enabling symmetry mirrors both parallel and perpendicular to the nanotube axis (such as the SWNTs from Fig. 3.2a and 3.2b), some others not (such as the SWNT from Fig. 3.2c). By correspondence with the terms used for molecules, the latter are commonly called “chiral” nanotubes. “Helical” should be preferred, however, in order to respect the definition of chirality, which makes all chiral molecules unable to be superimposed on their own image in a mirror. The various ways to roll graphene into tubes are therefore mathematically defined by the vector of helicity C_h , and the angle of helicity θ , as follows (referring to Fig. 3.1):

$$OA = C_h = na_1 + ma_2$$

with

$$a_1 = \frac{a\sqrt{3}}{2}x + \frac{a}{2}y \quad \text{and} \quad a_2 = \frac{a\sqrt{3}}{2}x - \frac{a}{2}y$$

where $a = 2.46 \text{ \AA}$

and

$$\cos \theta = \frac{2n + m}{2\sqrt{n^2 + m^2 + nm}}$$

where n and m are the integers of the vector \mathbf{OA} considering the unit vectors \mathbf{a}_1 and \mathbf{a}_2 .

The vector of helicity $\mathbf{C}_h (= \mathbf{OA})$ is perpendicular to the tube axis, while the angle of helicity θ is taken with respect to the so-called zig-zag axis, i. e., the vector of helicity that makes nanotubes of the “zig-zag” type (see below). The diameter D of the corresponding nanotube is related to \mathbf{C}_h by the relation:

$$D = \frac{|\mathbf{C}_h|}{\pi} = \frac{a_{CC}\sqrt{3(n^2 + m^2 + nm)}}{\pi},$$

where

$$1.41 \text{ \AA} \leq a_{C=C} \leq 1.44 \text{ \AA}.$$

(graphite) (C₆₀)

The C–C bond length is actually elongated by the curvature imposed, taking the average value for the C₆₀ fullerene molecule as a reasonable upper limit, and the value for flat graphenes in genuine graphite as the lower limit (corresponding to an infinite radius of curvature). Since \mathbf{C}_h , θ , and D are all expressed as a function of the integers n and m , they are sufficient to define any SWNT specifically, by noting them (n, m). Obtaining the values of n and m for a given SWNT is simple by counting the number of hexagons that separate the extremities of the \mathbf{C}_h vector following the unit vector \mathbf{a}_1 first, then \mathbf{a}_2 [3.12]. In the example of Fig. 3.1, the SWNT that will be obtained by rolling the graphene so that the two shaded aromatic cycles superimpose exactly is a (4,2) chiral nanotube. Similarly, SWNTs from Fig. 3.2a to 3.2c are (9,0), (5,5), and (10,5) nanotubes respectively, thereby providing examples of zig-zag-type SWNT (with an angle of helicity = 0°), armchair-type SWNT (with an angle of helicity of 30°) and a chiral SWNT, respectively. This also illustrates why the term “chiral” is sometimes inappropriate and should preferably be replaced by “helical”. Armchair (n, n) nanotubes, though definitely achiral from



Fig. 3.3 Image of two neighboring chiral SWNTs within a SWNT bundle as seen by high resolution scanning tunneling microscopy (by courtesy of Prof. Yazdani, University of Illinois at Urbana, USA)

a standpoint of symmetry, exhibit a “chiral angle” different from 0. “Zig-zag” and “armchair” qualifications for achiral nanotubes refer to the way carbon atoms are displayed at the edge of the nanotube cross section (Fig. 3.2a and 3.2b). Generally speaking, it is clear from Figs. 3.1 and 3.2a that having the vector of helicity perpendicular to any of the three overall C=C bond directions will provide zig-zag-type SWNTs, noted ($n, 0$), while having the vector of helicity parallel to one of the three C=C bond directions will provide armchair-type SWNTs, noted (n, n). On the other hand, because of the sixfold symmetry of the graphene sheet, the angle of helicity θ for the chiral (n, m) nanotubes is such as $0 < \theta < 30^\circ$. Figure 3.3 provides two examples of what chiral SWNTs look like, as seen by means of atomic force microscopy.

Planar graphenes in graphite have π electrons, which are satisfied by the stacking of graphenes that allows van der Waals forces to develop. Similar reasons make fullerenes gather and order into fullerite crystals and SWNTs into SWNT ropes (Fig. 3.4a). Spontaneously, SWNTs in ropes tend to arrange into an hexagonal array, which corresponds to the highest compactness achievable (Fig. 3.4b). This feature brings new periodicities

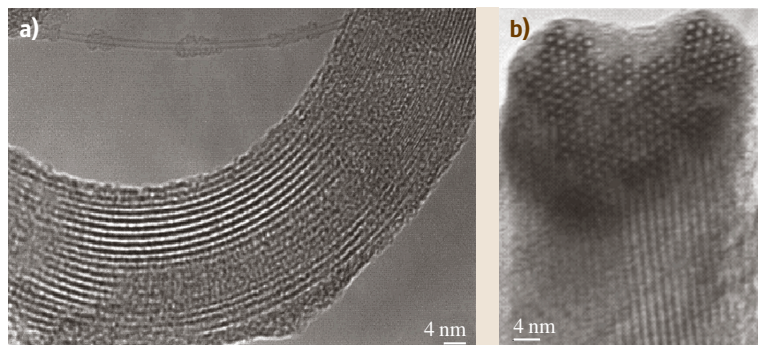


Fig. 3.4a,b High resolution transmission electron microscopy images of a SWNT rope (a) longitudinal view. At the top of the image an isolated single SWNT also appears. (b) cross section view (from [3.14])

with respect to graphite or turbostratic polyaromatic carbon crystals. Turbostratic structure corresponds to graphenes which are stacked with random rotations or translations instead of being piled up following sequential ABAB positions, as in graphite structure. This implies that no lattice atom plane exists anymore other than the graphene planes themselves (corresponding to the (001) atom plane family). These new periodicities make diffraction patterns specific and quite different from that of other sp^2 -carbon-based crystals, although hk reflections, which account for the hexagonal symmetry of graphene plane, are still present. On the other hand, $00l$ reflections, which account for the stacking sequence of graphenes in regular, “multilayered” polyaromatic crystals that does not exist in SWNT ropes, are absent. Such a hexagonal packing of SWNTs within the ropes requires that SWNTs exhibit similar diameters, which is the common case for SWNTs prepared by the electric arc or the laser vaporization processes. SWNTs prepared these ways are actually about 1.35 nm wide (diameter value for a (10,10) tube, among others), for reasons still unclear but related to the growth mechanisms specific to the conditions provided by these techniques (see Sect. 3.3).

3.1.2 Multiwall Nanotubes

Building multiwall carbon nanotubes is a little bit more complex, since it has to deal with the various ways graphenes can be displayed and mutually arranged within a filament morphology. Considering the usual textural versatility of polyaromatic solids, a similar versatility can be expected. Likewise, diffraction patterns no longer differentiate from that of anisotropic polyaromatic solids. The easiest MWNT to imagine is the concentric type (c-MWNT), in which SWNTs with regularly increasing diameters are coaxially displayed according to a Russian-doll model into a multiwall nanotube (Fig. 3.5). Such nanotubes are generally formed either by the electric-arc technique (without need of any catalyst) or by catalyst-enhanced thermal cracking of gaseous hydrocarbons or CO disproportionation (see Sect. 3.2). The number of walls (or number of coaxial tubes) can be anything, starting from two, with no upper limit. The intertube distance is approximately that of the intergraphene distance in turbostratic, polyaromatic solids, i. e. 0.34 nm (as opposed to 0.335 nm in genuine graphite), since the increasing radius of curvature imposed on the concentric graphenes prevents the carbon atoms from being displayed as in graphite,

i. e., each of the carbon atoms from a graphene facing alternatively either a ring center or a carbon atom from the neighboring graphene. But two cases allow such a nanotube to reach – totally or partially – the 3-D crystal periodicity of graphite. One is to consider a high number of concentric graphenes, i. e. concentric graphenes with long radius of curvature. In that case, the shift of the relative positions of carbon atoms from superimposed graphenes is so small with respect to that in graphite that some commensurability is possible. It may result in MWNTs with the association of both structures, i. e. turbostratic in the core and graphitic in the outer part [3.15]. The other case occurs for c-MWNTs exhibiting faceted morphologies, originating either from the synthesis process or more likely from

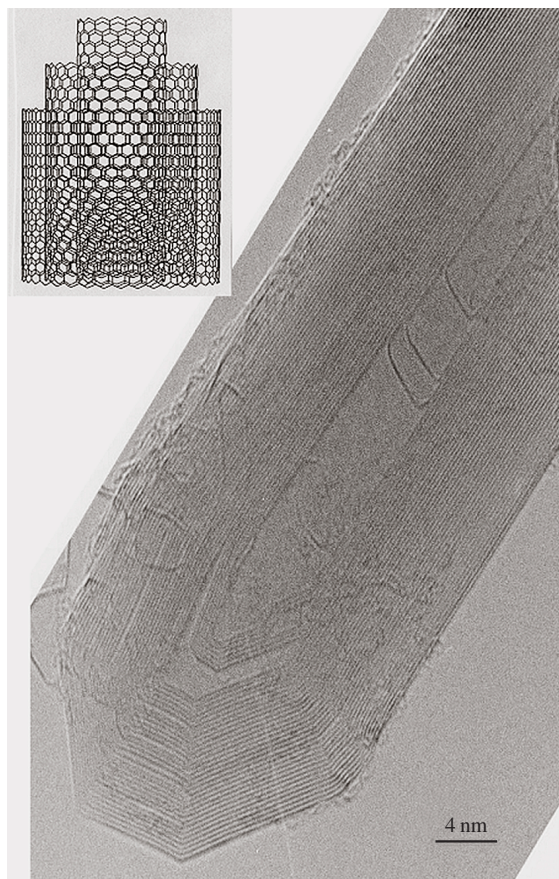


Fig. 3.5 High resolution transmission electron microscopy image (longitudinal view) of a concentric multiwall carbon nanotube (c-MWNT) prepared by electric arc. In *insert*, sketch of the Russian-doll-like display of graphenes

subsequent heat-treatments at high temperatures (e.g., 2,500 °C) in inert atmospheres. Obviously, facets allow graphenes to get back a flat arrangement of atoms – except at the junction between neighboring facets – in which the specific stacking sequence of graphite can develop.

Another frequent inner texture for multiwall carbon nanotubes is the so-called herringbone texture (h-MWNTs), in which graphenes make an angle with respect to the nanotube axis (Fig. 3.6). The angle value varies upon the processing conditions (e.g., the catalyst morphology or the atmosphere composition), from 0 (in which case the texture turns into that of a c-MWNT) to 90° (in that case, the filament is no longer a tube, see below), and the inner diameter varies so that the tubular feature can be lost [3.19], justifying that the latter can be called nanofibers rather than nanotubes. h-MWNTs are exclusively obtained by processes involving catalysts, generally catalyst-enhanced thermal cracking of hydrocarbons or CO disproportionation.

One unresolved question is whether the herringbone texture, which actually describes the texture projection rather than the overall three-dimensional texture, originates from the scroll-like spiral arrangement of a single graphene ribbon or from the stacking of independent truncated-cone-like graphenes. Although the former is more likely for energetic reasons since providing a minimal and constant amount of transiently unsatisfied bonds during the nanotube growth (similar to the well-known growth mechanism from a screw dislocation), the question is still debated.

Another common feature is the occurrence, at a variable frequency, of a limited amount of graphenes oriented perpendicular to the nanotube axis, thus forming the so-called “bamboo” texture. It cannot be a texture by its own but affects in a variable extent either c-MWNT (bc-MWNT) or h-MWNT (bh-MWNT) textures (Figs. 3.6 and 3.7). The question may be addressed whether such filaments, though hollowed, should still be called nanotubes, since the inner cavity is no longer opened all along the filament as it is for a genuine tube. They therefore are sometimes referred as “nanofibers” in literature.

Nanofilaments that definitely cannot be called nanotubes are those built from graphenes oriented perpendicular to the filament axis and stacked as piled-up plates. Although they actually correspond to h-MWNTs with the graphene/MWNT axis angle = 90°, the occurrence of inner cavity is no longer possible, and such filaments are therefore most often referred to as “platelet-nanofibers” in literature [3.19].

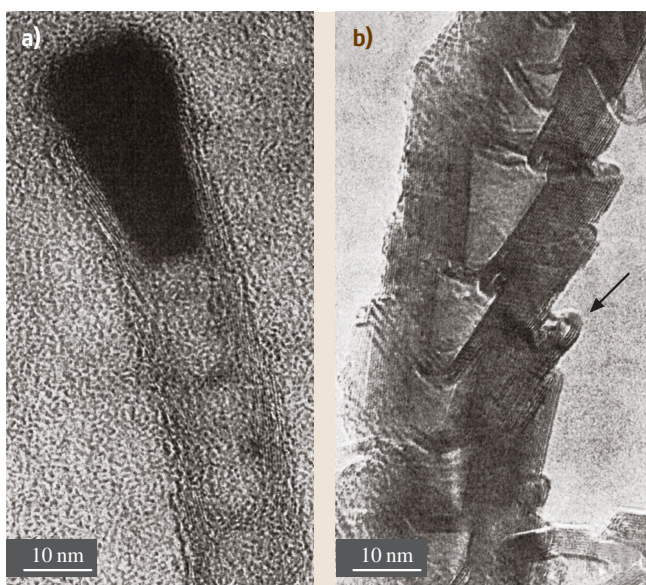


Fig. 3.6a,b One of the earliest high resolution transmission electron microscopy image of a herringbone (and bamboo) multi-wall nanotube (bh-MWNT, longitudinal view) prepared by CO disproportionation on Fe-Co catalyst. **(a)** as-grown. The nanotube surface is made of free graphene edges. **(b)** after 2,900 °C heat-treatment. Both the herringbone and the bamboo textures have become obvious. Graphene edges from the surface have buckled with neighbors (arrow), closing the access to the intergraphene spacing (adapted from [3.16])

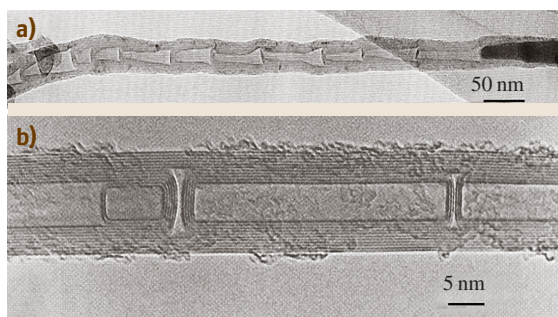


Fig. 3.7a,b Transmission electron microscopy images from bamboo-multi-wall nanotubes (longitudinal views). **(a)** low magnification of a bamboo-herringbone multi-wall nanotube (bh-MWNT) showing the nearly periodic feature of the texture, which is very frequent. (from [3.17]); **(b)** high resolution image of a bamboo-concentric multi-wall nanotube (bc-MWNT) (modified from [3.18])

As opposed to *SWNTs*, whose aspect ratio is so high that accessing the tube tips is almost impossible, aspect ratio for *MWNTs* (and carbon nanofibers) are generally lower and often allow one to image tube ends by transmission electron microscopy. Except for *c-MWNTs* from electric arc (see Fig. 3.5) that grow following a catalyst-free process, nanotube tips are frequently found associated with the catalyst crystal from which they have been formed.

MWNT properties (see Sect. 3.4) will obviously depend on the perfection and orientation of graphenes in the tube more than any other feature (e.g., the respective spiral angle of the constituting nanotubes for *c-MWNTs* has little importance). Graphene orientation is a matter of texture, as described above. Graphene perfection is a matter of nanotexture, which is commonly used to describe other polyaromatic carbon materials, and which is quantified by several parameters preferably obtained from high resolution transmission electron microscopy (Fig. 3.8). Both texture and nanotexture depend on the processing conditions. While the texture type is a permanent, intrinsic feature only able to go toward complete alteration upon severe degradation treatments (e.g., oxidation), however, nanotexture can be improved

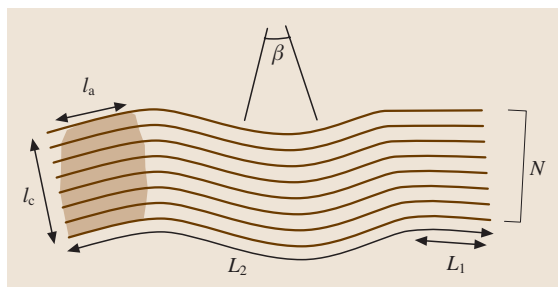


Fig. 3.8 Sketch explaining the various parameters obtained from high resolution (lattice fringe mode) transmission electron microscopy for quantifying nanotexture: L_1 is the average length of perfect (distortion-free) graphenes of coherent areas; N is the number of piled-up graphenes in the coherent (distortion-free) areas; L_2 is the average length of continuous though distorted graphenes within graphene stacks; β is the average distortion angle. L_1 and N are more or less related to L_a and L_c obtained from X-ray diffraction

by subsequent thermal treatments at high temperatures (e.g., $> 2,000\text{ }^\circ\text{C}$) or, reversibly, possibly degraded by chemical treatments (e.g., slight oxidation conditions).

3.2 Synthesis of Carbon Nanotubes

Producing carbon nanotubes so that the currently planned applications become marketable requires solving some problems that are more or less restrictive depending on the cases. One example is to specifically control the configuration (chirality), the purity, or the structural quality of *SWNTs*, with the production capacity adapted to the application. One condition would be to understand perfectly the mechanism of nanotube nucleation and growth, which remains the object of a lot of controversy in spite of an intense, worldwide experimental effort. This problem is partly explained by the lack of knowledge regarding several parameters controlling the synthesis conditions. For instance, neither the temperatures of nanotube condensation and formation nor the manner in which they are influenced by the synthesis parameters are known. Equally often unknown is the exact and accurate role of the catalysts in nanotube growth. Given the large number of experimental parameters and considering the large range of conditions that the several synthesis techniques correspond to, it is quite legitimate to think of more than one mechanism intervening in the nanotube formation.

3.2.1 Solid Carbon Source–Based Production Techniques for Carbon Nanotubes

Among the different *SWNT* production techniques, the three processes (laser ablation, solar energy, and electric arc) presented in this section have at least two common points: a high temperature ($1,000\text{ K} < T < 6,000\text{ K}$) medium and the fact that the carbon source originates from the erosion of solid graphite. In spite of these common points, both the morphologies of the carbon nanostructures and the *SWNT* yields can differ notably with respect to the experimental conditions.

Before being utilized for carbon nanotube synthesis, these techniques permitted the production of fullerenes. Laser vaporization of graphite was actually the very first method to demonstrate the existence of fullerenes, including the most popular one (because the most stable and therefore the most abundant), C_{60} [3.20]. On the other hand, the electric arc technique was (and still is) the first method to produce fullerenes in relatively large quantities [3.21]. As opposed to the fullerene formation, which requires the presence of carbon atoms

in high temperature media and the absence of oxygen, the utilization of these techniques for the synthesis of nanotubes requires an additional condition, i. e. the presence of catalysts in one of the electrode or the target.

In case of these synthesis techniques requiring relatively high temperatures to sublime graphite, the different mechanisms such as the carbon molecule dissociation and the atom recombination processes take place at different time scales, from nanosecond to microsecond and even millisecond. The formation of nanotubes and other graphene-based products appears afterward with a relatively long delay.

The methods of laser ablation, solar energy, and electric arc are based on an essential mechanism, i. e. the energy transfer resulting from the interaction between either the target material and an external radiation (laser beam or radiation emanating from solar energy) or the electrode and the plasma (in case of electric arc). This interaction is at the origin of the target or anode erosion leading to the formation of a plasma, i. e. an electrically neutral ionized gas, composed of neutral atoms, charged particles (molecules and ionized species), and electrons. The ionization degree of this plasma, defined by the ratio $(n_e/n_e + n_o)$, where n_e and n_o are the density of electrons and that of neutral atoms respectively, highlights the importance of energy transfer between the plasma and the material. The characteristics of this plasma and notably the fields of temperature and of concentration of the various species present in the plasma thereby depend not only on the nature and composition of the target or that of the electrode but also on the energy transferred.

One of the advantages of these different synthesis techniques is the possibility of varying a large number of parameters, which allow the composition of the high temperature medium to be modified and, consequently, the most relevant parameters to be determined, in order to define the optimal conditions for the control of carbon nanotube formation. But a major drawback of these techniques – as for any other technique for the production of SWNTs – is that SWNTs never come pure, i. e. they are associated with other carbon phases and catalyst remnants. Although purification processes are proposed in literature and by some commercial companies to rid these undesirable phases, they are all based on oxidation (e.g. acidic) processes that are likely to affect deeply the SWNT structure [3.14]. Subsequent thermal treatments at $\sim 1,200^\circ\text{C}$ under inert atmosphere, however, succeed somewhat in recovering the former structure quality [3.24].

Laser Ablation

After the first laser was built in 1960, physicists immediately made use of it as a means of concentrating a large quantity of energy inside a very small volume within a relatively short time. The consequences of this energy input naturally depends on the characteristics of the device employed. During the interaction between the laser beam and the material, numerous phenomena superimpose and/or follow each other within the time range, each of these processes being sensitive to such different parameters as the laser beam characteristics, the incoming power density (also termed “fluence”), the nature of the target, and the environment surrounding it. For instance, the solid target can merely heat up, or melt, or vaporize depending on the power provided.

While this technique was used successfully to synthesize fullerene-related structures for the very first time [3.20], the synthesis of SWNTs by laser ablation came only ten years later [3.22].

Laser Ablation – Experimental Devices

Two types of laser devices are utilized nowadays for carbon nanotube production: lasers operating in pulsed mode on the one hand and lasers operating in continuous mode on the other hand, the latter generally providing a smaller influence.

An example of the layout indicating the principle of a laser ablation device is given in Fig. 3.9. A graphite pellet containing the catalyst is put in the middle of an inert gas-filled quartz tube placed in an oven maintained at a temperature of $1,200^\circ\text{C}$ [3.22, 23]. The energy of the laser beam focused on the pellet permits it to vaporize and sublime the graphite by uniformly bombarding its surface. The carbon species swept by a flow of neutral gas are thereafter deposited as soot in different regions: on the conical water-cooled copper collector, on the quartz tube walls, and on the backside of the pellet.

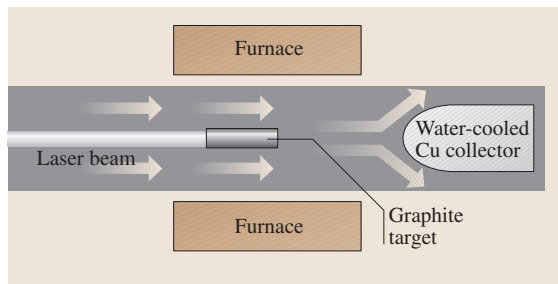


Fig. 3.9 Sketch of an early laser vaporization apparatus (adapted from [3.22, 23])

Various improvements have been made to this device in order to increase the production efficiency. For example, *Thess et al.* [3.25] employed a second pulsed laser that follows the initial impulsion but at a different frequency in order to ensure a more complete and efficient irradiation of the pellet. This second impulsion has the role of vaporizing the coarse aggregates issued from the first ablation and thereby making them participate in the active carbon feedstock involved in the nanotube growth. Other modifications were brought by *Rinzler et al.* [3.24], who inserted a second quartz tube of a smaller diameter coaxially disposed inside to the first one. This second tube has the role of reducing the vaporization zone and thereby permitting an increase in the quantity of sublimed carbon. They also arranged to place the graphite pellet on a revolving system so that the laser beam uniformly scans its whole surface.

Other groups have realized that, as far as the target contains both the catalyst and the graphite, the latter evaporates in priority and the pellet surface becomes more and more metal rich, resulting in a decrease of the efficiency in nanotube formation in the course of the process. To solve this problem, *Yudasaka et al.* [3.27] utilized two pellets facing each other, one entirely made from the graphite powder and the other from an alloy of transition metals (catalysts), and irradiated simultaneously.

A sketch of a synthesis reactor based on the vaporization of a target at a fixed temperature by a continuous CO₂ laser beam ($\lambda = 10.6 \mu\text{m}$) is shown in Fig. 3.10 [3.26]. The power can be varied from 100 W to 1,600 W. The temperature of the target is measured with an optical pyrometer, and these measurements are used to regulate the laser power to maintain a constant vaporization temperature. The gas, heated by the contact with the target, acts as a local furnace and creates an extended hot zone, making an external furnace unnecessary. The gas is extracted through a silica pipe, and the solid products formed are carried away by the gas flow through the pipe and then collected on a filter. The synthesis yield is controlled by three parameters: the cooling rate of the medium where the active, secondary catalyst particles are formed, the residence time, and the temperature (in the 1,000–2,100 K range) at which *SWNTs* nucleate and grow [3.28].

But devices equipped with facilities to gather in situ data such as the target temperature are few and, generally speaking, among the numerous parameters of the laser ablation synthesis technique. The most studied are the nature of the target, the nature and concentration of the

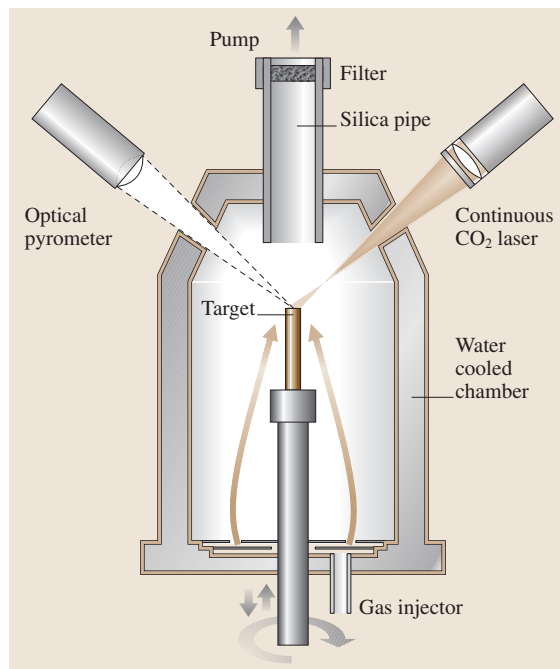


Fig. 3.10 Sketch of a synthesis reactor with a continuous CO₂ laser device (adapted from [3.26])

catalysts, the nature of the neutral gas flow, and the temperature of the outer oven (when any).

Laser Ablation – Results

In the absence of catalysts in the target, the soot collected mainly contains multiwall nanotubes (c-MWNTs). Their lengths can reach 300 nm. Their quantity and structure quality are dependent on the oven temperature. The best quality is obtained for an oven temperature set at 1,200 °C. At lower oven temperatures, the structure quality decreases, and the nanotubes start presenting many defects [3.23]. As soon as small quantities (few percents or less) of transition metals (Ni, Co) playing the role of catalysts are incorporated into the graphite pellet, products yielded undergo significant modifications, and *SWNTs* are formed instead of MWNTs. The yield of *SWNTs* strongly depends on the type of metal catalyst used and is seen to increase with furnace temperature, among other factors. The *SWNTs* have remarkably uniform diameter and they self-organize into rope-like crystallites 5–20 nm in diameter and tens to hundreds of micrometers in length (Fig. 3.11). The ends of all *SWNTs* appear to be perfectly closed with hemispherical end caps showing no evidence of any as-

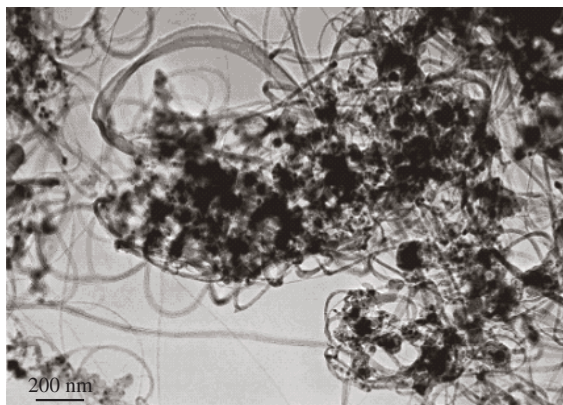


Fig. 3.11 Low magnification TEM images of a typical raw SWNT material obtained from the laser vaporization technique. Fibrous morphologies are SWNT bundles, and dark particles are catalyst remnants. Raw SWNT materials from electric arc exhibit a similar aspect (from [3.14])

sociated metal catalyst particle, although, as pointed out in Sect. 3.1, finding the two tips of a SWNT is rather challenging, considering the huge aspect ratio of the nanotube and their entanglement. Another feature of SWNTs produced with this technique is that they are supposedly “cleaner” than those produced employing other techniques, i. e., associated with a lower amount of an amorphous carbon phase, either coating the SWNTs or gathered into nano-particles. Such an advantage, however, stands only for synthesis conditions specifically set to ensure high quality SWNTs. It can no longer be true when conditions are such that high yields are preferred, and SWNTs from electric arc may appear cleaner than SWNTs from laser vaporization [3.14].

The laser vaporization technique is one of the three methods currently used to prepare SWNTs as commercial products. SWNTs prepared that way were first marketed by Carbon Nanotechnologies Inc. (Texas, USA), with prices as high as \$1,000/g (raw materials) until December 2002. As a probable consequence of the impossibility to lower the amount of impurities in the raw materials, they have recently decided to focus on fabricating SWNTs by the HiPCo technique (see Sect. 3.2.2). Though laser-based method are generally considered not competitive in the long term for the low-cost production of SWNTs compared to CCVD-based methods (see Sect. 3.2.2), prediction of prices as low as \$0.03 per gram of raw high concentration SWNT soot are expected in the near future (Acolt S.A., Switzerland).

Electric-Arc Method

Electric arcs between carbon electrodes have been studied as light sources and radiation standards for a very long time. Lately they have received renewed attention for their use in producing new fullerenes-related molecular carbon nanostructures such as genuine fullerenes or nanotubes. This technique was first brought to light by Krättschmer et al. [3.21] who utilized it to achieve the production of fullerenes in macroscopic quantities. In the course of investigating the other carbon nanostructures formed along with the fullerenes and more particularly the solid carbon deposit forming onto the cathode, Iijima [3.7] discovered the catalyst-free formation of perfect c-MWNT-type carbon nanotubes. Then, as mentioned in the introduction of this chapter, the catalyst-promoted formation of SWNTs was incidentally discovered after some amounts of transition metals were introduced into the anode in an attempt to fill the c-MWNTs with metals while they grow [3.8, 9]. Since then, a lot of work has been carried out by many groups using this technique to understand the mechanisms of nanotube growth as well as the role played by the catalysts (when any) for the synthesis of MWNTs and/or SWNTs [3.29–41].

Electric-Arc Method – Experimental Devices

The principle of this technique is to vaporize carbon in the presence of catalysts (iron, nickel, cobalt, yttrium, boron, gadolinium, and so forth) under reduced atmosphere of inert gas (argon or helium). After the triggering of the arc between two electrodes, a plasma is formed consisting of the mixture of carbon vapor, the rare gas (helium or argon), and the vapors of catalysts. The vaporization is the consequence of the energy transfer from the arc to the anode made of graphite doped with catalysts. The anode erosion rate is more or less important depending on the power of the arc and also on the other experimental conditions. It is noteworthy that a high anode erosion does not necessarily lead to a high carbon nanotube production.

An example of a reactor layout is shown in Fig. 3.12. It consists of a cylinder of about 30 cm in diameter and about 1 m in height, equipped with diametrically opposed sapphire windows located so that they face the plasma zone in view of observing the arc. The reactor possesses two valves, one for carrying out the primary evacuation (0.1 Pa) of the chamber, the other permitting it to fill with a rare gas up to the desired working pressure.

Contrary to the solar energy technique, SWNTs are deposited (provided appropriate catalysts are used) in

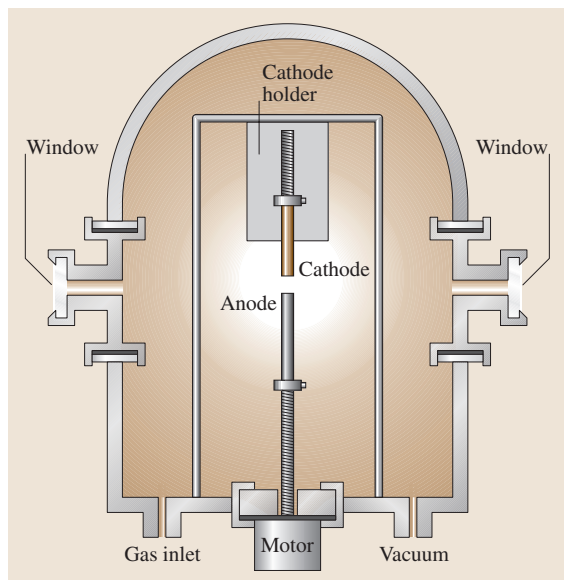


Fig. 3.12 Sketch of an electric arc reactor

different regions of the reactor: (1) the collaret, which forms around the cathode; (2) the web-like deposits found above the cathode; (3) the soot deposited all around the reactor walls and bottom. On the other hand, MWNTs are formed embedded in a hard deposit adherent to the cathode, whenever catalysts are used or not. The cathode deposits formed under the cathode. The formation of collaret and web is not systematic and depends on the experimental conditions as indicated in Table 3.1, as opposed to cathode deposit and soot that are systematically found.

Two graphite rods of few millimeters in diameter constitute the electrodes between which a potential difference is applied. The dimensions of these electrodes vary according to the authors. In certain cases, the cathode has a greater diameter than the anode in order to facilitate their alignment [3.32, 42]. Other authors utilize electrodes of the same diameter [3.41]. The whole device can be designed horizontally [3.33, 41] or vertically [3.34, 36–38]. The advantage of the latter is the symmetry brought by the verticality with respect to gravity, which facilitates computer modeling (regarding convection flows, for instance).

Two types of anodes can be utilized as soon as catalysts need to be introduced: (1) graphite anodes in which a coaxial hole is drilled several centimeters in length and in which catalyst and graphite powders are mixed; (2) graphite anodes in which the catalysts are homoge-

neously dispersed [3.43]. The former are by far the most popular, due to their ease of fabrication.

The optimization of the process regarding the nanotube yield and quality is attempted by studying the role of various parameters such as the type of doped anode (homogeneous or heterogeneous catalyst dispersion), the nature as well as the concentration of catalysts, the nature of the plasmagenic gas, the buffer gas pressure, the arc current intensity, and the distance between electrodes. Investigating the result of varying these parameters on the type and amount of carbon nanostructures formed is, of course, the preliminary work that has been done. Though electric arc reactors equipped with the related facilities are few (see Fig. 3.12), investigating the missing link, i.e. the effect of varying the parameters on the plasma characteristics (fields of concentration species and temperature), is likely to provide a more comprehensive understanding of the phenomena involved in nanotube formation. This has been recently developed by atomic and molecular optical emission spectroscopy [3.34, 36–39, 41].

Finally, mention has to be made of attempts to make the electric arc within liquid media such as liquid nitrogen [3.44] or water [3.45, 46], the goal being easier processing since they do not require pumping devices or a closed volume and therefore are likely to allow continuous synthesis. This adaptation has not, however, reached the state of mass production.

Electric-Arc Method – Results

In view of the numerous results obtained with this electric-arc technique, it appears clearly that both the nanotube morphology and the nanotube production efficiency strongly depend on the experimental conditions and, in particular, on the nature of the catalysts. It is worth noting that the products obtained do not consist solely in carbon nanotubes but also in nontubular forms of carbon such as nanoparticles, fullerene-like structures including C_{60} , poorly organized polyaromatic carbons, nearly amorphous nanofibers, multiwall shells, single-wall nanocapsules, and amorphous carbon as reported in Table 3.1 [3.35, 37, 38]. In addition, catalyst remnants are found all over the place, i.e. in the soot, collaret, web, and cathode deposit in various concentration. Generally, at pressure value of about 600 mbar of helium, for 80 A arc current and 1 mm electrode gap, the use of Ni/Y as coupled catalysts favors more particularly the synthesis of SWNTs [3.8, 33, 47]. For such conditions providing high SWNT yields, SWNT concentrations are higher in the collaret (in the range of 50–70%), then in the web (~50% or less), then in the soot. On the

Table 3.1 Different carbon morphologies obtained by changing the type of anode, the type of catalysts, and pressure value, in a series of arc-discharge experiments (electrode gap = 1 mm)

Catalyst (atom%) Arc conditions	0.6Ni + 0.6Co (homogeneous anode) $P \sim 60$ kPa $I \sim 80$ A	0.6Ni + 0.6Co (homogeneous anode) $P \sim 40$ kPa $I \sim 80$ A	0.5Ni + 0.5Co $P \sim 60$ kPa $I \sim 80$ A	4.2Ni + 1Y $P \sim 60$ kPa $I \sim 80$ A
Soot	<ul style="list-style-type: none"> • MWNT + MWS + POPAC or Cn \pm catalysts $\phi \sim 3$–35 nm • NANF + catalysts • AC particles + catalysts • [DWNT], [SWNT], ropes or isolated, + POPAC 	<ul style="list-style-type: none"> • POPAC and AC particles + catalysts $\phi \sim 2$–20 nm • NANF + catalysts $\phi \sim 5$–20 nm + MWS • [SWNT] $\phi \sim 1$–1.4 nm, distorted or damaged, isolated or ropes + Cn 	<ul style="list-style-type: none"> • AC and POPAC particles + catalysts $\phi \sim 3$–35 nm • NANF + catalysts $\phi \sim 4$–15 nm • [SWNT] $\phi \sim 1.2$ nm, isolated or ropes 	<ul style="list-style-type: none"> • POPAC and AC + particles + catalysts $\phi \leq 30$ nm • SWNT $\phi \sim 1.4$ nm, clean + Cn, short with tips, [damaged], isolated or ropes $\phi \leq 25$ nm • [SWNC] particles
Web	<ul style="list-style-type: none"> • [MWNT], DWNT, $\phi 2.7$–4–5.7 nm SWNT $\phi 1.2$–1.8 nm, isolated or ropes $\phi < 15$ nm, + POPAC \pm Cn • AC particles + catalysts $\phi \sim 3$–40 nm + MWS • [NANF] 	None	None	<ul style="list-style-type: none"> • SWNT, $\phi \sim 1.4$ nm, isolated or ropes $\phi \leq 20$ nm, + AC • POPAC and AC particles + catalysts $\phi \sim 3$–10–40 nm + MWS
Collaret	<ul style="list-style-type: none"> • POPAC and SWNC particles • Catalysts $\phi \sim 3$–250 nm, < 50 nm + MWS • SWNT $\phi 1$–1.2 nm, [opened], distorted, isolated or ropes $\phi < 15$ nm, + Cn • [AC] particles 	<ul style="list-style-type: none"> • AC and POPAC particles + catalysts $\phi \sim 3$–25 nm • SWNT $\phi \sim 1$–1.4 nm clean + Cn, [isolated] or ropes $\phi < 25$ nm • Catalysts $\phi \sim 5$–50 nm + MWS, • [SWNC] 	<ul style="list-style-type: none"> • Catalysts $\phi \sim 3$–170 nm + MWS • AC or POPAC particles + catalysts $\phi \sim 3$–50 nm • SWNT $\phi \sim 1.4$ nm clean + Cn isolated or ropes $\phi < 20$ nm 	<ul style="list-style-type: none"> • SWNT $\phi \sim 1.4$–2.5 nm, clean + Cn, [damaged], isolated or ropes $\phi < 30$ nm • POPAC or AC particles + catalysts $\phi \sim 3$–30 nm • [MWS] + catalysts or catalyst-free.
Cathode deposit	<ul style="list-style-type: none"> • POPAC and SWNC particles • Catalysts $\phi \sim 5$–300 nm MWS • MWNT $\phi < 50$ nm • [SWNT] $\phi \sim 1.6$ nm clean + Cn, isolated or ropes 	<ul style="list-style-type: none"> • POPAC and SWNC particles + Cn • Catalysts $\phi \sim 20$–100 nm + MWS 	<ul style="list-style-type: none"> • MWS, catalyst-free • MWNT $\phi < 35$ nm • POPAC and PSWNC particles • [SWNT], isolated or ropes • [Catalysts] $\phi \sim 3$–30 nm 	<ul style="list-style-type: none"> • SWNT $\phi \sim 1.4$–4.1 nm, clean + Cn, short with tips, isolated or ropes $\phi \leq 20$ nm. • POPAC or AC particles + catalysts $\phi \sim 3$–30 nm • MWS + catalysts $\phi < 40$ nm or catalyst-free • [MWNT]

Abundant – Present – [Rare]

Glossary: AC: amorphous carbon; POPAC: poorly organised polyaromatic carbon; Cn: fullerene-like structure, including C₆₀; NANF: nearly amorphous nanofiber; MWS: multiwall shell; SWNT: single-wall nanotube; DWNT: double-wall nanotube, MWNT: multiwall nanotube; SWNC: single-wall nanocapsule.

other hand, c-MWNTs are found in the cathode deposit. SWNT lengths are micrometric and, typically, outer diameters range around 1.4 nm. Taking the latter conditions as a reference experiment (Table 3.1, column 4), Table 3.1 illustrates the consequence of changing the parameters. For instance (Table 3.1, column 3), using Ni/Co instead of Ni/Y as catalysts prevents the formation of SWNTs. But when the Ni/Co catalysts are homogeneously dispersed in the anode (Table 3.1, column 1), the formation of nanotubes is promoted again, but MWNTs with two or three walls prevail over SWNTs, among which DWNTs (double-wall nanotubes) make a majority. But it is enough to decrease the ambient pressure from 60 to 40 kPa (Table 3.1, column 2) for getting back to conditions where the nanotube formation is impeached.

Recent works have attempted to replace graphite powder (sp^2 hybridized carbon) by diamond powder (sp^3 hybridized carbon) to mix with the catalyst powder and fill hollowed-type graphite anodes. The result was an unexpected but quite significant increase (up to +230%) in the SWNT yield [3.39,40]. Such experiments reveal, as for the comparison between the results from using homogeneous instead of heterogeneous anodes that the physical phenomena (charge and heat transfers) that occurred in the anode during the arc are of utmost importance, which was neglected until now.

It is clear that while the use of rare earth element (such as Y) as a single catalyst does not provide the conditions to grow SWNTs, associating it with a transition metal (such as Ni/Y) seems to correspond to the most appropriate combinations, leading to the highest SWNT yields [3.42]. On the other hand, using a single rare earth element may lead to unexpected results, such as the anticipated closure of graphene edges from a c-MWNT wall with the neighboring graphene edges from the same wall side, leading to the preferred formation of telescope-like and open c-MWNTs able to contain nested Gd crystals [3.36,38]. Such a need for bimetallic catalysts has just begun to be understood as a possible requirement to promote the transitory formation of nickel particles coated with yttrium carbide, whose lattice constants are somewhat commensurable with that of graphenes [3.48].

Figure 3.13 illustrates the kind of information provided by the analysis of the plasma by means of emission spectroscopy, i. e. radial temperature (Fig. 3.13a) or C_2 species concentration (Fig. 3.13b) profiles in the plasma. A common feature is that a huge vertical gradient (~ 500 K/mm) rapidly establishes (at ~ 0.5 mm from the center in the radial direction) from the bottom to the

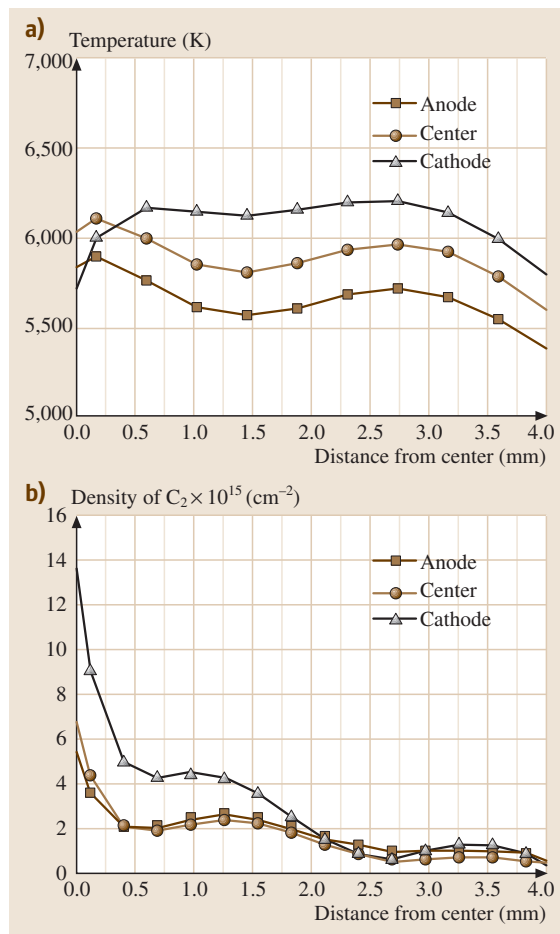


Fig. 3.13a,b Typical temperature (a) and C_2 concentration (b) profiles in the plasma at the anode surface (square), at the plasma center (dot), and at the cathode surface (triangle) for “standard” conditions (see text). Gradients are similar whatever the catalyst, although absolute value may vary

top of the plasma, as a probable consequence of convection phenomena (Fig. 3.13a). The zone of actual SWNT formation is beyond the limit of the volume analyzable in the radial direction, corresponding to colder areas. The C_2 concentration increases dramatically from the anode to the cathode and decreases dramatically in the radial direction (Fig. 3.13b). This demonstrates that C_2 moieties are secondary products resulting from the recombination of primary species formed from the anode. It also suggests that C_2 moieties may be the building blocks for MWNTs (formed at the cathode) but not for SWNTs [3.38,40].

Although many aspects of it still need to be understood, the electric-arc method is one of the three methods currently used to produce SWNTs as commercial products. At the French company Nanolegde S.A. (Montpellier, France), for instance, current production (for 2003) reaches ~ 20 kg/year (raw SWNTs, i. e. not purified), with a marketed price of ~ 90 Euros/g, which is much cheaper than any other production method so far. A decrease to 2–5 Euros/g is expected for sometime before 2007, with a SWNT production capacity of 4–5 tons/year. Amazingly, raw SWNTs from electric arc proposed by Bucky USA (Texas, USA) are still proposed at a marketed price of \$ 1,000/g.

Solar Furnace

Solar furnace devices were originally utilized by several groups to produce fullerenes [3.49–51]. *Heben* et al. [3.52] and *Laplaze* et al. [3.53] later modified their former devices in order to use them for carbon nanotube production. This modification consisted mainly in using more powerful ovens [3.54, 55].

Solar Furnace – Experimental Devices

The principle of this technique is again based on the sublimation in an inert gas of a mixture of graphite powder and catalysts formerly placed in a crucible. An example of such a device is shown in Fig. 3.14. The solar rays are collected by a plain mirror and reflected toward a parabolic mirror that focuses them directly onto a graphite pellet under controlled atmosphere. The high temperature of about 4,000 K permits both the carbon and the catalysts to vaporize. The vapors are then dragged by the neutral gas and condense onto the cold walls of the thermal screen. The reactor consists of a brass support cooled by water circulation, on which Pyrex[®] chambers with various shapes can be fixed (Fig. 3.14b). This support contains a watertight passage permitting the introduction of the neutral gas and a copper rod on which the target is mounted. The target is surrounded by a graphite tube that plays both the role of a thermal screen to reduce radiation losses (very important in the case of graphite) and the role of a duct to lead carbon vapors to a filter in order to avoid soot deposits on the Pyrex[®] chamber wall. A graphite crucible filled with powdered graphite (for fullerene synthesis) or a mixture of graphite and catalysts (for nanotube synthesis) is utilized in order to reduce the conduction losses.

These studies primarily investigated the target composition, the type and concentration of catalysts, the flow-rate, the composition and pressure of the plasma-genic gas inside the chamber, and the oven power. The

objectives are similar to that of works carried out with the other solid-carbon-source-based processes. When possible, specific in situ diagnostics (pyrometry, optical emission spectroscopy, etc.) are also performed in order to understand better the role of the various parameters (temperature measurements at the crucible surface, along the graphite tube acting as thermal screen, C₂ radical concentration in the immediate vicinity of the crucible).

Solar Furnace – Results

Some results obtained by different groups concerning the influence of the catalysts can be summarized as follows. With Ni/Co and at low pressure, the sample collected contains mainly MWNTs with bamboo texture, carbon shells, and some bundles of SWNTs [3.54]. At higher pressures, only bundles of SWNTs are obtained with fewer carbon shells. With Ni/Y and at a high pressure, relatively long bundles of SWNTs are observed. With Co, SWNT bundles are obtained in the soot with SWNT diameters ranging from 1 to 2 nm. *Laplaze* et al. [3.54] observed very few nanotubes but a large quantity of carbon shells.

In order to proceed to a large-scale synthesis of single-wall carbon nanotubes, which is still a challenge for chemical engineers, *Flamant* et al. [3.56] recently demonstrated that solar energy-based synthesis is a versatile method to obtain SWNTs and can be scaled from 0.1–0.5 g/h to 10 g/h and then to 100 g/h productivity using existing solar furnaces. Experiments at medium scale (10-g/h, 50 kW solar power) have proven the feasibility of designing and building such a reactor and of the scaling-up method. Numerical simulation was meanwhile performed in order to improve the selectivity of the synthesis, in particular by controlling the carbon vapor cooling rate.

3.2.2 Gaseous Carbon Source-Based Production Techniques for Carbon Nanotubes

As mentioned in the introduction of this chapter, the catalysis-enhanced thermal cracking of gaseous carbon source (hydrocarbons, CO) – commonly referred to as catalytic chemical vapor deposition (CCVD) – has been known to produce carbon nanofilaments for a long time [3.4], so that reporting all the works published in the field since the beginning of the century is almost impossible. Until the 90s, however, carbon nanofilaments were mainly produced to act as a core substrate for the subsequent growth of larger (micro-

metric) carbon fibers – so-called vapor-grown carbon fibers – by means of thickening through mere catalyst-free CVD processes [3.57, 58]. We therefore are going to focus instead on the more recent attempts made to prepare genuine carbon nanotubes.

The synthesis of carbon nanotubes (either single- or multiwalled) by CCVD methods involves the catalytic decomposition of a carbon containing source on small metallic particles or clusters. This technique involves either an heterogeneous process if a solid substrate has a role or an homogeneous process if everything takes place in the gas phase. The metals generally used for these reactions are transition metals, such as Fe, Co, and Ni. It is a rather “low temperature” process compared to arc-discharge and laser-ablation methods, with the formation of carbon nanotubes typically occurring between 600 °C and 1,000 °C. Because of the low temperature, the selectivity of the CCVD method is generally better for the production of MWNTs with respect to graphitic particles and amorphous-like carbon, which remain an important part of the raw arc-discharge SWNT samples, for example. Both homogeneous and heterogeneous processes appear very sensitive to the nature and the structure of the catalyst used, as well as to the operating conditions. Carbon nanotubes prepared by CCVD methods are generally much longer (few tens to hundreds of micrometers) than those obtained by arc discharge (few micrometers). Depending on the experimental conditions, it is possible to grow dense arrays of nanotubes. It is a general statement that MWNTs from CCVD contain more structural defects (i. e., exhibit a lower nanotexture) than MWNTs from arc, due to the lower temperature reaction, which does not allow any structural rearrangements. These defects can be removed by subsequently applying heat treatments in vacuum or inert atmosphere to the products. Whether such a discrepancy is also true for SWNTs remains questionable. CCVD SWNTs are generally gathered into bundles that are generally of smaller diameter (few tens of nm) than their arc-discharge and laser-ablation counterparts (around 100 nm in diameter). CCVD provides reasonably good perspectives of large-scale and low-cost processes for the mass production of carbon nanotubes, a key point for their applications at the industrial scale.

A last word concerns the nomenclature. Because work in the field started more than one century ago, denomination of the carbon objects prepared by this method has changed with time with regard to the authors, research areas, and fashions. The same objects are found to be called vapor grown carbon fibers, nanofilaments, nanofibers, and from now on,

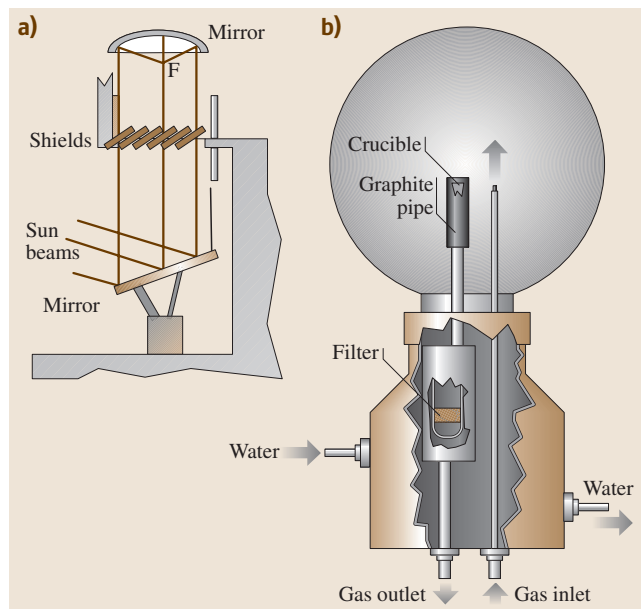


Fig. 3.14a,b Sketch of a solar energy reactor in use in Odeillo (France). (a) Gathering of sun rays, focused in F; (b) Example of Pyrex® chamber placed in (a) so that the graphite crucible is at the point F (adapted from [3.56])

nanotubes. Specifically regarding multilayered fibrous morphologies (since single-layered fibrous morphologies cannot be otherwise than SWNT anyway), the exact name should be vapor-grown carbon nanofilaments (VGCNF). Whether or not the filaments are then tubular is a matter of textural description, which should go with other textural features such as bamboo, herringbone, concentric, etc. (see Sect. 3.1.2). But the usage has decided otherwise. In the following, we will therefore use MWNTs for any hollowed nanofilament, whether they contain transversally oriented graphene walls or not. Any other nanofilament will be named “nanofiber.”

Heterogeneous Processes

Heterogeneous CCVD processes are basically simple and consist, within a furnace heated to the desired temperature, in passing a gaseous flow containing a given proportion of a hydrocarbon (mainly CH₄, C₂H₂, C₂H₄, or C₆H₆, usually as a mixture with either H₂ or an inert gas such as Ar) over small transition metal particles (Fe, Co, Ni). The latter are previously deposited onto an inert substrate, for instance, by spraying a suspension of the metal particles on it, or any other method. The reac-

tion is chemically defined as catalysis-enhanced thermal cracking



Catalysis-enhanced thermal cracking was used as early as the late 19th century (see beginning of chapter). Further extensive works before the 90s include those by Baker et al. [3.6, 59], or *Endo* et al. [3.60, 61]. Several review papers have been published since then, such as [3.62], in addition to many regular papers.

CO can be used instead of hydrocarbons, the reaction is then chemically defined as catalysis-enhanced disproportionation



Heterogeneous Processes – Experimental Devices

The ability of catalysis-enhanced CO disproportionation in making carbon nanofilaments was reported by *Davis* et al. [3.63] as early as 1953, probably for the first time. Extensive following works were performed by *Boehm* [3.64], *Audier* et al. [3.16, 65–67], and *Gadelle* et al. [3.68–71].

Although formation mechanisms for *SWNTs* and *MWNTs* can be quite different (see Sect. 3.3, or refer to a review article such as [3.72]), many of the parameters of the catalytic processes have a similar and important role on the type of nanotubes formed: the temperature, the duration of the treatment, the gas composition and flow rate, and of course the catalyst nature and size. At a given temperature, depending mainly on the nature of both the catalyst and the carbon-containing gas, the catalytic decomposition will take place at the surface of the metal particles, followed by a mass-transport of the freshly produced carbon either by surface or volume diffusion until the carbon concentration reaches the solubility limit, and the precipitation starts.

It is now agreed that the formation of *CCVD* carbon nanotubes occurs on metal particles of a very small size, typically in the nanometer-size range [3.72]. These catalytic metal particles are prepared mainly by reduction of transition metals compounds (salts, oxides) by H_2 , prior to the nanotube formation step (where the carbon containing gas is required). It is possible, however, to produce these catalytic metal particles in situ in presence of the carbon source, allowing for a one-step process [3.73]. Because the control of the metal particle size is the key point (they have to be kept at a nanometric size), their coalescence is generally avoided by supporting them on an inert support such as an oxide (Al_2O_3 ,

SiO_2 , zeolites, $MgAl_2O_4$, MgO , etc.), or more rarely on graphite. A low concentration of the catalytic metal precursor is required to limit the coalescence of the metal particles that may happen during the reduction step.

There are two main ways for the preparation of the catalyst: (a) the impregnation of a substrate with a solution of a salt of the desired transition metal catalyst, and (b) the preparation of a solid solution of an oxide of the chosen catalytic metal in a chemically inert and thermally stable host oxide. The catalyst is then reduced to form the metal particles on which the catalytic decomposition of the carbon source will lead to carbon nanotube growth. In most cases, the nanotubes can then be separated from the catalyst (Fig. 3.15).

Heterogeneous Processes – Results with CCVD Involving Impregnated Catalysts

A lot of work was already done in this area even before the discovery of fullerenes and carbon nanotubes, but although the formation of tubular carbon structures by catalytic processes involving small metal particles was clearly identified, the authors did not focus on the preparation of *SWNTs* or *MWNTs* with respect to the other carbon species. Some examples will be given here to illustrate the most striking improvements obtained.

With the impregnation method, the process generally involves four different and successive steps: (1) the impregnation of the support by a solution of a salt (nitrate, chloride) of the chosen metal catalyst; (2) the drying and calcination of the supported catalyst to get the oxide of the catalytic metal; (3) the reduction in a H_2 -containing atmosphere to make the catalytic metal particles and at last (4) the decomposition of a carbon-containing gas over the freshly prepared metal particles that will lead to the nanotube growth. For example, *Ivanov* et al. [3.74] have prepared nanotubes by the decomposition of C_2H_2 (pure or in mixture with H_2) on well-dispersed transition metal particles (Fe, Co, Ni, Cu) supported on graphite or SiO_2 . Co- SiO_2 was found to be the best catalyst/support combination for the preparation of *MWNTs*, but most of the other combinations led to carbon filaments, sometimes covered with amorphous-like carbon. The same authors have developed a precipitation-ion-exchange method that provides a better dispersion of metals on silica compared to the classical impregnation technique. The same group has then proposed the use of a zeolite-supported Co catalyst [3.75, 76], resulting in very finely dispersed metal particles (from 1 to 50 nm in diameter). Only on this catalyst could they observe *MWNTs* with a diameter around 4 nm and only two or three walls. *Dai* et al. [3.77] have prepared *SWNTs* by CO dispro-

portionation on nano-sized Mo particles. The diameters of the nanotubes obtained are closely related to that of the original particles and range from 1 to 5 nm. The nanotubes obtained by this method are free of amorphous carbon coating. It is also found that a synergetic effect occurs in the case of an alloy instead of the components alone, and one of the most striking examples is the addition of Mo to Fe [3.78] or Co [3.79].

Heterogeneous Processes – Results with CCVD Involving Solid-Solutions-Based Catalysts

A solid solution of two metal oxides is formed when some ions of one of the metals are found in substitution of the other metal ions. For example, Fe_2O_3 can be prepared in solid solution into Al_2O_3 to give a $\text{Al}_{2-2x}\text{Fe}_{2x}\text{O}_3$ solid solution. The use of a solid solution allows a perfect homogeneity of the dispersion of each oxide one in the other. These solid solutions can be prepared by different ways but the co-precipitation of mixed-oxalates and the combustion synthesis have been used mainly for the preparation of nanotubes. The synthesis of nanotubes by catalytic decomposition of CH_4 over $\text{Al}_{2-2x}\text{Fe}_{2x}\text{O}_3$ solid solutions was originated by Peigney et al. [3.73] and then studied extensively by the same group using different oxides such as spinel-based solid solutions ($\text{Mg}_{1-x}\text{M}_x\text{Al}_2\text{O}_4$ with $\text{M} = \text{Fe}, \text{Co}, \text{Ni}$, or a binary alloy [3.80, 81] or magnesia-based solid solutions [3.80, 82] ($\text{Mg}_{1-x}\text{M}_x\text{O}$, with $\text{M} = \text{Fe}, \text{Co}$ or Ni)). Because of the very homogeneous dispersion of the catalytic oxide, it is possible to produce very small catalytic metal particles, at the high temperature required for the decomposition of CH_4 (which was chosen for its greater thermal stability compared to other hydrocarbons). The method proposed by these authors involves the heating of the solid solution from room temperature to a temperature between 850°C and $1,050^\circ\text{C}$ in a mixture of H_2 and CH_4 , typically containing 18 mol.% of CH_4 . The nanotubes obtained depend clearly on the nature of both the transition metal (or alloy) used and the inert oxide (matrix), the latter because the Lewis acidity seems to play an important role [3.83]. For example, in the case of solid solutions containing around 10 wt% of Fe, the amount of carbon nanotubes obtained is decreasing in the following order depending of the matrix oxide: $\text{MgO} > \text{Al}_2\text{O}_3 > \text{MgAl}_2\text{O}_4$ [3.80]. In the case of MgO-based solid solutions the nanotubes can be very easily separated from the catalyst by dissolving it, in diluted HCl, for example [3.82]. The nanotubes obtained are typically gathered into small diameter bundles (less than 15 nm) with lengths up to $100\ \mu\text{m}$. The nanotubes are

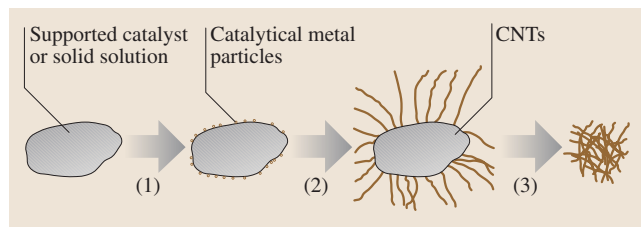


Fig. 3.15 Formation of nanotubes by the CCVD-based impregnation technique. (1) Formation of the catalytic metal particles by reduction of a precursor; (2) Catalytic decomposition of a carbon-containing gas, leading to the growth of carbon nanotubes (CNTs); (3) Removal of the catalyst to recover the CNTs (from [3.80])

mainly SWNTs and DWNTs, with diameters ranging between 1 and 3 nm.

Obtaining pure nanotubes by the CCVD method requires, as for all the other techniques, the removal of the catalyst. When a catalyst supported (impregnation) in a solid solution is used, the supporting – and catalytically inactive – oxide is the main impurity, both in weight and volume. When oxides such as Al_2O_3 or SiO_2 (or even combinations) are used, aggressive treatments involving hot caustic solutions (KOH, NaOH) for Al_2O_3 or the use of HF for SiO_2 are required. These treatments have no effect, however, on the other impurities such as other forms of carbon (amorphous-like carbon, graphitized carbon particles and shells, and so on). Oxidizing treatments (air oxidation, use of strong oxidants such as HNO_3 , KMnO_4 , H_2O_2) are thus required and allow for the removal of most of the unwanted forms of carbon but are resulting in a low yield of remaining carbon nanotubes, which are often quite damaged. Flahaut et al. [3.82] were the first to use a MgCoO solid solution to prepare SWNTs and DWNTs that could be easily separated without any damage by a fast and safe washing with an aqueous HCl solution.

In most cases, only very small quantities of catalyst (typically less than 500 mg) have been used, and most claims for “high yield” productions of nanotubes are based on laboratory experimental data, without taking into account all the technical problems related to the scaling up of a laboratory-scale CCVD reactor. At the present time, although the production of MWNTs is possible at an industrial scale, the production of SWNTs at an affordable cost is still a challenge.

Homogeneous Processes

The homogenous route, also called “floating catalyst method,” differs from the other CCVD-based meth-

ods because it uses only gaseous species and does not require the presence of any solid phase in the reactor. The basic principle of this technique, similar to the other CCVD processes, is to decompose a carbon source (ethylene, xylene, benzene, carbon monoxide, etc.) on nanometric transition metallic (generally Fe, Co, or Ni) particles in order to obtain carbon nanotubes. The catalytic particles are formed directly in the reactor, however, and are not introduced before the reaction, as it happens in the supported CCVD, for instance.

Homogeneous Processes – Experimental Devices

The typical reactor used in this technique is a quartz tube placed in an oven to which the gaseous feedstock, containing the metal precursor, the carbon source, some hydrogen, and a vector gas (N₂, Ar, or He), is sent. The first zone of the reactor is kept at a lower temperature, and the second zone, where the formation of tubes occurs, is heated to 700–1,200 °C. The metal precursor is generally a metal-organic compound, such as a zero-valent carbonyl compound like Fe(CO)₅ [3.84], or a metallocene [3.85–87], for instance ferrocene, nickelocene or cobaltocene. It may be advantageous to make the reactor vertical, in order for the effect of gravity to be symmetrically dispatched on the gaseous volume inside the furnace and to help in maintaining for a while the solid products in fluidized bed.

Homogeneous Processes – Results

The metal-organic compound decomposes in the first zone of the reactor to generate the nanometric metallic particles that can catalyze the nanotubes formation. In the second part of the reactor, the carbon source is decomposed to atomic carbon which then is responsible for the formation of nanotubes.

This technique is quite flexible and both single-walled nanotubes [3.88] and multiwalled nanotubes [3.89] have been obtained depending on the carbon feedstock gas; it has also been exploited for some years in the production of vapor grown carbon nanofibers [3.90].

The main drawback of this type of process is again, as for heterogeneous processes, the difficulty to control the size of the metal nanoparticles, and thus the nanotube formation is often accompanied by the production of undesired carbon forms (amorphous carbon or polyaromatic carbon phases found as various phases or as coatings). In particular, encapsulated forms have been often found, as the result of the creation of metallic par-

ticles that are too big to be active for growing nanotubes (but are still effective for catalytically decomposing the carbon source) and be totally recovered by graphene layers.

The same kind of parameters as for heterogeneous processes have to be controlled in order to finely tune this process and obtain selectively the desired morphology and structure of the nanotubes formed, such as: the choice of the carbon source; the reaction temperature; the residence time; the composition of the incoming gaseous feedstock with a particular attention paid to the role played by hydrogen proportion, which can control the orientation of graphenes with respect to the nanotube axis thus switching from c-MWNT to h-MWNT [3.69]; and the ratio of the metallorganic precursor to the carbon source (for lower values, SWNTs are obtained [3.85]). As recently demonstrated, the overall process can be improved by adding other compounds such as ammonia or sulfur-containing species to the reactive gas phase. The former allows aligned nanotubes and mixed C-N nanotubes [3.91] to be obtained, the latter results in a significant increase in productivity [3.90].

It should be emphasized that only small productions have been achieved so far, and the scale up toward industrial exploitation seems quite difficult because of the large number of parameters that have to be considered. A critical one is to be able to increase the quantity of metallorganic compound that has to be sent in the reactor, as a requirement to increase the production, without obtaining too big particles. This problem has not yet been solved. An additional problem inherent in the process is the possibility of clogging the reactor due to the deposition of metallic nanoparticles on the reactor walls followed by carbon deposition.

A significant breakthrough concerning this technique could be the process developed at Rice University, the so-called HiPCoTM process to produce SWNTs of very high purity [3.92]. This gas phase catalytic reaction uses carbon monoxide to produce, from [Fe(CO)₅], a SWNT material claimed to be relatively free of by-products. The temperature and pressure conditions required are applicable to industrial plants. The company Carbon Nanotechnologies Inc. (Houston, TX, USA) actually sells raw SWNT materials prepared that way, at a marketed price of \$375/g, doubled if purified (2003 data). Other companies are more specialized in MWNTs such as Applied Sciences Inc. (Cedarville, Ohio, USA), which currently has a production facility of ~40 tons/year of ~100 nm large MWNTs (Pyrograf-III), or Hyperion Catalysis (Cambridge, MA, USA), which makes MWNT-based materials.

Templating

Another technique interesting to describe briefly, though definitely not suitable for mass production, is the templating technique. It is the second method only (the first being the electric-arc technique, when considering the formation of MWNTs on the cathode) able to synthesize carbon nanotubes without any catalyst. Any other work reporting the catalyst-free formation of nanotubes is likely to have been fooled by metallic impurities present in the reactor or by some other factors having brought a chemical gradient to the system. Another original aspect is that it allows aligned nanotubes to be obtained naturally, without the help of any subsequent alignment procedure. But recovering the nanotubes only requires the template to be removed (dissolved), which means the former alignment of the nanotubes is lost.

Templating – Experimental Devices

The principle of the technique is to deposit a solid carbon coating obtained from CVD method onto the walls of an appropriate porous substrate whose pores are displayed as parallel channels. The feedstock is again a hydrocarbon, as a common carbon source. The substrate can be alumina or zeolite for instance, however, which present natural channel pores, while the whole is heated to a temperature able to crack the hydrocarbon selected as carbon source (Fig. 3.16).

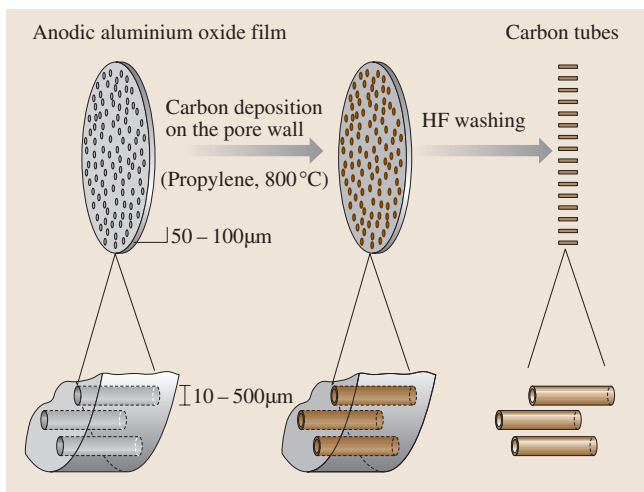


Fig. 3.16 Principle of the templating technique for the catalyst-free formation of single-walled or concentric-type multi-walled carbon nanotubes (from [3.93])

Templating – Results

Provided the chemical vapor deposition mechanism (which is actually better described as a chemical vapor infiltration mechanism) is well controlled, the synthesis results in the coating of the channel pore walls by a variable number of graphenes. Both MWNTs (exclusively concentric type) or SWNTs can be obtained. The smallest SWNTs (diameters ~ 0.4 nm) ever obtained mentioned in Sect. 3.1 have actually been synthesized by this technique [3.11]. Lengths are directly determined by channel lengths, i. e. by the thickness of the substrate plate. A main advantage is the purity of the tubes (no catalyst remnants, and little other carbon phases). On the other hand, the nanotube structure is not closed at both ends, which can be an advantage or a drawback, depending on the application. For instance, recovering the tubes requires the porous matrix to dissolve using one of the chemical treatment previously cited. The fact that tubes are open makes them even more sensitive to the acid attack.

3.2.3 Miscellaneous Techniques

In addition to the major techniques described in Sects. 3.2.1 and 3.2.2, many attempts can be found in literature to produce nanotubes by various ways, with a generally specific goal, such as looking for a low-cost or a catalyst-free production process. None has been sufficiently convincing so far to be presented as a serious alternative to the major processes described previously. Some examples are provided in the following.

Hsu et al. [3.94] have succeeded in preparing MWNTs (including coiled MWNTs, a peculiar morphology resembling a spring) by a catalyst-free (although Li was present) electrolytic method, by running a 3–5 A current between two graphite electrodes (a graphite crucible as the anode and a graphite rod as the cathode). The graphite crucible was filled with lithium chloride, while the whole was heated in air or argon at ~ 600 °C. As with many other techniques, by-products such as encapsulated metal particles, carbon shells, amorphous carbon, and so on, are formed.

Cho et al. [3.95] have proposed a pure chemistry route, by the polyesterification of citric acid onto ethylen glycol at 50 °C, followed by a polymerization at 135 °C, then carbonized at 300 °C under argon, then oxidized at 400 °C in air. Despite the latter oxidation step, the solid product surprisingly contains short MWNTs, although obviously with a poor nanotexture. By-products such as carbon shells and amorphous carbon are also formed.

Li et al. [3.96] have also obtained short MWNTs by a catalyst-free (although Si is present) pyrolytic method which involves heating silicon carbonitride nanograins in a BN crucible to 1,200–1,900 °C in nitrogen within a graphite furnace. No details are given about the possible occurrence of by-products, but they are likely considering the complexity of the chemical system (Si-C-B-N) and the high temperatures involved.

Terranova et al. [3.98] have investigated the catalyzed reaction between a solid carbon source and atomic hydrogen. Graphite nanoparticles (~ 20 nm) are sent with a stream of H₂ onto a Ta filament heated at 2,200 °C. The species produced, whatever they are, then hit a Si polished plate warmed to 900 °C and supporting transition metal particles. The whole chamber is under a dynamic vacuum of 40 torr. SWNTs are supposed to form according to the authors, although images are poorly convincing. One major drawback of the method, besides its complexity compared to others, is the difficulty of recovering the “nanotubes” from the Si substrates onto which they seem to be firmly bonded.

A last example is an attempt to prepare nanotubes by diffusion flame synthesis [3.99]. A regular gaseous hydrocarbon source (ethylene, . . .) added with ferrocene vapor is sent within a laminar diffusion flame made from air and CH₄ whose temperature range is 500–1,200 °C. SWNTs are actually formed, together with encapsulated metal particles, soot, and so on. In addition to a low yield, the SWNT structure is quite poor.

3.2.4 Synthesis of Aligned Carbon Nanotubes

Several applications (such as field-emission-based display, see Sect. 3.6) require that carbon nanotubes grow as highly aligned bunches, in highly ordered arrays, or located at specific positions. In that case, the purpose of the process is not mass production but controlled growth and purity, with subsequent control of nanotube morphology, texture, and structure. Generally speaking, the more promising methods for the synthesis of aligned nanotubes are based on CCVD processes, which involve molecular precursors as carbon source, and method of thermal cracking assisted by the catalytic activity of transition metal (Co, Ni, Fe) nanoparticles deposited onto solid supports. Few attempts have been made so far to obtain such materials with SWNTs. But the catalyst-free templating methods related to that described in Sect. 3.2.2 are not considered here, due to the lack of support after the template removal, which does not allow the former alignment to be maintained.

During the CCVD-growth, nanotubes can self-assemble into nanotube bunches aligned perpendicular to the substrate if the catalyst film on the substrate has a critical thickness [3.100], the driving forces for this alignment are the van der Waals interactions between the nanotubes, which allow them to grow perpendicularly to the substrates. If the catalyst nanoparticles are deposited onto a mesoporous substrate, the mesoscopic pores may also cause a certain effect on the alignment when the growth starts, thus controlling the growth direction of the nanotubes. Two kinds of substrates have been used so far in this purpose: mesoporous silica [3.101, 102] and anodic alumina [3.103].

Different methods have been reported in the literature for metal particles deposition onto substrates: (i) deposition of a thin film on alumina substrates from metallic-salt precursor impregnation followed by oxidation/reduction steps [3.104], (ii) embedding catalyst particles in mesoporous silica by sol-gel processes [3.101], (iii) thermal evaporation of Fe, Co, Ni, or Co-Ni metal alloys on SiO₂ or quartz substrates under high vacuum [3.105, 106], (iv) photolithographic patterning of metal-containing photoresist polymer with the aid of conventional black and white films as a mask [3.107] and, electrochemical deposition at the bottom of the pores in anodic aluminum oxide templates [3.103].

Depositing the catalyst nanoparticles onto a previously patterned substrate allows one to control the frequency of local occurrence and the display of the MWNT bunches formed. The as-produced materials mainly consist in arrayed, densely packed, freestanding, aligned MWNTs (Fig. 3.17), which is quite

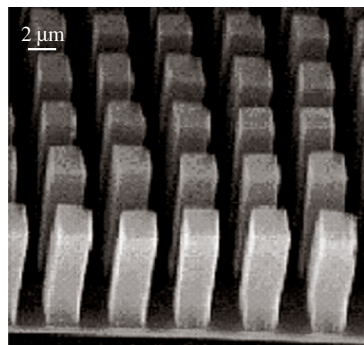


Fig. 3.17 Example of a free-standing MWNT array obtained from the pyrolysis of a gaseous carbon source over catalyst nanoparticles previously deposited onto a patterned substrate. Each square-base rod is a bunch of MWNTs aligned perpendicular to the surface (from [3.97])

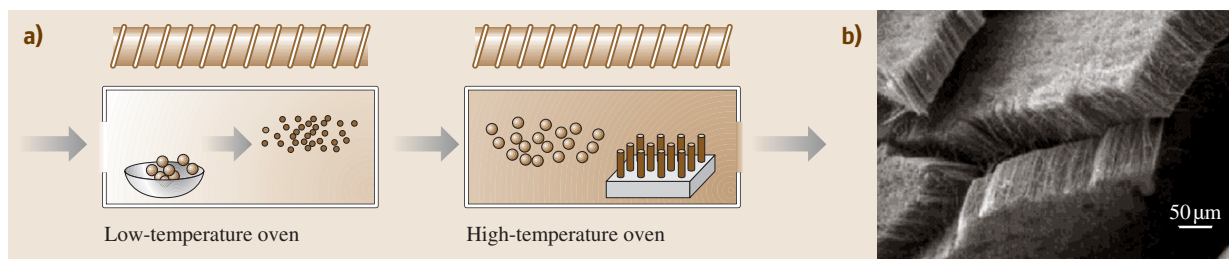


Fig. 3.18a–c Sketch of a double-furnace CCVD device for the organo-metallic/hydrocarbon co-pyrolysis process. In (a): sublimation of the precursor; in (b): decomposition of the precursor and MWNTs growth onto the substrate. (c) Example of the densely packed and aligned MWNT material obtained (from [3.108])

suitable for field emission-based applications for instance [3.97].

When a densely packed coating of vertically aligned MWNTs is desired (Fig. 3.18b), another route is the pyrolysis of hydrocarbons in the presence of organometallic precursor molecules like ferrocene or iron pentacarbonyl, operating in a dual furnace system (Fig. 3.18a). The organo-metallic precursor (e.g., ferrocene) is first sublimed at low temperature in the first furnace or is injected as a solution along with the hydrocarbon feedstock, then the whole components are pyrolyzed at higher temperature in the second furnace [3.88, 108–111]. The parameters that must be taken into account are the heating or feeding rate of ferrocene, the flow rate of the vector gas (Ar or N₂) and of the gaseous hydrocarbon, and the temperature of pyrolysis (650–1,050 °C). Generally speaking, the co-deposition process using [Fe(CO)₅] as catalyst source implies its thermal decomposition at elevated temperatures to produce atomic iron that

deposits on the substrates in the hot zone of the reactor. As the nanotube growth occurs simultaneously with the introduction of [Fe(CO)₅], the temperatures chosen for the growth depend on the carbon feedstock utilized, e.g., they can vary from 750 °C for acetylene to 1,100 °C for methane. Mixtures of [FeCp₂] and xylene or [FeCp₂] and acetylene have also been used successfully for the production of freestanding MWNTs.

The nanotube yield and quality are directly linked with the amount and size of the catalyst particles, and since the planar substrates used do not exhibit high surface area, the dispersion of the metal can be a key step in the process. It has been observed that an etching pre-treatment of the surface of the deposited catalyst thin film with NH₃ may be critical for an efficient growth of nanotubes by bringing the appropriate metal particle size distribution. It may also favor the alignment of MWNTs and prevent the formation of amorphous carbon from thermal cracking of acetylene [3.112].

3.3 Growth Mechanisms of Carbon Nanotubes

Growth mechanisms of carbon nanotubes are still debated. But researchers have been impressively imaginative and have made a number of hypotheses. One reason is that conditions allowing carbon nanofilaments to grow are very diverse, which means that related growing mechanisms are many. For given conditions, the truth is even probably a combination or a compromise between some of the proposals. Another reason is that phenomena are quite fast and difficult to observe in situ. It is generally agreed, however, that growth should occur so that the number of dangling bonds is limited, for energetic reasons.

3.3.1 Catalyst-Free Growth

As already mentioned, in addition to the templating technique which merely relates to chemical vapor infiltration mechanism for pyrolytic carbon, the growth of c-MWNT as a deposit onto the cathode in the electric-arc method is a rare example of catalyst-free carbon nanofilament growth. The driving forces are obviously related to the electric field, i.e. related to charge transfers from an electrode to the other via the particles contained in the plasma. How the MWNT nucleus forms is not clear, but once it has started, it may include the direct incorpora-

tion of C_2 species to the primary graphene structure as it was formerly proposed for fullerenes [3.113]. This is supported by recent C_2 radical concentration measurements that revealed an increasing concentration of C_2 from the anode being consumed to the growing cathode (Fig. 3.13), indicating, first, that C_2 are secondary species only, and second, that C_2 species could actually participate actively in the growth mechanism of c-MWNTs in the arc method.

3.3.2 Catalytically Activated Growth

Growth mechanisms involving catalysts are more difficult to ascertain, since they are more diverse. Although a more or less extensive contribution of a VLS (Vapor-Liquid-Solid [3.114]) mechanism is rather well admitted, it is quite difficult to find comprehensive and plausible explanations able to account for both the various conditions used and the various morphologies observed. What follows is an attempt to provide overall explanations of most of the phenomena, while remaining consistent with the experimental data. We did not consider hypotheses for which there are a lack of experimental evidence, such as the moving nano-catalyst mechanism, which proposed that dangling bonds from a growing SWNT may be temporarily stabilized by a nano-sized catalyst located at the SWNT tip [3.23], or the scooter mechanism, which proposed that C dangling bonds are temporarily stabilized by a single catalyst atom, moving all around the SWNT cross section edge, allowing subsequent C atom addition [3.115].

From the various results, it appears that the most important parameters are probably the thermodynamic conditions (only temperature will be considered here), the catalyst particle size, and the presence of a substrate. Temperature is critical and basically corresponds to the discrepancy between CCVD methods and solid-carbon-source based method.

Low Temperature Conditions

Low temperature conditions are typical from CCVD conditions, since nanotubes are frequently found to grow far below $1,000^\circ\text{C}$. If conditions are such that the catalyst is a crystallized solid, the nanofilament is probably formed according to a mechanism close to a VLS mechanism, in which three steps are defined: (i) adsorption then decomposition of C-containing gaseous moieties at the catalyst surface; (ii) dissolution then diffusion of the C-species through the catalyst, thus forming a solid solution; (iii) back precipitation of solid car-

bon as nanotube walls. The texture is then determined by the orientation of the crystal faces relative to the filament axis (Fig. 3.19), as demonstrated beyond doubt by transmission electron microscopy images such as that in *Rodriguez et al.* [3.19]. This mechanism can therefore provide either c-MWNT, or h-MWNT, or platelet nanofiber.

If conditions are such that the catalyst is a liquid droplet, either because of higher temperature conditions or because of lower temperature melting catalyst, a mechanism similar to that above can still occur, really VLS (vapor = gaseous C species, liquid = molten catalyst, S = graphenes), but there are obviously no more crystal faces to orientate preferentially the rejected graphenes. Energy minimization requirements will therefore tend to make them concentric and parallel to the filament axis.

With large catalyst particles (or in the absence of any substrate), the mechanisms above will generally follow a “tip growth” scheme, i. e., the catalyst will move forward while the rejected carbon form the nanotube behind, whether there is a substrate or not. In that case,

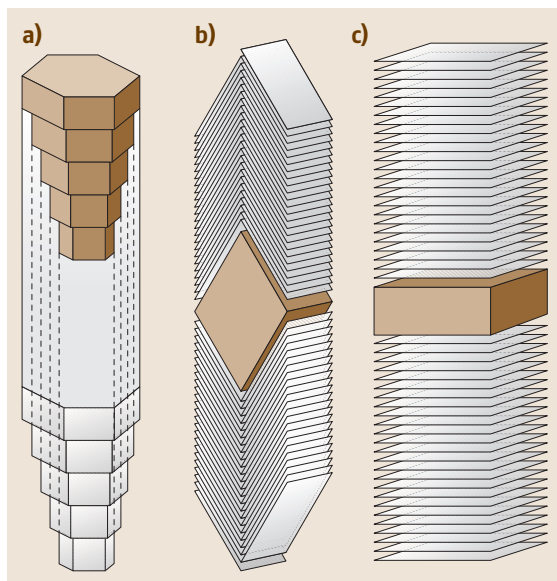


Fig. 3.19 Illustration of the relationships between the catalyst crystal outer morphology and the subsequent carbon nanofilament inner texture. Crystal are drawn from their images in the projected plane perpendicular to the electron beam in a transmission electron microscope, i. e. crystal morphology in the out-of-plane dimension is not ascertained (adapted from [3.19])

chances are high that one end is open. On the contrary, when catalyst particles deposited onto a substrate are small enough (nanoparticles) to be refrained to move by the interaction forces with the substrate, the growth mechanism will follow a “base growth” scheme, i. e. the carbon nanofilament grows away from the substrate leaving the catalyst nanoparticle attached to the substrate (Fig. 3.20).

The bamboo texture that affects both the herringbone and the concentric texture may reveal a specificity of the dissolution-rejection mechanism, i. e. a periodic, discontinuous dynamics of the phenomenon. Once the catalyst has reached the saturation threshold regarding its content in carbon, it expulses it quite suddenly. Then it becomes again able to incorporate a given amount of carbon without having any catalytic activity for a little while, then over-saturation is reached again, etc. Factors controlling such a behavior, however, are not determined.

It is then clear that, in any of the mechanisms above, 1 catalyst particle = 1 nanofilament. This explains why, although making SWNT by CCVD methods is possible, controlling the catalyst particle size is critical, since it thereby controls the subsequent nanofilament to be grown from it. Reaching a really narrow size distribution in CCVD is quite challenging, specifically as far as nanosizes are concerned when growing SWNTs is the goal. Only particles < 2 nm will be able to make it (Fig. 3.20), since larger SWNTs would energetically not be favored [3.10]. Another specificity of the CCVD method and from the related growth mechanisms is that the process can be effective all along the isothermal zone of the reactor furnace since continuously fed with a carbon-rich feedstock, which is generally in excess, with a constant composition at a given time of flight of the species. Coarsely, the longer the isothermal zone in gaseous carbon excess conditions, the longer the nanotubes. This is why the nanotube lengths can be much longer than that obtained by solid-carbon-source-based methods.

Table 3.2 provides guidelines for the relationships between the synthesis conditions and the type of nanotube formed.

High Temperature Conditions

High temperature conditions are typical from solid-carbon-source based methods such as electric arc, laser vaporization, or solar furnace (see Sect. 3.2). The huge temperatures involved (several thousands °C) atomize both the carbon source and the catalyst. Of course, catalyst-based SWNTs do not form in the area of highest temperatures (contrary to c-MWNT in the electric arc

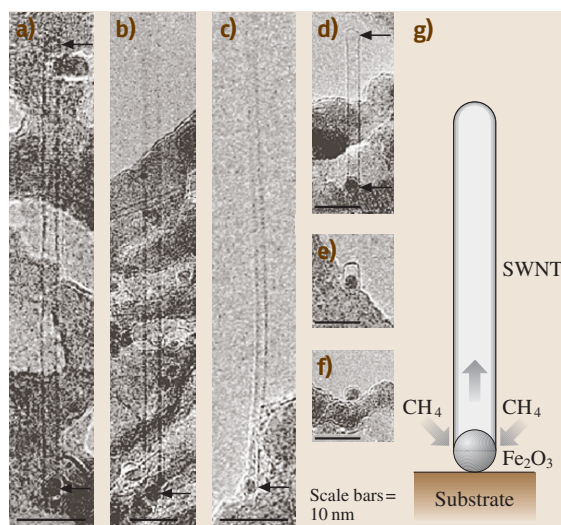


Fig. 3.20 High resolution transmission electron microscopy images of several SWNTs grown from iron-based nanoparticles by CCVD method, showing that particle sizes determine SWNT diameters in that case (adapted from [3.116])

method), but the medium is made of atoms and radicals all mixed, some of which are likely to condense into the same droplet (since it will be liquid at the beginning). At some distance from the atomization zone, the medium is therefore made of carbon metal alloy droplets and of secondary carbon species that range from C₂ to higher order molecules such as corannulene which is made of a central pentagon surrounded by 5 hexagons. (The preferred formation of such a molecule can be explained by the former association of carbon atoms into a pentagon, because it is the fastest way to limit dangling bonds at low energetic cost, thereby providing a fixation site for other carbon atoms (or C₂) which also will tend to close into a ring, again to limit dangling bonds. Since adjacent pentagons are not energetically favoured, these cycles will be hexagons. Such a molecule is thought to be a probable precursor for fullerenes. Fullerenes are actually always produced, even in conditions which produce SWNTs.) The same event of saturation in C of the carbon-metal alloy droplet occurs as described in Sect. 3.3.2, resulting in the precipitation of excess C outside the particle upon the effect of the decreasing thermal gradient in the reactor, which decreases the solubility threshold of C in the metal [3.117]. Once the “inner” carbon atoms reach the catalyst particle surface, they meet the “outer” carbon species, including corannulene, that will con-

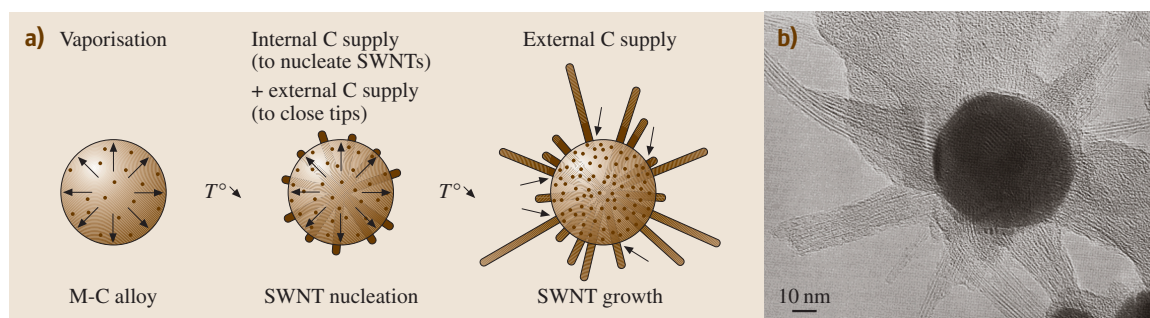
Table 3.2 Guidelines indicating the relationships between possible carbon nanoflament morphologies and some basic synthesis conditions

		Increasing temperature and physical state of catalyst →			Substrate		Thermal gradient	
		Solid (crystallized)	Liquid from melting	Liquid from clusters	Yes	No	Low	High
Catalyst particle size	< ~ 3 nm	SWNT	SWNT	?	base-growth			
	> ~ 3 nm	MWNT (c,h,b) platelet nanofiber (heterogeneous related to catalyst particle size)	c-MWNT	SWNT	tip-growth	tip-growth	long length	short length
Nanotube diameter				homogeneous (independent) from particle size)				
Nanotube/particle		one nanotube/particle		several SWNTs/particle				

tribute to cap the merging nanotubes. Once formed and capped, nanotubes can grow both from the inner carbon atoms (Fig. 3.21a), according to the VLS mechanism proposed by *Saito* et al. [3.117], and from the outer carbon atoms, according to the adatom mechanism proposed by *Bernholc* et al. [3.118]. In the latter, carbon atoms from the surrounding medium in the reactor are attracted then stabilized by the carbon/catalyst interface at the nanotube/catalyst surface contact, promoting their subsequent incorporation at the tube base. The growth mechanism therefore mainly follows the base growth scheme. But once the nanotubes are capped, C₂ species still remaining in the medium and which meet the growing nanotubes far from the nanotube/catalyst interface, may still incorporate the nanotubes from both the side

wall or the tip, thereby giving rise to some proportion of Stone–Wales defects [3.40]. The occurrence of a nanometer-thick surface layer of yttrium carbide (onto the main Ni-containing catalyst core), whose some lattice distances are commensurable with that of the C–C distance in graphene, as recently revealed by *Gavillet* et al. [3.48], could possibly play a beneficial role in the stabilization effect at the nanotube/catalyst interface and explain why SWNT yield is enhanced by such bimetallic alloys (as opposed to single metal catalysts).

A major difference with the low temperature mechanisms described for CCVD methods is that many nanotubes are formed from a single, relatively large (~ 10–50 nm) catalyst particle (Fig. 3.21b), whose size distribution is therefore not as critical as for the low

**Fig. 3.21** (a) Mechanism proposed for SWNT growth (see text). (b) Transmission electron microscopy image of SWNT growing radial to a large Ni catalyst particle surface in the electric arc experiment. (modified from [3.17])

temperature mechanisms (particles that are too large, however, would induce polyaromatic shells instead of nanotubes). That is why **SWNT** diameters are much more homogeneous than for **CCVD** methods. Why the most frequent diameter is ~ 1.4 nm is again a matter of energy balance. Single-wall nanotubes larger than ~ 2.5 nm are not stable [3.10]. On the other hand, strain to the C–C angles increases as the radius of curvature decreases. Such diameter (1.4 nm) should therefore correspond to the best energetic compromise. Another difference with the low temperature mechanisms for **CCVD** is that temperature gradients are huge, and the gas phase composition surrounding the catalysts droplets is also subjected to rapid changes (as opposed to what

could happen in a laminar flow of a gaseous feedstock whose carbon source is in excess). This explains why nanotubes from arc are generally shorter than nanotubes from **CCVD**, and why mass production by **CCVD** should be favored. In the latter, the catalytic role of the metallic particle can be recurrent as long as the conditions are maintained. In the former, surrounding conditions change continuously, and the window for efficient catalysis effect can be very narrow. Lowering temperature gradients in solid carbon source-based **SWNT** producing methods such as the electric-arc reactor should therefore be a way to increase the **SWNT** yield and length [3.119]. Amazingly, this is in opposition to fullerene production from arc.

3.4 Properties of Carbon Nanotubes

Carbon is a unique light atom that can form one-, two-, or threefold strong chemical bonds. The planar threefold configuration forms graphene planes that can, under certain growth conditions (see Sect. 3.3), adopt a tubular geometry. Properties of the so-called carbon nanotubes may change drastically depending on whether **SWNTs** or **MWNTs** are considered (see Sect. 3.1).

3.4.1 Variability of Carbon Nanotube Properties

Properties of **MWNTs** are generally not much different from that of regular polyaromatic solids (which may exhibit graphitic, or turbostratic, or intermediate crystallographic structure), and variations are then mainly driven by the textural type of the **MWNTs** considered (concentric, herringbone, bamboo) and the quality of the nanotexture (see Sect. 3.1), both of which control the extent of anisotropy. Actually, for polyaromatic solids, whose structural entities are built with stacked graphenes, bond strength is quite different depending on whether the in-plane direction is considered (which includes only very strong – covalent – and therefore very short – 0.142 nm bonds) or the direction perpendicular to it (which includes only very weak – van der Waals – and therefore very loose – ~ 0.34 nm bonds). Such heterogeneity is not found in single (isolated) **SWNTs**. But the heterogeneity is back along with the related consequences when **SWNTs** associate into bundles. Therefore, properties – and applicability – for **SWNTs** may also change dramatically depending on whether single **SWNT** or **SWNT** ropes are involved.

In the following, we will emphasize **SWNT** properties, as far as their original structure often leads to original properties with respect to that of regular polyaromatic solids. But we will also sometimes cite properties of **MWNTs** for comparison.

3.4.2 General Properties

SWNT-type carbon nanotube diameters fall in the nanometer range and can be hundreds of micrometers long. **SWNTs** are narrower in diameter than the thinnest line able to be obtained by electron beam lithography. **SWNTs** are stable up to 750 °C in air (but start being damaged earlier through oxidation mechanisms, as demonstrated by their subsequent ability to be filled with molecules, see Sect. 3.5) and up to $\sim 1,500$ – $1,800$ °C in inert atmosphere beyond which they transform into regular, polyaromatic solids (i. e., phases built with stacked graphenes instead of single graphenes) [3.120]. They have half the mass density of aluminum. While the length of **SWNTs** can be macroscopic, the diameter has a molecular dimension. As a molecule, properties are closely influenced by the way atoms are displayed along the molecule direction. The physical and chemical behavior of **SWNTs** are therefore related to their unique structural features [3.121].

3.4.3 SWNT Adsorption Properties

An interesting feature of **SWNTs** is their very high surface area, the highest ever due to the fact that a single graphene sheet is probably the unique example of a ma-

terial energetically stable in normal conditions while consisting of a single layer of atoms. Ideally, i. e. not considering SWNTs in bundles but isolated SWNTs, and provided the SWNTs have one end opened (by oxidation treatment for instance), the real surface area can be equal to that of a single, flat graphene, i. e. $\sim 2,700 \text{ m}^2/\text{g}$ (accounting for both sides).

But practically, nanotubes – specifically SWNTs – are more often associated with many other nanotubes to form bundles, then fibers, films, papers, etc. than as a single entity. Such architectures develop various porosity ranges important for determining adsorption properties (the latter aspects are also developed in Sect. 3.6.2, focused on applications). It is thus most appropriate to discuss adsorption on SWNT-based materials in term of adsorption on the outer or inner surfaces of such bundles. Furthermore, theoretical calculations have predicted that the molecule adsorption on the surface or inside of the nanotube bundle is stronger than that on an individual tube. A similar situation exists for MWNTs where adsorption could occur either on or inside the tubes or between aggregated MWNTs. Additionally, it has been shown that the curvature of the graphene sheets constituting the nanotube walls can result in a lower heat for adsorption with respect to that of a planar graphene (see Sect. 3.1.1).

Accessible SWNT Surface Area

Various studies dealing with the adsorption of nitrogen on MWNTs [3.122, 123] and SWNTs [3.124] have highlighted the porous nature of these two materials. Pores in MWNTs can be divided mainly into inner hollow cavities of small diameter (narrowly distributed, mainly 3–10 nm) and aggregated pores (widely distributed, 20–40 nm), formed by interaction of isolated MWNTs. It is also worth noting that the ultra-strong nitrogen capillarity in the aggregated pores contributes to the major part of the total adsorption, showing that the aggregated pores are much more important than the inner cavities of the MWNTs for adsorption. Adsorption of N_2 has been studied on as-prepared and acid-treated SWNTs, and the results obtained point out the microporous nature of SWNT materials, as opposed to the mesoporous MWNT materials. Also, as opposed to isolated SWNTs (see above), surface areas well above $400 \text{ m}^2\text{g}^{-1}$ have been measured for SWNT-bundle-containing materials, with internal surface areas of $300 \text{ m}^2\text{g}^{-1}$ or higher.

The theoretical specific surface area of carbon nanotubes ranges over a broad scale, from 50 to $1,315 \text{ m}^2\text{g}^{-1}$ depending on the number of walls, the diameter, or the

number of nanotubes in a bundle of SWNTs [3.125]. Experimentally, the specific surface area of SWNTs is often larger than that of MWNTs. Typically, the total surface area of as-grown SWNTs ranges between 400 and $900 \text{ m}^2\text{g}^{-1}$ (micropore volume, $0.15\text{--}0.3 \text{ cm}^3\text{g}^{-1}$), whereas values ranging between 200 and $400 \text{ m}^2\text{g}^{-1}$ for as-produced MWNTs are often reported. In the case of SWNTs, the diameter of the tubes and the number of tubes in the bundle will affect mainly the BET value. It is worth noting that opening/closing of the central canal noticeably contributes to the adsorption properties of nanotubes. In the case of MWNTs, chemical treatments such as KOH activation are efficient to develop a microporosity, and surface areas as high as $1,050 \text{ m}^2\text{g}^{-1}$ have been reported [3.126]. Thus it appears that opening or cutting as well as chemical treatments (purification step for example) of carbon nanotubes can considerably affect their surface area and pore structure.

Adsorption Sites and Binding Energy of the Adsorbates

An important problem to solve when considering adsorption on nanotubes is the identification of the adsorption sites. Adsorption of gases in a SWNT bundle can occur inside the tubes (pore), in the interstitial triangular channels between the tubes, on the outer surface of the bundle, or in a groove formed at the contact between adjacent tubes on the outside of the bundle (Fig. 3.22). Starting from closed-end SWNTs, simple molecules can adsorb on the walls of the outer nanotubes of the bundle and preferably on the external grooves. For the more attractive sites, corresponding to the first adsorption stages, it seems that adsorption or condensation in the interstitial channel of SWNT bundles depends on the size of the molecule (or on the SWNT diameters) and on their interaction energies [3.127]. Then, adapted treatments to open the tubes will favour the gas adsorption (e.g., O_2 , N_2 in the inner walls [3.128, 129]). For hydro-

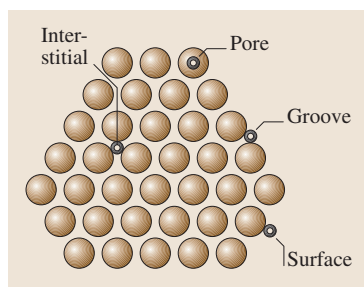


Fig. 3.22 Sketch of a SWNT bundle illustrating the four different adsorption sites

gen and other small molecules, computational methods have shown that, for open *SWNTs*, the pore, interstitial, and groove sites are energetically more favourable than the surface site, with respect to the increasing number of carbon nanotubes interacting with the adsorbed molecules [3.130].

For *MWNTs*, adsorption can occur in the aggregated pores, inside the tube or on the external walls. In the latter case, the presence of defects, as incomplete graphene layers, has to be taken into consideration. Although adsorption between the graphenes (intercalation) has been proposed in the case of hydrogen adsorption in *h-MWNTs* or platelet nanofibers [3.132], it is unlikely for many molecules due to steric effect and should not prevail for small molecules due to long diffusion path.

Few studies deal with adsorption sites in *MWNTs*, however it has been shown that butane adsorbs more in the case of *MWNTs* with smaller outside diameters, which is consistent with another statement that the strain brought to curved graphene surfaces affects sorption. Most of the butane adsorbs to the external surface of the *MWNTs* while only a small fraction of the gas condensed in the pores [3.133]. Comparative adsorption of krypton or of ethylene on *MWNTs* or on graphite has allowed scientists to determine the dependence of the adsorption and wetting properties on the specific morphology of the nanotubes. Higher condensation pressure and lower heat of adsorption were found on nanotubes with respect to graphite [3.134]. These differences result mainly from a decrease in the lateral interactions between the adsorbed molecules, related to the curvature of the graphene sheets.

A limited number of theoretical as well as experimental works exist on the values of the binding energies for gases on carbon nanotubes. If most of these studies report low binding energies on *SWNTs*, consistent with a physisorption, some experimental results, in particular in the case of hydrogen, are still controversial (see Sect. 3.6.2). In the case of platelet nanofibers, the initial dissociation of hydrogen on graphite edge sites, which constitute the majority of the nanofiber surface has been proposed [3.135]. For carbon nanotubes, a mechanism that involves H_2 dissociation on residual metal catalyst followed by H spillover and adsorption on the most reactive nanotube sites could be envisaged [3.136]. Doping nanotubes with alkali may enhance hydrogen adsorption, due to the charge transfer from the alkali metal to the nanotube, which polarizes the H_2 molecule and induces dipole interaction [3.137].

Generally speaking, the adsorbates can be either charge donors or acceptors to the nanotubes. The observed trends in the binding energies of gases with different van der Waals radii suggest that the groove sites of *SWNTs* are the preferred low coverage adsorption sites due to their higher binding energies. Finally, several studies have shown that, at low coverage, the binding energy of the adsorbate on *SWNT* is between 25% and 75% higher than the binding energy on a single graphene. This discrepancy can be attributed to an increase of the effective coordination in the binding sites, such as the groove sites, in *SWNTs* bundles [3.138, 139]. Representative results concerning the adsorption properties of *SWNTs* and *MWNTs* are summarized on Table 3.3.

Table 3.3 Adsorption properties and sites of *SWNTs* and *MWNTs*. Letters in column 5 refer to Fig. 3.22. Data of two last columns are from [3.131]

Type of nanotube	Porosity (cm^3g^{-1})	Surface area (m^2/g)	Binding energy of the adsorbate	Adsorption sites	Attractive potential per site (eV)	Surface area per site (m^2/g)
<i>SWNT</i> (bundle)	Microporous V_{micro} : 0.15–0.3	400–900	Low, mainly physisorption 25–75% > graphite	Surface (A)	0.049	483
				Groove (B)	0.089	22
				Pore (C)	0.062	783
				Interstitial (D)	0.119	45
<i>MWNT</i>	Mesoporous	200–400	Physisorption	Surface Pore Aggregated pores	—	—

3.4.4 Transport Properties

The narrow diameter of *SWNTs* has a strong influence on its electronic excitations due to its small size compared to the characteristic length scale of low energy electronic excitations. Combined with the particular shape of the electronic band structure of graphene, carbon nanotubes are ideal quantum wires. The conduction and the valence band of the graphene touch on the 6 corners (*K* points) of the Brillouin zone [3.140]. By rolling the graphene to form a tube, new periodic boundary conditions for the electronic wave functions superimpose, which give rise to one-dimensional sub-bands: $C_n K = 2q$ where q is an integer and C_n the vector $na_1 + ma_2$ characteristic of the diameter and the helicity of the tube (see Sect. 3.1). If one of these sub-bands passes through one of the *K* points, the nanotube will be metallic, otherwise it will be semiconductor with a gap inversely proportional with the diameter. For a tube with a diameter of 3 nm, the gap falls in the range of the thermal energy at room temperature. As pointed out in Sect. 3.1 already, knowing (n, m) then allows one to predict whether or not the tube exhibits a metallic behavior. To summarize, we can say that the electronic structure of *SWNTs* depends both on the orientation of the honeycomb lattice with respect to the tube axis and the radius of curvature imposed to the bent graphene sheet. This explains why properties of *MWNTs* quickly become no different from regular, polyaromatic solids as the number of walls (graphenes) increases, since the radius of curvature increases meanwhile. In addition, the conduction occurs essentially through the external tube (for *c-MWNTs*), but the interactions with the internal coaxial tubes may make the electronic properties vary. For small diameter *MWNTs* exhibiting a low number of walls, typically two (*DWNTs*), the relative lattice orientation of the two superimposed graphenes remains determinant, and the resulting overall electronic behavior can either be metallic or semiconductor upon structural considerations [3.141]. Another consequence, valid for any nano-sized carbon nanotube whatever the number of walls, is that applying stresses to the tube is also likely to change its electronic behavior, as a consequence of the variation brought to the position of the sub-bands with respect to the *K* points of the Brillouin zone [3.142].

The details of electronic properties of *SWNTs* are not well understood yet, and numerous theoretical and experimental works have revealed fascinating effects [3.143]. An assembly of agglomerated tubes (ropes) increases the complexity. Moreover, investigating the electron properties of a single *SWNT* requires

one to characterize and control the properties of the electrical contacts. Likewise, the interaction with the substrate influence the bulk transport properties a lot when *SWNTs* embedded in a medium (e.g., a composite) are considered. The conduction of charge carriers in metallic *SWNTs* is thought to be ballistic (i.e., independent from length) due to the expected small number of defects [3.144–146] with a predicted electric conductance twice the fundamental conductance unit $G_0 = 4e/h$ because of the existence of two propagating modes. Because of the reduced scattering, metallic *SWNTs* can transport huge current densities (max 10^9 A/cm²) without being damaged, i.e. about three orders of magnitude higher than in Cu. On the other hand, in a one-dimensional system, electrons often localize due to structural defects or disorder. In case the contact resistance is too high, a tunnel barrier is formed, and the charge transport is dominated by tunneling effects. Several transport phenomena were reported in the literature of this regime: weak localization due to quantum interferences of the electronic wave functions that leads to an increase of the resistivity [3.147–149], Coulomb blockade at low temperature that characterizes by conductance oscillations as the gate voltage increases [3.148], superconductivity induced by superconductor contacts [3.150], or spin polarization effects induced by ferromagnetic contacts [3.151]. Furthermore, due to enhanced Coulomb interactions, one-dimensional metals are expected to show drastic changes in the density of states at the Fermi level and are described by a Luttinger liquid [3.148]. This behavior is expected to result in the variation of conductance vs. temperature that follows a power law, with a zero conductance at low temperature.

As mentioned previously, *SWNTs* are model systems to study one-dimensional charge transport phenomena. Due to the of mesoscopic dimension of the morphology, the one-dimensional structure of the nanotube has strong singularities in the electronic density of states (*DOS*) that fall in the energy range of visible light. As a consequence, visible light is strongly absorbed. It has been observed that flash illumination with a broadband light can lead to spontaneous burning of a macroscopic sample of agglomerated (i.e., ropes) carbon nanotubes in air and room temperature [3.152].

As a probable consequence of both the small number of defects (at least the kind of defects that oppose phonon transport) and the cylindrical topography, *SWNTs* exhibit a large phonon mean free path, which results in a high thermal conductivity. The thermal conductivity of *SWNTs* is comparable to that of a single, isolated

graphene layer or high purity diamond [3.153] or possibly higher ($\sim 6,000$ W/mK).

Finally, carbon nanotubes may also exhibit a positive or negative magneto-resistance depending on the current, the temperature, and the field, whether they are MWNTs [3.154] or SWNTs [3.149].

3.4.5 Mechanical Properties

While tubular nano-morphology is also observed for many two-dimensional solids, carbon nanotubes are unique through the particularly strong threefold bonding (sp^2 hybridization of the atomic orbitals) of the curved graphene sheet, which is stronger than in diamond (sp^3 hybridization) as revealed by their difference in C–C bond length (0.142 vs. 0.154 nm for graphene and diamond respectively). This makes carbon nanotubes – SWNTs or c-MWNTs – particularly stable against deformations. The tensile strength of SWNTs can be 20 times that of steel [3.155] and has actually been measured equal to ~ 45 GPa [3.156]. Very high tensile strength values are also expected for ideal (defect-free) c-MWNTs, since combining perfect tubes concentrically is not supposed to be detrimental to the overall tube strength, provided the tube ends are well capped (otherwise, concentric tubes could glide relative to each other, inducing high strain). Tensile strength values as high as ~ 150 GPa have actually been measured for perfect MWNTs from electric arc [3.157], although the reason for such a high value compared to that measured for SWNTs is not clear. It probably reveals the difficulty in carrying out such measurements in a reliable manner. At least, flexural modulus, for perfect MWNTs should logically exhibit higher values than SWNTs [3.155], with a flexibility that decreases as the number of walls increases. On the other hand, measurements performed on defective MWNTs obtained from CCVD gave a range of 3–30 GPa [3.158]. Tensile modulus, also, reaches the highest values ever, 1 TPa for MWNTs [3.159], and possibly even higher for SWNTs, up to 1.3 TPa [3.160,161]. Figure 3.23 illustrates how spectacularly defect-free carbon nanotubes could revolutionize the current panel of high performance fibrous materials.

3.4.6 Reactivity

The chemical reactivity of graphite, fullerenes, and carbon nanotubes exhibits some common features. Like any small object, carbon nanotubes have a large surface with which they can interact with their environment (see Sect. 3.4.1). It is worth noting, however, that the

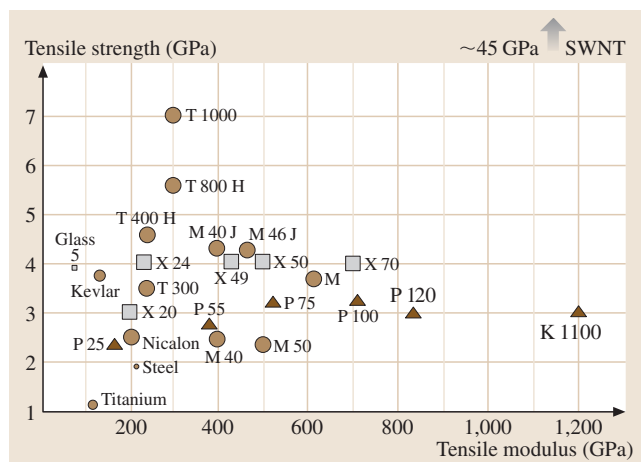


Fig. 3.23 Plot of the tensile strength versus tensile modulus for current fibrous materials, as compared to SWNTs. Large circles are PAN-based carbon fibers, which include the highest tensile strength fiber available on the market (T1000 from Torayca); Triangles are pitch-based carbon fibers, which include the highest tensile modulus fiber on the market (K1100 from Amoco)

chemistry of nanotubes differs from that of regular polyaromatic carbon materials because of their unique shape, small diameter, and structural properties. Compared to graphite, perfect SWNTs have no chemically active dangling bonds (the reactivity of polyaromatic solids is known to occur mainly through graphene edges). Compared to fullerenes, the ratio of “weak” sites (C–C bonds involved in heterocycles) over strong sites (C–C bonds between regular hexagons) is only slightly different from 0 for ideally perfect tubes (as opposed to 1 in C_{60} fullerenes – C_{60} molecules have 12 pentagons (therefore accounting for $5 \times 12 = 30$ C–C bonds) and 20 hexagons, each of them having three C–C bonds not involved in an adjacent pentagon but shared with a neighboring hexagon (therefore accounting for $20 \times 3 \times 1/2 = 30$ C–C bonds involved in hexagons only). Although graphene faces are chemically relatively inert, the radius of curvature imposed on the graphene in nanotubes enforces the three formerly planar C–C bonds characteristic of the genuine sp^2 hybridization to accept distortions in bond angles that make them closer and closer to the situation of three of the four C–C bonds in diamond (characteristic of the genuine sp^3 hybridization) as the radius of curvature decreases. Even though it is not enough to bring a genuine chemical reactivity to the carbon atoms, a consequence is to consider that either nesting sites are created at the concave sur-

face, or strong physisorption sites are created above each carbon atom of the convex surface, both with a bonding efficiency that increases as the nanotube diameter decreases.

As already pointed out in Sect. 3.1, the chemical reactivity of SWNTs (and c-MNWTs) is supposed to come mainly from the caps, since they contain six pentagons each, as opposed to the tube body, which supposedly contains hexagons only. Indeed, oxidizing treatments applied to carbon nanotubes (air oxidation, wet-chemistry oxidation) are known to open the nanotube tips rather selectively [3.162]. But the ability of SWNTs to be opened by oxidation methods then filled with foreign molecules such as fullerenes (see Sect. 3.5) reveals the occurrence of side defects [3.14], whose identification and occurrence were discussed then proposed to be an average of one Stone–Wales defect every 5 nm along the tube length, involving an amount of about

2% of the carbon atoms for the example of a regular (10,10) SWNT [3.163] – a Stone–Wales defect is made of four adjacent heterocycles, two pentagons and two heptagons, displayed by pairs in opposition. Such a defect actually allows localized double bonds to be formed between the carbon atoms involved in the defect (instead of the electrons participating to the delocalized electron cloud above the graphene as usual, enhancing the chemical reactivity, e.g. toward chlorocarbenes [3.163]). This means that the overall chemical reactivity of carbon nanotubes should strongly depend on the way they are synthesized. For example, SWNTs prepared by the arc-discharge method are supposed to contain fewer structural defects compared to CCVD-synthesized SWNTs, which have a higher chemical reactivity. Of course, the reactivity of h-MWNT-type nanotubes is intrinsically higher, due to the occurrence of accessible graphene edges at the nanotube surface.

3.5 Carbon Nanotube–Based Nano-Objects

3.5.1 Hetero–Nanotubes

Hetero-nanotubes are defined here as carbon nanotubes whose carbon atoms, part or all of them, are substituted with another element while the overall honeycomb lattice-based graphene structure is maintained. Elements involved are, therefore, boron and/or nitrogen. Benefits can be new behaviors (e.g., BN nanotubes are electrical insulators), improved properties (e.g., regarding the resistance to oxidation), or better control of the properties. One current challenge is actually to control the processing so that the desired SWNT structure is selectively synthesized (metallic or semiconductor). In this regard, it was demonstrated that substituting some C atoms by N or B atoms lead to SWNTs whose electrical behavior is systematically metallic [3.164, 165].

Some examples of hetero-nanotubes, though mainly MWNTs, are found in literature, whose hetero-atom involved is generally nitrogen due to the ease of introducing some gaseous or solid nitrogen and/or boron containing species (e.g., N₂, NH₃, BN, HfB₂) in existing MWNT synthesis devices [3.164, 166] until complete substitution of carbon [3.167, 168]. An amazing result of such attempts to synthesize hetero-MWNTs was the subsequent formation of “multilayered” c-MWNTs, i.e. MWNTs whose constituting coaxial tubes were alternatively made of carbon graphenes and boron nitride graphenes [3.169]. On the other hand, exam-

ples of hetero-SWNTs are few. But the synthesis of B- or N-containing SWNTs has been recently reported [3.165, 170].

3.5.2 Hybrid Carbon Nanotubes

Hybrid carbon nanotubes are here defined as carbon nanotubes, SWNTs or MWNTs, whose inner cavity has been filled, partially or entirely, by foreign atoms, molecules, compounds, or crystals. Such hybrids are thereby noted as X@SWNT (or X@MWNT, if appropriate, where X is the atom, molecule, etc. involved) [3.171].

Motivation

Why filling carbon nanotubes? The very small inner cavity of nanotubes is an amazing tool to prepare and study the properties of confined nanostructures of any nature, such as salts, metals, oxides, gases, or even discrete molecules like C₆₀, for example. Because of the almost one-dimensional structure of carbon nanotubes (specifically considering SWNTs), different physical and/or chemical properties can be expected for the encapsulated foreign materials or possibly for the overall hybrid materials. Indeed, when the volume available inside a carbon nanotube is small enough, the foreign material can be made mainly of “surface atoms” of reduced coordination. The overall former motivation was then to tenta-

tively form metal nanowires likely to be interesting for electronic applications (quantum wires). Metals were the preferred fillers, and nanotubes were mostly considered merely as nano-molds, likely to be removed afterward. But it is likely that the removal of the SWNT “container” to liberate the confined one-dimensional structure may destroy or at least transform it because of the stabilizing effect brought by the interactions with the nanotube wall.

Filling nanotubes while they grow (in situ filling) was one of the pioneering methods. In most cases, however, the filling step is separated from the step of synthesis of the nanotubes. Three methods can then be distinguished: (a) wet chemistry procedures, and physical procedures, involving (b) capillarity filling by a molten material or (c) filling by a sublimated material.

Generally speaking, the estimation of the filling rate is problematic and most of the time is taken merely from the TEM observation, without any statistics on the number of tubes observed. Moreover, as far as SWNTs are concerned, the fact that the nanotubes are gathered into bundles makes difficult the observation of the exact number of filled tubes, as well as the estimation of the filled length for each tube.

Filling carbon nanotubes with materials that could not have been introduced directly is also possible. This can be accomplished by first filling the nanotubes with an appropriate precursor (i. e., able to sublime, or melt, or solubilize) that will later be transformed by chemical reaction or by a physical interaction such as electron beam irradiation, for example [3.172]. In the case of secondary chemical transformation, the reduction by H₂ is the most frequently used to obtain nanotubes filled with metals [3.173]. Sulfides can be obtained as well by using H₂S as reducing agent [3.173].

Because the inner diameter of SWNTs is generally smaller than that of MWNTs, it is more difficult to fill them, and the driving forces involved in the phenomena are not yet totally understood (see the review paper by [3.163]). Consequently, more than one hundred articles dealing with filled MWNTs were already published by the time this chapter was written. We, therefore, did not attempt to review all the works. We chose to cite the pioneering works, then to focus on the more recent works dealing with the more challenging topic of filling SWNTs.

In Situ Filling Method

Most of the first hybrid carbon nanotubes ever synthesized were directly obtained in the course of their processing. This concerns only MWNTs, prepared by the arc-discharge method in its early hours, for which the

filling materials were easily introduced in the system by drilling a central hole in the anode and filling it with the heteroelements. First attempts were all reported the same year [3.174–178], with elements such as Pb, Bi, YC₂, TiC, etc. Later on, *Loiseau* et al. [3.179] showed that MWNTs could also be filled to several μm in length by elements such as Se, Sb, S, and Ge, but only as nanoparticles with elements such as Bi, B, Al and Te. Sulfur was suggested to play an important role during the in situ formation of filled MWNTs by arc-discharge [3.180]. This technique is no longer the preferred one because of the difficulty in controlling the filling ratio and yield and in achieving mass production.

Wet Chemistry Filling Method

The wet chemistry method requires the opening of the nanotubes tips by chemical oxidation prior to the filling step. This is generally obtained by refluxing the nanotubes in diluted nitric acid [3.181–183], although other oxidizing liquid media may work as well, e.g. [HCl + CrO₃] [3.184] or chlorocarbenes formed from the photolytic dissociation of CHCl₃ [3.163] as a rare example of a nonacidic liquid route for opening SWNTs. If a dissolved form (salt, oxide, etc.) of the desired metal is meanwhile introduced during the opening step, some of it will get inside the nanotubes. An annealing treatment (after washing and drying of the treated nanotubes) may then lead to the oxide or to the metal, depending on the annealing atmosphere [3.162]. Although the wet chemistry method looked promising because a wide variety of materials can be introduced within nanotubes this way, and because it operates at temperature not much different from room temperature, attention has to be paid to the oxidation method that has to be carried out as the first steps. The damages brought to the nanotubes by severe treatments (e.g., nitric acid) make them improper for use with SWNTs. Moreover, the filling yield is not very important, as a probable consequence of the presence of the solvent molecules that also enter the tube cavity, and the subsequent filled lengths rarely exceed 100 nm. Recent results have been obtained, however, using wet chemistry filling by *Mittal* et al. [3.184] who have filled SWNTs ropes by CrO₃ with an average yield of ~ 20%.

Molten State Filling Method

The physical method involving a liquid (molten) phase is more restrictive, first, because some materials may start decomposing when they melt, and second because the melting point has to be compatible with the nanotubes, i. e. thermal treatment temperature should remain below the temperature of transformation or damaging

of the nanotubes. Because the filling is occurring by capillarity, the surface tension threshold of the molten material was found to be 100–200 N/cm² [3.185]. But this threshold was proposed for MWNTs, whose inner diameters (5–10 nm) are generally larger than those of SWNTs (1–2 nm). In a typical filling experiment, the MWNTs are closely mixed with the desired amount of filler by gentle grinding, and the mixture is then vacuum-sealed in a silica ampoule. The ampoule is then slowly heated to a temperature above the melting point of the filler, then is slowly cooled. The use of this method does not require any opening of the nanotubes prior to the heat treatment. The mechanism of nanotube opening is not yet established clearly, but it is certainly related to the chemical aggressivity of the molten materials toward carbon and more precisely toward graphene defects in the tube structure (see Sect. 3.4.4).

Most of the works on SWNTs involving this method were performed by Sloan and coworkers at Oxford University [3.187], although other groups followed the same procedure [3.86, 181, 183]. Precursors to fill the nanotubes were mainly metals halides. Although little is known yet about the physical properties of halides crystallized within carbon nanotubes, the crystallization itself of molten salts within small diameter SWNTs has been studied in detail, revealing a strong interaction between the one-dimensional crystals and the surrounding graphene wall. For example, Sloan et al. [3.188] have described two-layer 4 : 4 coordinated KI crystals formed within SWNTs of around 1.4 nm diameter. These two-

layer crystals are “all surface” and have no “internal” atoms. Significant lattice distortions occur compared to the bulk structure of KI, where the normal coordination is 6 : 6 (meaning that each ion is surrounded by six identical closer neighbors). Indeed, the distance between two ions across the SWNT capillary is 1.4 times the same distance along the tube axis. This denotes an accommodation of the KI crystal to the confined space provided by the inner nanotube cavity in the constrained crystal direction (across the tube axis). This implies that the interactions between the ions and the surrounding carbon atoms are strong. The volume dimension available within the nanotubes thus somehow controls the crystal structure of inserted materials. For instance, the structure and orientation of encapsulated PbI₂ crystals inside their capillaries were found to arrange in different ways inside SWNTs and DWNTs, with respect to the diameter of the confining nanotubes [3.186]. In the case of SWNTs, most of the obtained encapsulated one-dimensional PbI₂ crystals exhibit a strong preferred orientation with their (110) planes aligning at an angle of ca. 60° to the SWNT axes as shown in Fig. 3.24a and 3.24b. Due to the extremely small diameter of the nanotube capillaries, individual crystallites are often only a few polyhedral layers thick, as outlined in Fig. 3.24d to 3.24h. As a result of lattice terminations enforced by capillary confinement, the edging polyhedra must be of reduced coordination, as indicated in Fig. 3.24g and 3.24h. In the case of PbI₂ formed inside DWNTs, similar crystal growth behavior was generally observed to occur in narrow nanotubes with diameters comparable to that of SWNTs. As the diameter of the encapsulating capillaries increases, however, different preferred orientations are frequently observed (Fig. 3.25). In this example, the PbI₂ crystal is oriented with the [121] direction parallel to the direction of the electron beam (Fig. 3.25a to 3.25d). If the PbI₂@DWNT hybrid is viewed “side-on” (as indicated by the arrow in Fig. 3.25e) polyhedral slabs are seen to arrange along the capillary, oriented at an angle of ca. 45° with respect to the tubule axis.

Sublimation Filling Method

This method is even more restrictive than the previous one, since it is applicable only to a very limited number of compounds due to the requirement for the filling materials to sublime within the temperature range of thermal stability of the nanotubes. Examples are therefore few. Actually, except for an attempt to fill SWNTs with ZrCl₄ [3.189], the only example published so far is the formation of C₆₀@SWNT (whose popular nickname

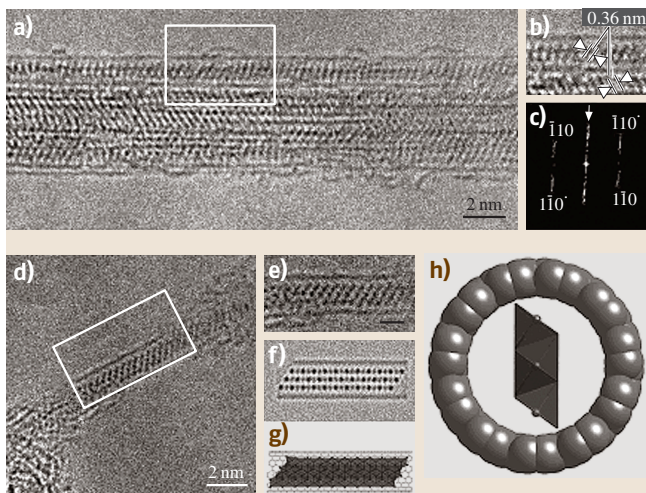


Fig. 3.24 HRTEM images and corresponding structural model for PbI₂ filled SWNTs (from [3.186])

is “peapods”), reported for the first time in 1998 [3.190], where regular ~ 1.4 nm large SWNTs are filled with C_{60} fullerene molecule chains (Fig. 3.26a). Of course, the process requires a pre-opening of the SWNTs by some method, as discussed previously, typically either acid attack [3.191] or heat-treatment in air [3.192]. Then the opened SWNTs are put into a sealed glass tube together with fullerene powder and placed into a furnace heated above the sublimation temperature for fullerite ($> \sim 350$ °C). Since there is no limitation related to Laplace’s law or the presence of solvent since only gaseous molecules are involved, filling efficiency may actually reach $\sim 100\%$ [3.192].

Remarkable behaviors have been revealed since then, such as the ability of the C_{60} molecules to move freely within the SWNT cavity (Fig. 3.26b and 3.26c) upon random ionization effects from electron irradiation [3.193], or to coalesce into 0.7 nm large inner elongated capsules upon electron irradiation [3.194], or into a 0.7 nm large nanotube upon subsequent thermal treatment above 1,200 °C [3.193, 195]. Annealing of C_{60} @SWNT materials may thus appear as an efficient way to produce DWNTs with nearly constant inner (~ 0.7 nm) and outer (~ 1.4 nm) diameters. DWNTs produced this way are actually the smallest MWNTs synthesized so far.

Based on the successful synthesis of so-called endofullerenes previously achieved [3.13], further development of the process has recently led to the synthesis of more complex nanotube-based hybrid materials such as $La_2@C_{80}$ @SWNTs [3.196], $Gd@C_{82}$ @SWNTs [3.197], or $Er_xSc_{3-x}N@C_{80}$ @SWNT [3.198] among other examples. These provide even more extended perspective regarding the potential applications of peapods, which are still being investigated.

Finally the last example to cite is the successful attempt to produce peapods by a related method, by using accelerated fullerene ions (instead of neutral gaseous molecules) to enforce the fullerenes to enter the SWNT structure [3.199].

3.5.3 Functionalized Nanotubes

Based on the reactivity of carbon nanotubes as discussed in Sect. 3.4.6, the functionalization reactions can be divided into two main groups. One is based on the chemical oxidation of the nanotubes (tips, structural defects) leading to carboxylic, carbonyl, and/or hydroxyl functions. These functions are then used for additional reactions, to attach oligomeric or polymeric functional

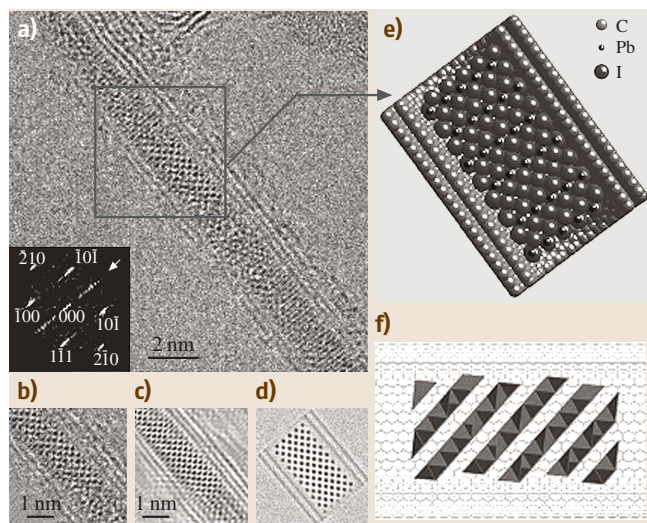


Fig. 3.25 HRTEM images (experimental and simulations), and corresponding structural model for a PbI_2 filled double-wall carbon nanotube (from [3.186])

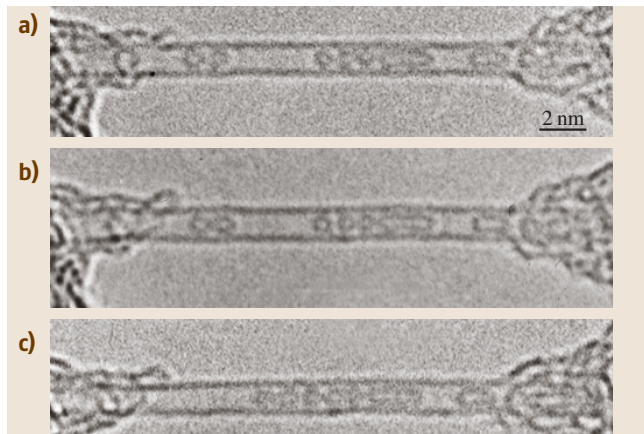


Fig. 3.26a–c HRTEM images of (a) example of five regular C_{60} molecules encapsulated together with two higher fullerenes (C_{120} and C_{180}) as distorted capsules (on the right) within a regular 1.4 nm diameter SWNT. (a)–(c) Example of the diffusion of the C_{60} -molecules along the SWNT cavity. The time between each image of the sequence is about 10 s. The fact that nothing occurs between (a) and (b) reveals the randomness of the ionisation events generated by the microscope electron beam and assumed to be responsible for the molecule displacement

entities. The second group is based on direct addition to the graphitic-like surface of the nanotubes (i. e. without any intermediate step). Examples of the latter reactions

include oxidation or fluorination (an important first step for further functionalization with other organic groups). Properties and applications of functionalized nanotubes have been reviewed recently [3.200].

Oxidation of Carbon Nanotubes

Carbon nanotubes are often oxidized and therefore opened before chemical functionalization to increase their chemical reactivity (creation of dangling bonds). Chemical oxidation of nanotubes is mainly achieved using either wet chemistry or gaseous oxidants such as oxygen (typically air) or CO_2 . Depending on the synthesis process, the oxidation resistance of the nanotubes can vary. When oxidation is carried out through gas phases, thermo-gravimetric analysis (TGA) is of great use to determine at which temperature the treatment should be applied. It is important to know that TGA accuracy increases as the heating rate diminishes, while the literature often provides TGA analyses obtained in nonoptimized conditions, leading to overestimated oxidation temperatures. The presence of catalyst remnants (metals, more rarely oxides), the type of nanotubes (SWNTs, c-MWNTs, h-MWNTs), and the oxidizing agent (air, O_2 is an inert gas, CO_2 , etc.) as well as the flow rate used make difficult the comparison of published results. It is generally agreed, however, that amorphous carbon burns first, followed by SWNTs and then multiwall materials (shells, MWNTs), even if TGA is often unfortunately not able to clearly separate the different oxidation steps. The more common method used for nanotube oxidation is that of aqueous solutions of oxidizing reagents. The main one is nitric acid, either concentrated or diluted (around 3 moles per liter in most cases), but oxidants such as potassium dichromate ($\text{K}_2\text{Cr}_2\text{O}_7$), hydrogen peroxide (H_2O_2), or potassium permanganate (KMnO_4) are very often used as well. HCl, like HF, do not damage nanotubes because these acids are not oxidizing.

Functionalization of Oxidized Carbon Nanotubes

Carboxylic groups located at the nanotube tips can be coupled with different chemical groups. Oxidized nanotubes are usually reacted with thionyl chloride (SOCl_2) to generate the acyl chloride, even if a direct reaction is theoretically possible with alcohols or amines, for example. Reaction of SWNTs with octadecylamine (ODA) was reported by Chen et al. [3.201] after reaction of oxidized SWNTs with SOCl_2 . The functionalized SWNTs have substantial solubility in chloroform (CHCl_3), dichloromethane (CH_2Cl_2), aro-

matic solvents, and carbon disulfide (CS_2). Many other reactions between functionalized nanotubes (after reaction with SOCl_2) and amines have been reported in the literature and will not be reviewed here. Non-covalent reactions between the carboxylic groups of oxidized nanotubes and octadecylammonium ions are possible [3.202], providing solubility in tetrahydrofuran (THF) and CH_2Cl_2 . Functionalization by glucosamine using similar procedures [3.203] allowed the water solubilization of SWNTs, which is of special interest when considering biological applications of functionalized nanotubes. Functionalization with lipophilic and hydrophilic dendra (with long alkyl chains and oligomeric poly(ethyleneglycol) groups) has been achieved by amination and esterification reactions [3.204], leading to solubility of the functionalized nanotubes in hexane, chloroform, and water. It is interesting to note that in the latter case, the functional groups could be removed just by modifying the pH of the solution (base- and acid-catalyzed hydrolysis reaction conditions, [3.205]). A last example is the possible interconnection of nanotubes via chemical functionalization. This has been recently achieved by Chiu et al. [3.206] using the already detailed acyl chloride way and a bifunctionalized amine to link the nanotubes by the formation of amide bonds.

Sidewall Functionalization of Carbon Nanotubes

The covalent functionalization of the nanotube walls is possible by means of fluorination reactions. It was first reported by Mickelson et al. [3.207], with F_2 gas (the nanotubes can then be defluorinated, if required, with anhydrous hydrazine). As recently reviewed by Khabashesku et al. [3.208], it is then possible to use these fluorinated nanotubes to carry out subsequent derivatization reactions. Thus, sidewall-alkylated nanotubes can be prepared by nucleophilic substitution (Grignard synthesis or reaction with alkyllithium precursors [3.209]). These alkyl sidewall groups can be removed by air oxidation. Electrochemical addition of aryl radicals (from the reduction of aryl diazonium salts) to nanotubes has also been reported by Bahr et al. [3.210]. Functionalization of the nanotube external wall by cycloaddition of nitrenes, addition of nucleophilic carbenes, or addition of radicals has been described by Holzinger et al. [3.211]. Electrophilic addition of dichlorocarbene to SWNTs occurs by reaction with the deactivated double bonds in the nanotube wall [3.212]. Silanization reactions are another way to functionalize nanotubes, although only tested with MWNTs. Velasco-Santos et al. [3.213] have reacted oxidized MWNTs with an organosilane (RsiR'_3 ,

with R being an organo-functional group attached to silicon) and obtained organo-functional groups attached to the nanotubes by silanol groups.

Noncovalent sidewall functionalization of nanotubes is important because the covalent bonds are associated with changes from sp^2 to sp^3 in the hybridization of the carbon atoms involved, which corresponds to a loss of the graphite-like character. As a consequence, physical properties of functionalized nanotubes, specifically **SWNTs**, may be modified. One possibility for achieving noncovalent functionalization of nanotubes is to wrap the nanotubes in a polymer [3.214], which allows their solubilization (thus improving the processing possibilities) while preserving their physical properties.

3.6 Applications of Carbon Nanotubes

Carbon nanotubes can be inert and can have a high aspect ratio, high tensile strength, low mass density, high heat conductivity, large surface area, and versatile electronic behavior including high electron conductivity. While these are the main characteristics of the properties for individual nanotubes, a large number of them can form secondary structures such as ropes, fibers, papers, thin films with aligned tubes, etc., with their own specific properties. The combination of these properties makes them ideal candidates for a large number of applications provided their cost is sufficiently low. The cost of carbon nanotubes depends strongly on both the quality and the production process. High quality single shell carbon nanotubes can cost 50–100 times more than gold. But synthesis of carbon nanotubes is constantly improving, and sale prizes fall by 50% per year. Application of carbon nanotubes is therefore a very fast moving area with new potential applications found every year, even several times per year. Making an exhaustive list is again a challenge we will not take. Below are listed applications considered “current” (Sect. 3.6.1) either because already marketed, or because up-scaling synthesis is being processed, or because prototypes are currently developed by profit-based companies. Other applications are said to be “expected” (Sect. 3.6.2).

3.6.1 Current Applications

High mechanical strength of carbon nanotubes makes them a near to ideal force sensor in scanning probe microscopy (**SPM**) with a higher durability and the ability to image surfaces with a high lateral resolution, the latter

Finally, it is worth keeping in mind that all these chemical reactions are not specific to nanotubes and may occur to most of the carbonaceous impurities present in the raw materials. This makes difficult the characterization of the functionalized samples and thus requires one to perform the experiments starting with very pure carbon nanotube samples, which is unfortunately not always the case for the results reported in the literature. On the other hand, purifying the nanotubes to start with may also bias the functionalization experiments since purification requires chemical treatments. But the demand for such products does exist already, and purified then fluorinated **SWNTs** can be found on the market at \$ 900/g (Carbon Nanotechnologies Inc., 2003).

being a typical limitation of conventional force sensors (ceramic tips). The idea was first proposed and experimented by Dai et al. [3.77] using c-MWNTs. It was extended to **SWNTs** by Hafner et al. [3.215], since small diameters of **SWNTs** were supposed to bring higher resolution than MWNTs due to the extremely short radius of curvature of the tube end. But commercial nanotube-based tips (e.g., Piezomax, Middleton, WI, USA) use MWNTs for processing convenience. It is also likely that the flexural modulus of **SWNTs** is too low and therefore induces artifacts affecting the lateral resolution when scanning a rough surface. On the other hand, the flexural modulus of c-MWNTs is supposed to increase with the number of walls, but the radius of curvature of the tip meanwhile increases.

Near-Field Microscope Probes

SWNT or MWNT, such nanotube-based **SPM** tips also offer the perspective of being functionalized, in the prospect of making selective images based on chemical discrimination by “chemical force microscopy” (**CFM**). Chemical function imaging using functionalized nanotubes represents a huge step forward in **CFM** because the tip can be functionalized very accurately (ideally at the very nanotube tip only, where the reactivity is the highest), increasing the spatial resolution. The interaction between chemical species present at the end of the nanotube tip and a surface containing chemical functions can be recorded with great sensitivity, allowing the chemical mapping of molecules [3.216, 217].

Today the cost of nanotube-based **SPM** tips is in the range of \$ 200/tip. Such a high cost is explained both

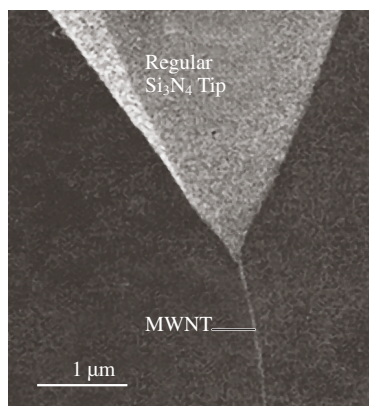


Fig. 3.27 Scanning electron microscopy image of a carbon nanotube (MWNT) mounted onto a regular ceramic tip as a probe for atomic force microscopy

by the processing difficulty, which ideally requires one to grow or mount a single MWNT in the appropriate direction at the tip of a regular SPM probe (Fig. 3.27), and by the need to individually control the tip quality. Such a market has been estimated at $\sim \$20$ M/year.

Field Emission-Based Devices

Based on a pioneering work by *de Heer* et al. [3.218], carbon nanotubes have been demonstrated to be efficient field emitters and are currently being incorporated in several applications, including flat panel display for television sets or computers (whose a first prototype was exhibited by Samsung in 1999) or any devices re-

quiring an electron producing cathode, such as X-ray sources. The principle of a field-emission-based screen is demonstrated in Fig. 3.28a. Briefly, a potential difference is brought between emitting tips and an extraction grid so that electrons are taking out from the tips and sent onto an electron sensitive screen layer. Replacing the glass support and protection of the screen by some polymer-based material will even allow the develop of flexible screens. As opposed to regular (metallic) electron emitting tips, the structural perfection of carbon nanotubes allows higher electron emission stability, higher mechanical resistance, and longer life time. First of all, it allows energy savings since it needs lower (or no) heating temperature of the tips and requires much lower threshold voltage. As an illustration for the latter, producing a current density of 1 mA/cm^2 is possible for a threshold voltage of $3 \text{ V}/\mu\text{m}$ with nanotubes, while it requires $20 \text{ V}/\mu\text{m}$ for graphite powder and $100 \text{ V}/\mu\text{m}$ for regular Mo or Si tips. The subsequent reductions in cost and energy consumption are estimated at 1/3 and 1/10 respectively. Generally speaking, the maximum current density obtainable ranges between 10^6 A/cm^2 and 10^8 A/cm^2 depending on the nanotubes involved (e.g., SWNT or MWNT, opened or capped, aligned or not) [3.219–221]. Although nanotube side-walls seem to emit as well as nanotube tips, many works have dealt (and are still dealing) with growing nanotubes perpendicular to the substrate surface as regular arrays (Fig. 3.28b). Besides, using SWNTs instead of MWNTs does not appear necessary for many of these applications when they are used as bunches. On the other hand, when considering single, isolated nanotubes, SWNTs are generally less preferable since they allow much lower electron doses than do MWNTs, although they are likely meanwhile to provide an even higher coherent source (an useful feature for devices such as electron microscopes or X-ray generators).

The market associated with this application is huge. With such major companies involved as Motorola, NEC, NKK, Samsung, Thales, Toshiba, etc., the first commercial flat TV sets and computers using nanotube-based screens are about to be seen in stores, and companies such as Oxford Instruments and Medirad are about to commercialize miniature X-ray generators for medical applications on the basis of nanotube-based cold cathodes developed by Applied Nanotech Inc.

Chemical Sensors

The electrical conductance of semiconductor SWNTs was recently demonstrated to be highly sensitive to the change in the chemical composition of the surround-

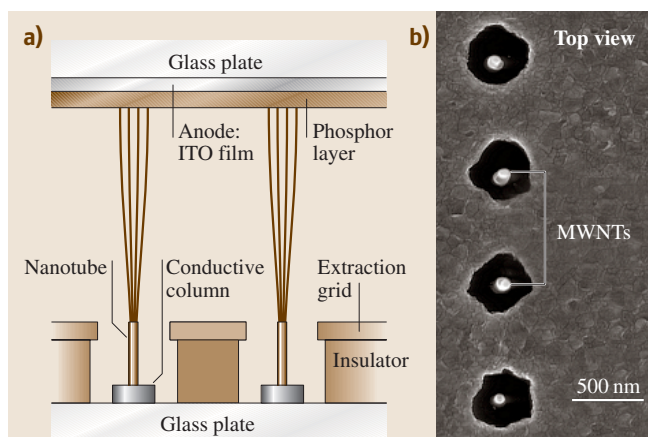


Fig. 3.28 (a) Principle of a field-emitter-based screen. (b) Scanning electron microscope image of a nanotube-based emitter system (top view). Round dots are MWNT tips seen through the holes corresponding to the extraction grid. By courtesy of *Legagneux* (Thales Research & Technology, Orsay, USA)

ing atmosphere at room temperature, due to the charges transfer between the nanotubes and the molecules from the gases adsorbed onto the *SWNT* surface. It has also been shown that there is a linear dependence between the concentration of the adsorbed gas and the difference in electrical properties, and that the adsorption is reversible. First tries involved NO_2 or NH_3 [3.222] and O_2 [3.223]. *SWNT*-based chemical NO_2 and NH_3 sensors are characterized by extremely short response time (Fig. 3.29), thus being different from conventionally used sensors [3.222, 224]. High sensitivity toward water or ammonia vapors has been measured on *SWNT*- SiO_2 composite [3.225]. This study indicated the presence of p-type *SWNT*s dispersed among the predominant metallic *SWNT*s, and that chemisorption of gases on the surface of the semiconductor *SWNT*s is responsible for the sensing action. The determination of CO_2 and O_2 concentrations on *SWNT*- SiO_2 composite has also been reported [3.226]. By doping nanotubes with palladium nanoparticles, Kong et al. [3.227] have also shown that

the modified material could reveal the presence of hydrogen up to 400 ppm whereas the as-grown material was totally ineffective.

Generally speaking, the sensitivity of the new nanotube-based sensors is three orders of magnitude higher than that of standard solid state devices. In addition, the interest in using nanotubes as opposed to current sensors is the simplicity and the very small size of the system in which they can be placed, the fact that they can operate at room temperature, and their selectivity, which allows a limited number of sensor device architectures to be built for a variety of industrial purposes, while the current technology requires a large diversity of devices based on mixed metal oxide, opto-mechanics, catalytic beads, electrochemistry, etc. The market opportunity is expected to be \$ 1.6 billion by 2006, including both the biological area and the chemical industrial area. Nanotube-based sensors are currently developed in both large and small companies, such as Nanomix (USA), for example.

Catalyst Support

Carbon materials are attractive supports in heterogeneous catalytic processes due to their ability to be tailored to specific needs: indeed, activated carbons are already currently employed as catalyst supports because of their high surface area, their stability at high temperatures (under not oxidizing atmosphere), and the possibility of controlling both their porous structure and the chemical nature of their surface [3.228, 229]. The attention has been brought to nano-sized fibrous morphologies of carbon that appeared during the last decade, showing novel interesting potentialities as supports [3.230]. Carbon nanofibers (also improperly called graphite nanofibers) and carbon nanotubes have been used successfully and shown to present, as catalyst-supporting materials, properties superior to that of such other regular catalyst-supports as activated carbon, soot, or graphite [3.231]. The use of graphite nanofibers as a direct catalyst for oxidative dehydrogenation has also been reported [3.232].

The morphology and size of carbon nanotubes, especially since they do present huge lengths vs. diameters (= aspect ratio), can play a significant role in catalytic applications due to their ability to disperse catalytically active metal particles. Their electronic properties are also of primary importance [3.233] since this conductive support may be exerting electronic perturbation as well as geometric constraint on the dispersed metal particles. A recent comparison between the interaction of transition metal atoms with carbon nanotube walls

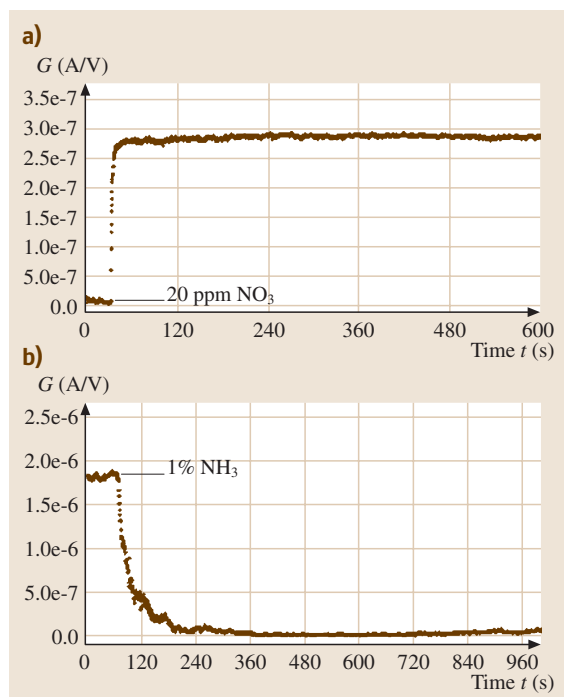


Fig. 3.29a,b Demonstration of the ability of *SWNT*s in detecting molecule traces in inert gases. (a) Increase in a single *SWNT* conductance when 20 ppm of NO_2 are added to an argon gas flow. (b) Same with 1% NH_3 added to the argon gas flow (from [3.222])

and that with graphite indicates major differences in bonding sites, magnetic moments, and charge-transfer direction [3.234]. Thus the possibility of strong metal-support interaction has to be taken into account. Their mechanical strength is also important and makes them resistant to attrition in view of recycling. Their external or internal surface presents strong hydrophobicity and strong adsorption ability toward organic molecules. Finally, for MWNT-based catalyst-supports, the relatively high surface area and the absence of microporosity (i. e., pores < 2 nm) associated with a high meso- and macropore volume (see Sect. 3.4.3) result in significant improvements of the catalytic activity, in the case of liquid-phase reactions when compared to catalysts supported on activated carbon. With nanotube supports, the mass transfer limitation of the reactants to the active sites is actually prevented due to the absence of microporosity, and the apparent contact time of the products with the catalyst is diminished, leading to more active and more selective catalytic effects.

The most widely used technique to prepare carbon nanotube-supported catalysts is the incipient wetness impregnation, in which the purified support is impregnated with a solution of the metal precursor, then dried, calcinated and/or reduced in order to obtain metal particles dispersed on the support. The chemical treatment and/or the modification of the carbon nanotube surface was found to be a useful tool to control its hydrophobic or hydrophilic character [3.236]. A strong metal/support interaction can thus be expected from the occurrence of functionalized groups created by the oxidation of the support surface, resulting in smaller particle sizes [3.237]. A more sophisticated technique to achieve the grafting of metal particles onto carbon nanotubes consists of functionalizing the outer surface of the tubes and then performing a chemical reaction with a metal complex, thus resulting in a good dispersion of the metallic particles (Fig. 3.30) [3.235].

Selected examples of some carbon nanotube-based catalysts together with the related preparation routes and catalytic activities are listed in Table 3.4.

The market is huge for this application since it most often concerns the “heavy” chemical industry. It implies and requires mass production of low-cost nanotubes, processed by methods other than solid-carbon-source-based methods (see Sect. 3.2.1). Such an application also requires some surface reactivity, making the h-MWNT type nanotubes with a poor nanotexture (see Sect. 3.1.2) the most suitable starting material for preparing such catalyst supports. Catalysis-enhanced thermal cracking



Fig. 3.30 Transmission electron microscopy image showing rhodium nanoparticles supported on MWNT surface (from [3.235])

of gaseous carbon precursors is therefore preferred, and pilot plants are already being built by major chemical industrial companies (e.g., Ato-Fina, France).

3.6.2 Expected Applications Related to Adsorption

The adsorption and interaction of gases, liquids, or metal with carbon nanotubes has attracted much attention in the past several years. The applications resulting from the adsorption properties of carbon nanotubes can be arbitrarily divided into two groups. The first group is based on the consequences of molecule adsorption on nanotube electronic properties, whose main application is the chemical sensors (see Sect. 3.6.1). The second group includes gas storage, gas separation, or the use of carbon nanotubes as adsorbent and results from the morphological characteristics of carbon nanotubes (surface area, aspect ratio, and so forth). Among the three latter potential applications, the possibility of storing gases, and more particularly hydrogen, on carbon nanotubes has received most of the attention.

Table 3.4 Preparation and catalytic performances of some nanotube-supported catalysts

Catalyst	Preparation route	Catalytic reaction	Comments
Ru/MWNT+SWNT [3.230]	Liquid phase impregnation, no pretreatment of the tubes	Liquid phase cinnamaldehyde hydrogenation	Different kind of metal support interaction compared to activated carbon
Pt/MWNT electrodes [3.149]	Electrode-less plating with pre-functionalization of MWNT	Oxygen reduction for fuel cells applications	High electrocatalytic activity
Rh/MWNT [3.235]	Surface mediated organo-metallic synthesis, pre-functionalization of MWNT	Liquid phase hydroformylation and hydrogenation	Higher activity of Rh/MWNT compared to Rh/activated carbon
Ru-alkali/MWNT [3.238]	Liquid phase impregnation, no pretreatment of the tubes	Ammonia synthesis, gas phase reaction	Higher activity with MWNT than with graphite
Rh-phosphine/MWNT [3.239]	Liquid phase grafting from [RhH(CO)(PPh ₃) ₃]	Liquid phase hydroformylation	Highly active and regioselective catalyst

Gas Storage – Hydrogen

The development of lightweight and safe system for hydrogen storage is necessary for a wide use of highly efficient H₂-air fuel cells in transportation vehicles. The U.S. Department of Energy Hydrogen Plan has set a standard by providing a commercially significant benchmark for the amount of reversible hydrogen adsorption. This benchmark requires a system-weight efficiency (the ratio of H₂ weight to system weight) of 6.5 wt% hydrogen and a volumetric density of 63 kgH₂/m³.

From now on, the failure to produce a practical storage system for hydrogen has prevented hydrogen from coming to the commercial forefront as a transportation fuel. The ideal hydrogen storage system needs to be light, compact, relatively inexpensive, safe, easy to use, and reusable without the need for regeneration. While research and development are continuing on such technologies as liquid hydrogen systems, compressed hydrogen systems, metal hydride systems, and superactivated carbon systems, all have serious disadvantages. For example, liquid hydrogen systems are very expensive, primarily because the hydrogen must be cooled to about -252 °C. For example, a liquid hydrogen system will cost about four times more than an equivalent amount of gasoline. Further, liquid hydrogen must be kept cooled to prevent it from boiling away, even when the vehicle is parked.

Compressed hydrogen is much cheaper than liquid hydrogen but also much bulkier.

Metal hydride systems store hydrogen as a solid in combination with other materials. For example, metal hydrides are produced by bathing a metal, such as palladium or magnesium, in hydrogen. The metal splits the

dihydrogen gas molecules and binds the hydrogen atoms to the metal until released by heating. The disadvantages of a metal hydride system are its weight (typically about eight times more than an equivalent amount of liquid hydrogen or an equivalent amount of gasoline) and the need to warm it up to release the hydrogen.

Superactivated carbon is the basis of another system for storing hydrogen that initially showed commercial potential. Superactivated carbon is a material similar to the highly porous activated carbon used in water filters but can gently hold hydrogen molecules by physisorption at sub-zero temperatures. The colder the carbon, the less heat is needed to disturb the weak forces holding the carbon and hydrogen together. Again, a major disadvantage of such a system is that preventing the hydrogen from escaping requires it to constantly remain at very low temperatures, even when the vehicle is parked.

Consequently there still remains a great need for a material that can store hydrogen and is light, compact, relatively inexpensive, safe, easy to use, and reusable without regeneration. Recently some articles or patents concerning the very high, reversible adsorption of hydrogen in carbon nanotubes or platelet nanofibers have aroused tremendous interest in the research community, stimulating much experimental and theoretical works. Most of the works on hydrogen adsorption on carbon nanotubes have been recently reviewed [3.240–243].

A group from Northeastern University [3.132, 244] was the first to report the supposedly successful hydrogen storage in carbon layered nanostructures possessing some crystallinity. The authors claimed that, in platelet nanofibers (3–50 nm in width), hydrogen can be stored up to 75 wt%, meaning a C/H ratio of 1/9. Complete

hydrogen desorption occurs only at very high temperature. The same authors have recently pointed out the dramatic role of the treatment that has to be applied to the carbon nanofibers prior to H₂ adsorption [3.244]. This thermal treatment, though simple (1,000 °C in an inert gas), is a critical procedure in order to remove chemisorbed gases from the edge and step regions of the carbon structures. Failure to achieve this condition results in a dramatic decrease in the hydrogen adsorption performance of the materials. In this work, the authors have performed the experiments at room temperature, and 100 bar of H₂, hydrogen uptake between 20 and 40 wt% were recorded. The authors have also demonstrated by XRD measurements that structural perturbation of the material was produced following hydrogen treatment, and that it was manifested by an expansion of the graphitic interplane distance (from 0.34 before H₂ adsorption to 0.347 after H₂ uptake).

Hydrogen adsorption and desorption measurements on nanofibers similar to that used by Rodriguez et al. [3.19] were also performed by Ahn et al. [3.245]. The authors have measured a hydrogen uptake of 2.4 wt%. In fact, in their study, none of the graphite nanofiber material tested has indicated hydrogen storage abilities that exceed the values already reported for activated carbons.

Adsorption of H₂ on platelet nanofibers was computed by Monte Carlo simulations [3.246]. The graphene spacing was optimized to maximize the weight fraction of H₂ adsorbed. Given the results of their calculations, the authors concluded that no physically realistic graphite-hydrogen potential can account for the tremendous adsorption ability reported by the group from Penn State.

Rzepka et al. [3.247] have also used theoretical Monte Carlo calculation to calculate the amount of physically adsorbed hydrogen molecules in carbon slit pores of dimensions similar to that used by the Penn State group (i. e., 0.34 nm as the interplanar distance between graphenes in the nanofibers). They reached the conclusion that no hydrogen can be adsorbed at all. Even if the interplanar distance is assumed to expand during the adsorption process, the maximum calculated adsorption is 1 wt% for $d = 0.7$ nm. These authors concluded that the Penn State experimental results could not be attributed to some “abnormal capillary condensation effect” as initially claimed. Since then, nobody has been able to duplicate it experimentally.

Meanwhile, hydrogen storage experiments were also attempted on SWNTs. The first work was reported by Dillon et al. [3.248] who used temperature-programmed

desorption measurements. A major drawback of their experimental procedure was that they used only 1 mg of *unpurified* soot containing 0.1% of SWNTs. They attributed the reversible hydrogen capacity of 0.01 wt% observed to the SWNTs only, therefore leading to a presumable capacity of 5–10 wt% for a pure nanotubes sample. TPD experiments shown H₂ desorption between –170 and +100 °C. Despite the weakness of the demonstration, the paper, which was published not much before that of Chambers et al. [3.132], has induced a worldwide excitement for the field.

Hydrogen adsorption measurements were also performed on SWNT samples of high purity [3.249]. At –193 °C, 160 bar of H₂ were admitted and the hydrogen adsorption was found to exceed 8 wt%. In this case, the authors proposed that hydrogen is first adsorbed on the outer surfaces of the crystalline material. But no data concerning H₂ desorption are given.

In recent reports, Dresselhaus and coworkers [3.240, 250] reported hydrogen storage in SWNTs (1.85 nm of average diameter) at room temperature. A hydrogen storage capacity of 4.2 wt% was achieved reproducibly under 100 bar for a SWNT-containing material of about 0.5 g that was previously soaked in hydrochloric acid and then heat-treated (500 °C) in vacuum. The purity of the sample was estimated from TGA and TEM observations to be about 50 to 60%. Moreover, 78% of the adsorbed hydrogen could be released under ambient pressure at room temperature, while the release of the residual stored hydrogen required some heating at 200 °C.

A valuable input to the topic was brought by Hirscher et al. [3.251], who demonstrated that several of the supposedly successful experiments regarding the storage of H₂ in SWNTs were actually misled by the hydrogen storage capacity of Ti nanoparticles originating from the sonoprobe frequently used at one step or another of the procedure, specifically when the SWNT material is previously purified.

Density functional theory (DFT) was used [3.252] to estimate H₂ adsorption in SWNTs. From their calculations, within the regime of operating conditions where adsorptive storage seems attractive, the storage properties of H₂ in a SWNT system appear to fall far short of the DOE target. In their model, rolling graphite into a cylindrical sheet does not significantly alter the nature of the carbon–H₂ interaction, in contradiction with the latest calculations, which indicate that the possibilities of physisorption increase as the radius of curvature of SWNTs decreases [3.253].

More recently, however, Lee et al. [3.254, 255] have also used DFT calculations to search for hydrogen ad-

sorption sites and predict maximum storage capacity in SWNTs. They have found two chemisorption sites, at the exterior and the interior of the tube wall. Thus they predict a maximum hydrogen storage capacity that can exceed 14 wt% ($160 \text{ kgH}_2/\text{m}^3$). The authors have also considered H_2 adsorption in multiwall carbon nanotubes and have predicted lower storage capacities for the latter.

Calculations are constrained, however, by the starting hypotheses. While considering the same (10,10) SWNT, although calculations based on DFT predict a 14.3% storage [3.254], calculations based on a geometrical model predict 3.3% [3.240], and calculations based on quantum mechanical molecular dynamics model predict 0.47% [3.256].

In conclusion, neither the experimental results, obviously biased by some problem in the procedures, nor theoretical results are yet able to demonstrate that an efficient storage of H_2 is achievable for carbon nanotubes, whatever the type. But the definitive failure statement cannot yet be claimed. Further efforts have to be made to enhance H_2 adsorption of these materials, in particular (i) by adjusting the surface properties that can be modified by chemical or mechanical treatments, and (ii) by adjusting the material structure (pore size and curvature). Whether the best carbon material will then be nanotube-based is another story.

Gas Storage – Gases Other than Hydrogen

Encouraged by the potential applications related to hydrogen adsorption, several research groups have tried to use carbon nanotubes as a stocking and transporting mean for other gases such as: oxygen, nitrogen, noble gases (argon and xenon), and hydrocarbons (methane, ethane, and ethylene). These studies have shown that carbon nanotubes could become the world's smallest gas cylinders combining low weight, easy transportability, and safe use with acceptable adsorbed quantities. Thanks to their nano-sizes, nanotubes might also be used in medicine where physically confining special gases (like ^{133}Xe for instance) prior to injection would be extremely useful.

Kusnetzova et al. [3.257] have conducted experiments with xenon and found that a very significant enhancement (280 times more, up to a molar ratio $N_{\text{Xe}}/N_{\text{C}} = 0.045$) can be achieved by opening the SWNT bundles by thermal activation at 800°C . With this treatment the gas can be adsorbed inside the nanotubes and the rates of adsorption are also increased.

The possibility of storing argon in carbon nanotubes has been studied with encouraging results by Gadd et al. [3.258]: their experiments show that large

amounts of argon can be trapped into catalytically grown MWNTs (20–150 nm) by hot isostatic pressing (HIP-ing) for 48 hours at 650°C under an argon pressure of 1,700 bar. Energy dispersive X-ray spectroscopy was used to determine that the gas was located inside the tubes and not on their walls. Further studies determined the argon pressure inside the tubes at room temperature. The authors estimated this feature to be around 600 bars, indicating that the equilibrium pressure was attained in the tubes during the HIP-ing and that MWNTs would be a convenient material for storing that gas.

Gas Separation

As SWNTs or MWNTs have regular geometries that can, to some extent, be controllable, they could be used to develop precise separation tools. If the sorption mechanisms are known, it should be possible to control sorption of various gases through combinations of temperature, pressure, and nanotube morphology. Since the large-scale production of nanotubes is now constantly progressing and may result in low costs, accurate separation methods based on carbon nanotubes have started to be investigated.

A theoretical study has aimed to determine the effect of different factors such as the diameter of the tubes, the density and the type of the gas used on the flow of molecules inside the nanotubes. An atomistic simulation with methane, ethane, and ethylene [3.259] has shown that the molecule mobility decreases with the decrease of the diameter of the tube for each of the three gases. Ethane and ethylene have a smaller mobility due to the stronger interaction they seem to have with the nanotube walls. In another theoretical study on the possibility of hydrocarbon mixture separation on SWNT bundles, the authors conclude on the possibility of using carbon nanotubes to separate methane/n-butane and methane/isobutene mixtures [3.260], with an efficiency that increases as the average tube diameter decreases. An experimental work was also performed by the same group on the sorption of butane on MWNTs [3.133].

Simulation by grand canonical Monte Carlo for separation of hydrogen and carbon monoxide by adsorption on SWNT has also been reported [3.261]. In most of the situations studied, SWNTs are found to adsorb more CO than H_2 , and an excellent separation effect could probably be obtained, again, by varying the SWNT average diameter.

Adsorbents

Carbon nanotubes were recently found to be able to adsorb some toxic gases such as dioxins [3.262], fluo-

ride [3.263], lead [3.264], or alcohols [3.265] better than the materials used so far, such as activated carbon. These pioneering works opened a new field of applications as cleaning filters for many industrial processes having hazardous by-products. Adsorption of dioxins, which are very common and persistent carcinogenic by-products of many industrial processes, is a good example of the interest of nanotubes in this field. Ecological consciousness has imposed emission limits on dioxin-generating sources in many countries, but finding materials that can act as effective filters, even at extremely low concentrations, is a big issue. Long et al. [3.262] have found that nanotubes can attract and trap more dioxins than activated carbons or other polyaromatic materials that are currently used as filters. This improvement is probably due to the stronger interaction forces that exist between dioxin molecules and the nanotube curved surfaces compared to those for flat graphene sheets.

The adsorption capacity of $\text{Al}_2\text{O}_3/\text{MWNT}$ for fluoride from water has been reported to be 13.5 times that of activated carbon and 4 times that of Al_2O_3 [3.263]. The same group has also reported an adsorption capacity of lead from water by MWNTs higher than that by activated carbon [3.264]. The possibility to using graphite nanofibers to purify water from alcohols has also been explored [3.265]. These experimental results suggest that carbon nanotubes may be promising adsorbents for the removal of polluting agents from water.

Bio-Sensors

Attaching molecules of biological interest to carbon nanotubes is an ideal way to realize nanometer-sized biosensors. Indeed, the electrical conductivity of such functionalized nanotubes would depend on modifications of the interaction of the probe with the studied media, because of chemical changes or as result of their interaction with target species. The science of attaching biomolecules to nanotubes is rather recent and was inspired by similar research in the fullerene area. Some results have already been patented, and what was looking like a dream a couple of years ago may become reality in the near future. The use of the internal cavity of nanotubes for drug delivery would be another amazing application, but little work has been carried out so far to investigate the harmfulness of nanotubes in the human body. MWNTs have been used by Mattson et al. [3.266] as a substrate for neuronal growth. They have compared the activity of untreated MWNTs with that of MWNTs coated with a bioactive molecule (4-hydroxynonenal) and observed that on these latter functionalized nanotubes, neurons elaborated multiple neurites. This is an

important result illustrating the feasibility of using nanotubes as substrate for nerve cell growth.

Davis et al. [3.267] have immobilized different proteins (metallothionein, cytochrome c and c_3 , β -lactamase I) in MWNTs and checked that these molecules were still catalytically active compared to the nonimmobilized ones. They have shown that confining a protein within a nanotube provides some protection toward the external environment. Protein immobilization via non-covalent sidewall functionalization was proposed by Chen et al. [3.268] by using a bifunctional molecule (1-pyrenebutanoic acid, succinimidyl ester). This molecule is maintained to the nanotube wall by the pyrenyl group, and amine groups or biological molecules can react with the ester function to form amid bonds. This method was also used to immobilize ferritin and streptavidin onto SWNTs. It has the main advantage of not modifying the SWNT wall and keeping unperturbed the sp^2 structure, maintaining the physical properties of the nanotubes. Shim et al. [3.269] have functionalized SWNTs with biotin and observed specific binding with streptavidin, illustrating biomolecular recognition possibilities. Dwyer et al. [3.270] have functionalized SWNTs by covalently coupling DNA strands to them using EDC(1-ethyl-3-(3-dimethylaminopropyl) carbodiimide hydrochloride) but did not test biomolecular recognition; other proteins such as bovine serum albumin (BSA) [3.271] have been attached to nanotubes using the same process (diimide-activated amidation with EDC) and most of the attached proteins remained bioactive. Instead of working with individual nanotubes (or more likely nanotube bundles in the case of SWNTs), Nguyen et al. [3.272] have functionalized nanotubes arrayed with a nucleic acid, still using EDC as the coupling agent, in order to facilitate the realization of biosensors based on protein-functionalized nanotubes. Recently Azamian et al. [3.273] have immobilized a series of biomolecules (cytochrome c, ferritin, and glucose oxydase) on SWNTs and observed that the use of EDC was not always necessary, indicating that the binding was predominantly noncovalent. In the case of glucose oxydase, they have tested the catalytic activity of functionalized nanotubes immobilized on a glassy carbon electrode and observed a tenfold greater catalytic response compared to that in the absence of modified SWNTs.

Functionalization of nanotubes with biomolecules is still in its infancy, and their use as biosensors may lead to practical applications earlier than expected. For example, functionalized nanotubes can be used as AFM tips (see Sect. 3.6.1) allowing to perform “chemical

force microscopy” (CFM), allowing single-molecule measurements. Even in the case of nonfunctionalized CNT-based tips, important improvements have been obtained for the characterization of biomolecules (see the review by [3.215]).

Composites

Because of their exceptional morphological, electrical, thermal, and mechanical characteristics, carbon nanotubes are particularly promising materials as reinforcement in composite materials with metal, ceramic, or polymer matrix. Key basic issues include the good dispersion of the nanotubes, the control of the nanotube/matrix bonding, the densification of bulk composites and thin films, and the possibility of aligning the nanotubes. In addition, the nanotube type (SWNT, c-MWNT, h-MWNT, etc.) and origin (arc, laser, CCVD, etc.) is also an important variable since determining the structural perfection, surface reactivity, and aspect ratio of the reinforcement.

Considering the major breakthrough that carbon nanotubes are expected to make in the field, the following will give an overview of the current work on metal-, ceramic- and polymer-matrix composites reinforced with nanotubes. We will not consider nanotubes merely coated with another material will not be considered here. We discussed filled nanotubes in Sect. 3.5.2. Applications involving the incorporation of nanotubes to materials for purposes other than structural will be mentioned in Sect. 3.6.2.

Metal Matrix Composites

Nanotube-metal matrix composites are still rarely studied. The materials are generally prepared by standard powder metallurgy techniques, but the dispersion of the nanotubes is not optimal. Thermal stability and electrical and mechanical properties of the composites are investigated. The room temperature electrical resistivity of hot-pressed CCVD MWNTs-Al composites increases slightly by increasing the MWNT volume fraction [3.274]. The tensile strength and elongation of nonpurified arc-discharge MWNT-Al composites are only slightly affected by annealing at 873 K in contrast to that of pure Al [3.275]. The Young’s modulus of nonpurified arc-discharge MWNTs-Ti composites is about 1.7 times that of pure Ti [3.276]. The formation of TiC, probably resulting from the reaction between amorphous carbon and the matrix, was observed, but the MWNTs themselves were not damaged. An increase of the Vickers hardness by a factor 5.5 over that of pure Ti was associated with the suppression of coarsening

of the Ti grains, the TiC formation, and the addition of MWNTs with an extremely high Young’s modulus. CCVD MWNTs-Cu composites [3.277] also show a higher hardness and a lower friction coefficient and wear loss. A deformation of 50–60 % of the composites was observed. A MWNTs-metallic glass Fe82P18 composite [3.278] with a good dispersion of the MWNTs was prepared by the rapid solidification technique.

Ceramic Matrix Composites

Carbon nanotube-containing ceramic-matrix composites are a bit more frequently studied, most efforts made to obtain tougher ceramics [3.279]. Composites can be processed following the regular processing route, in which the nanotubes are usually mechanically mixed with the matrix (or a matrix precursor) then densified using hot-pressing sintering of the slurry or powders. Zhan et al. [3.280] ball-milled SWNT bundles (from the HiPCo technique) and nanometric alumina powders, producing a fairly homogeneous dispersion, supposedly without damaging the SWNTs. On the other hand, interesting results were obtained using the spark plasma sintering (SPS) technique, which was able to prepare fully dense composites without damage to the SWNTs [3.281]. Other original composite processing include sol-gel route, by which bulk and thin film composites were prepared [3.282], and in situ SWNT growth in ceramic foams, using procedures closely related to that described in Sect. 3.2.2 [3.283].

Ma et al. [3.284] prepared MWNT-SiC composites by hot-pressing mixtures of CCVD MWNTs and nano-SiC powders. They claimed that the presence of the MWNTs provides an increase of about 10% of both the bending strength and fracture toughness, but the dispersion of the MWNTs looks poor. Several detailed studies [3.82, 285–288] have dealt with the preparation of nanotube-Fe-Al₂O₃, nanotube-Co-MgO, and nanotube-Fe/Co-MgAl₂O₄ composites by hot-pressing of the corresponding composite powders. The nanotubes were grown in situ in the starting powders by a CCVD method [3.73, 80, 289–293] and thus are very homogeneously dispersed between the metal-oxide grains, in a way that could be impossible to achieve by mechanical mixing. The nanotubes (mostly SWNTs and DWNTs) gather in long, branched bundles smaller than 50 nm in diameter, which appear to be very flexible. Depending on the matrix and hot-pressing temperature, a fraction of the nanotubes seems to be destroyed during hot-pressing in a primary vacuum. The increase of the quantity of nanotubes (ca. 2–12 wt%) leads to a refinement of the microstructure but also to a strong decrease in rela-

tive density (70–93%). Probably because of this, the fracture strength and the toughness of the nanotube-containing composites are generally lower than those of the nanotube-free metal-oxide composites and only marginally higher than those of the corresponding ceramics. SEM observations revealed both the trapping of some of the nanotubes within the matrix grains or at grain boundaries and a relatively good wetting in the case of alumina. Most nanotubes are cut near the fracture surface after some pull-out and could contribute to a mechanical reinforcement.

Siegel et al. [3.294] claimed that the fracture toughness of 10 vol.% MWNTs-alumina hot-pressed composites is increased by 24% (to $4.2 \text{ MPa m}^{1/2}$) over that of pure alumina. But the density and grain size are not reported, so it is difficult to consider this result as an evidence for the beneficial role of the MWNTs themselves. A confirmation could be found in the work by Sun et al. [3.281] who developed a colloidal route to coat the nanotubes with alumina particles prior to another mixing step with alumina particles then densification by SPS. A very large gain in fracture toughness (calculated from Vickers indentation) is reported (from $3.7 \text{ MPa m}^{1/2}$ for pure Al_2O_3 to $4.9 \text{ MPa m}^{1/2}$ for an addition of 0.1 wt% of SWNT nanotubes, and to $9.7 \text{ MPa m}^{1/2}$ for an addition of 10 wt%). But it is possible that the beneficial input of the nanotubes is due to the previous coating of the nanotubes before sintering, resulting in an improved bonding with the matrix.

Bulk properties other than mechanical are also worth being investigated. Interestingly, the presence of well dispersed nanotubes confers an electrical conductivity to the otherwise insulating ceramic-matrix composites. The percolation threshold is very low – in the range 0.2–0.6 wt% of carbon – due to the very high aspect ratio of nanotubes. Varying the nanotube quantity in the starting powders allows the electrical conductivity to be controlled in the range $0.01\text{--}10 \text{ S cm}^{-1}$. Moreover, the extrusion at high temperatures in vacuum allows the nanotubes to be aligned in the matrix, thus inducing an anisotropy in the electrical conductivity [3.295]. One of the early works involved MWNTs in a superconducting $\text{Bi}_2\text{Sr}_2\text{CaCu}_2\text{O}_{8+\delta}$ matrix [3.296]. The application of SWNTs for thermal management in partially stabilized zirconia [3.297] and of MWNTs-lanthanum cobaltate composites for application as an oxygen electrode in zinc/air [3.298] were reported more recently. The friction coefficient was also shown to increase and the wear loss to decrease upon the increase in nanotube volume fraction in carbon/carbon composites [3.299].

The latter is one of the few examples in which carbon has been considered as a matrix. Another one is the work reported by Andrews et al. [3.300], who introduced 5 wt% of SWNTs into a pitch material before spinning the whole as a SWNT-reinforced pitch-fiber. Subsequent carbonization transformed it into a SWNT-reinforced carbon fiber. Due to the contribution of the SWNTs, which were aligned by the spinning stresses, the resulting gain in tensile strength, modulus, and electrical conductivity with respect to the nonreinforced carbon fiber was claimed to be 90, 150, and 340%, respectively.

Polymer Matrix Composites

Nanotube-polymer composites, first reported by Ajayan et al. [3.301] are now intensively studied, notably epoxy- and polymethylmethacrylate (PMMA)-matrix composites. Regarding the mechanical characteristics, the three key issues affecting the performance of a fiber-polymer composite are the strength and toughness of the fibrous reinforcement, its orientation, and a good interfacial bonding crucial for the load transfer to occur [3.302]. The ability of the polymer to form large-diameter helices around individual nanotubes favors the formation of a strong bond with the matrix [3.302]. Isolated SWNTs may be more desirable than MWNTs or bundles for dispersion in a matrix because of the weak frictional interactions between layers of MWNTs and between SWNTs in bundles [3.302]. The main mechanisms of load transfer are micromechanical interlocking, chemical bonding, and van der Waals bonding between the nanotubes and the matrix. A high interfacial shear stress between the fiber and the matrix will transfer the applied load to the fiber over a short distance [3.303]. SWNTs longer than 10–100 μm would be needed for significant load-bearing ability in the case of non-bonded SWNT-matrix interactions, whereas the critical length for SWNTs cross-linked to the matrix is only 1 μm [3.304]. Defects are likely to limit the working length of SWNTs [3.305], however.

The load transfer to MWNTs dispersed in an epoxy resin was much higher in compression than in tension [3.303]. It was proposed that all the walls of the MWNTs are stressed in compression, whereas only the outer walls are stressed in tension because all the inner tubes are sliding within the outer. Mechanical tests performed on 5 wt% SWNT-epoxy composites [3.306] showed that SWNTs bundles were pulled out of the matrix during the deformation of the material. The influence of the nanotube/matrix interfacial interaction was evidenced by Gong et al. [3.307]. It was also reported that coating regular carbon fiber with MWNTs prior to their

dispersion into an epoxy matrix improves the interfacial load transfer, possibly by local stiffening of the matrix near interface [3.308].

As for ceramic matrix composites, the electrical characteristics of SWNT- and MWNT-epoxy composites are described with the percolation theory. Very low percolation threshold (below 1 wt%) is often reported [3.309–311]. Industrial epoxy loaded with 1 wt% unpurified CCVD-prepared SWNTs showed an increase in thermal conductivity of 70% and 125% at 40 K and at room temperature, respectively [3.309]. Also, the Vickers hardness rose with the SWNT loading up to a factor of 3.5 at 2 wt%. Thus both the thermal and mechanical properties of such composites are improved without the need to chemically functionalize the SWNTs.

Likewise, the conductivity of laser-prepared SWNT-PMMA composites increases with the load in SWNTs (1–8 wt% SWNTs) [3.302]. Thermogravimetric analysis shows that, compared to pure PMMA, the thermal degradation of PMMA films occurs at a slightly higher temperature when 26 wt% MWNTs are added [3.312]. Improving the wetting between the MWNTs and the PMMA by coating the MWNTs with poly(vinylidene fluoride) prior to melt-blending with PMMA resulted in an increased storage modulus [3.313]. The impact strength in aligned SWNT-PMMA composites was significantly increased with only 0.1 wt% of SWNTs, possibly because of a weak interfacial adhesion, and/or of the high flexibility of the SWNTs, and/or the pullout and sliding effects of individual SWNTs within bundles [3.314]. The transport properties of arc-discharge SWNTs-PMMA composite films (10 μm thick) were studied in great detail [3.315, 316]. The electrical conductivity increases by nine orders of magnitude from 0.1 to 8 wt% SWNTs. The room temperature conductivity is again well described with the standard percolation theory, confirming the good dispersion of the SWNTs in the matrix.

Polymer composites with other matrices include CCVD-prepared MWNT-polyvinyl alcohol [3.317], arc-prepared MWNT-polyhydroxyaminoether [3.318], arc-prepared MWNT-polyurethane acrylate [3.319, 320], SWNT-polyurethane acrylate [3.321], SWNT-polycarbonate [3.322], MWNT-polyaniline [3.323], MWNT-polystyrene [3.324], SWNT-polyethylene [3.325], CCVD-prepared MWNT-polyacrylonitrile [3.326], MWNT-oxotitanium phthalocyanine [3.327], arc-prepared MWNT-poly(3-octylthiophene) [3.328], SWNT-poly(3-octylthiophene) [3.329], and CCVD MWNTs-poly(3-hexylthiophene) [3.330]. These works deal mainly with films 100–200 micrometer thick and

aim to study the glass transition of the polymer, mechanical, and electrical characteristics as well as photoconductivity.

A great deal of work is also devoted to nanotube-polymer composites for applications as materials for molecular optoelectronics, using primarily poly(m-phenylenevinylene-co-2,5-dioctoxy-p-phenylenevinylene) (PmPV) as the matrix. This conjugated polymer tends to coil, forming a helical structure. The electrical conductivity of the composite films (4–36 wt% MWNTs) is increased by eight orders of magnitude compared to that of PmPV [3.331]. Using the MWNT-PmPV composites as the electron-transport-layer in light-emitting diodes results in a significant increase in brightness [3.332]. The SWNTs act as a hole-trapping material blocking the holes in the composites, this being probably induced through long-range interactions within the matrix [3.333]. Similar investigations were carried out on arc-discharge SWNTs-polyethylene dioxythiophene (PEDOT) composite layers [3.334] and MWNTs-polyphenylenevinylene composites [3.335].

To conclude, two critical issues have to be considered for the application of nanotubes as reinforcement for advanced composites. One is to choose between SWNTs and MWNTs. The former seem more beneficial for the purpose of mechanical strengthening, provided they are isolated or arranged into cohesive yarns so that the load is able to be conveniently transferred from a SWNT to another. Unfortunately, despite recent advances [3.336–339], this is still a technical challenge. The other issue is to tailor the nanotube/matrix interface with respect to the matrix. This is a current topic for many laboratories involved in the field.

Multifunctional Materials

One of the major benefits expected from incorporating carbon nanotubes in other solid or liquid materials is bringing some electrical conductivity to them while not affecting the other properties or behaviors of these materials. As already mentioned in the previous section, the percolation threshold is reached at very low load with nanotubes. Tailoring the electrical conductivity of a bulk material is then achievable by adjusting the nanotube volume fraction in the formerly insulating material while not making this fraction too large anyway. As demonstrated by Maruyama [3.3], there are three regimes of interest regarding the electrical conductivity: (i) electrostatic discharge, e.g., to prevent fire or explosion hazard in combustible environments or perturbations in electronics, which requires electrical resistivity less than $10^{12} \Omega \text{ cm}$; (ii) electrostatic painting, which requires

the material to be painted to be electrical conductive enough (electrical resistivity below $10^6 \Omega \text{ cm}$) to prevent the charged paint droplets to be repelled; (iii) electromagnetic interference shielding, which is achieved for electrical resistivity lower than $10 \Omega \text{ cm}$.

Materials are often asked to be multifunctional, e.g. having both high electrical conductivity and high toughness, or high thermal conductivity and high thermal stability, etc. The association of several materials, each of them bringing one of the desired features, therefore generally meets this need. Exceptional features and properties of carbon nanotubes make them likely to be a perfect multifunctional material in many cases. For instance, materials for satellites are often required to be electrical conductive, mechanically self-supporting, able to transport the excess heat away, sometimes be pro-

tected against electromagnetic interferences, etc., while exhibiting minimal weight and volume. All these properties should be possible with a single nanotube-containing composite material instead of complex multi-materials combining layers of polymers, aluminum, copper, etc. Table 3.5 provides an overview of various fields in which nanotube-based multifunctional materials should find an application.

Nano-Electronics

As reported in Sects. 3.1.1 and 3.4.4, SWNT nanotubes can be either metallic (with an electrical conductivity higher than that of copper), or semiconductor. This has inspired the design of several components for nano-electronics. First, metallic SWNTs can be used as mere ballistic conductors. Moreover, as early as 1995,

Table 3.5 Applications for nanotube-based multifunctional materials (from [3.3]), by courtesy of B. Maruyama (WPAFB, Dayton, Ohio)

Fiber fraction	Applications system	Mechanical			Electrical			Thermal		Thermo-mechanical	
		Strength/stiffness	Specific strength	through-thickness strength	Static dissipation	Surface Conduction ^a	EMI shielding	Service ^b temp.	conduction/dissipation ^c	Dimensional Stability ^d	CTE reduction ^e
Low Volume fraction (fillers)											
Elastomers	Tires	×			×				×		
Thermo Plastics	Chip package Electronics/Housing	×			×			×	×		
Thermosets	Epoxy products Composites	×	×	×		×				×	×
High Volume Fraction											
Structural composites	Space/aircraft components		×	×							
High conduction composites	Radiators Heat exchangers EMI shield	×							×	×	×

^a For electrostatic painting, to mitigate lightning strikes on aircraft, etc.
^b To increase service temperature rating of product
^c To reduce operating temperatures of electronic packages
^d Reduces warping
^e Reduces microcracking damage in composites

realizing a rectifying diode by joining one metallic SWNT to one semiconductor SWNT (hetero-junction) was proposed by *Lambin* et al. [3.340], then later by *Chico* et al. [3.341] and *Yao* et al. [3.342]. Also, field-effect transistors (FET) can be built by the attachment of a semiconductor SWNT across two electrodes (source and drain) deposited on an insulating substrate that serves as a gate electrode [3.343, 344]. Recently the association of two such SWNT-based FETs has made a voltage inverter [3.345].

All the latter developments are fascinating and provide promising perspectives for nanotube-based electronics. But progress is obviously needed before making SWNT-based integrated circuits on a routine basis. A key point is the need to be able to prepare selectively either metallic or semiconductor nanotubes. Although a way has been proposed to destroy selectively metallic SWNTs from bundles of undifferentiated SWNTs [3.347], the method is not scalable and selective synthesis would be preferable. Also, defect-free nanotubes are required. Generally speaking, it relates to another major challenge, which is to be able to fabricate at industrial scale integrated circuits including nanometer-size components that only sophisticated imaging methods (AFM) are able to visualize.

Nano-Tools, Nano-Devices, Nano-Systems

Due to the ability of graphene to expand slightly when electrically charged, nanotubes have been found to act conveniently as actuators. *Kim* et al. [3.346] demonstrated it by designing “nano”-tweezers able to grab, manipulate, release nano-objects (the “nano”-bead having been handled for the demonstration was actually

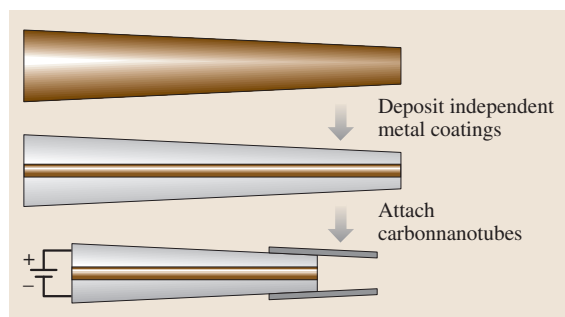


Fig. 3.31 Sketch explaining how the first nano-tweezers were designed. First is a glass micropipette (dark cone, top). Then two Au coatings (in grey, middle) are deposited so that they are not in contact. Then a voltage is applied to the electrodes (from [3.346])

closer to micrometer than nanometer), and measure their electrical properties. This was made possible quite simply by depositing two non-interconnected gold coatings onto a pulled glass micropipette (Fig. 3.31), then attaching two MWNTs (or two SWNT-bundles) $\sim 20\text{--}50$ nm in diameter to each of the gold electrodes. Applying a voltage (0–8.5 V) between the two electrodes then makes the tube tips to open and close reversibly in a controlled manner.

A similar experiment, again rather simple, was proposed by *Baughman* et al. the same year (1999) [3.348], consisting in mounting two SWNT-based paper strips (“bucky-paper”) on both sides of an insulating double-side tape. The two bucky-paper strips were previously loaded with Na^+ and Cl^- , respectively. When 1 V was applied between the two paper strips, both expand, but the strip loaded with Na^+ expands a bit more, forcing the whole system to bend. Though performed in a liquid environment, such a behavior has inspired the authors to predict a future for their system as “artificial muscles.”

Another example of amazing nano-tools is the nano-thermometer proposed by *Gao* et al. [3.349]. A single MWNT was used, in that case, partially filled with liquid gallium. Upon the effect of temperature variations in the range 50–500 °C, the gallium goes up and down reversibly within the nanotube cavity at reproducible level with respect to the values of the temperature applied.

Of course, nano-tools such as nano-tweezers or nano-thermometers will hardly reach a commercial development so to justify industrial investments. But such experiments are more than amazing laboratory curiosities. They definitely demonstrate the ability of carbon nanotubes as parts for future nano-devices, including nanomechanics-based systems.

Supercapacitors

Supercapacitors include two electrodes immersed in an electrolyte (e.g., 6 M KOH), separated by an insulating ion-permeable membrane. Charging the capacitors is achieved by applying a potential between the two electrodes, making the cations and the anions moving toward the electrode oppositely charged. Suitable electrodes should exhibit a high electrical conductivity and a high surface area since the capacitance is proportional to it. Actually, the surface area should originate mainly from the appropriate combination of mesopores (to allow the electrolyte components to circulate well, which is related to the charging speed) and micropores (whose walls are the surface of attraction and fixation sites for the ions). Based on early works by

Niu et al. [3.350], such a combination was found to be reached with the specific architecture offered by packed and entangled h-MWNTs with a poor nanotexture (see Sect. 3.1.2). But, activation pre-treatments are necessary. For instance, a capacitor made from nanotubes with surface area = 220 m²/g exhibited a capacitance of 20 F/g, which increased up to 100 F/g after an activation treatment was applied to the nanotubes so that their surface area reaches 880 m²/g [3.126]. Alternatively, again due to their specific architecture induced by their huge aspect ratio, nanotubes can also be used as supports for conductive polymer coatings, e.g., polypyrrole or polyaniline [3.351], which otherwise would make

a too dense phase (i. e. not allowing an easy circulation and penetration of ions). Supercapacitors built from such composites can overcome more than 2,000 charging cycles, with current density as high as 350 mA/g [3.352]. Capacitors including nanotubes already have capacitance as high as 180–200 F/g, i. e. equivalent to that obtained with electrodes built from regular carbon materials, with the advantage of faster charging [3.126]. Current works will certainly lead to further optimization of both the nanotube material architecture and the nanotube-supported conductive polymers, giving reasonable perspectives for the commercial use of nanotubes as components for supercapacitors.

References

- 3.1 M. Hillert, N. Lange: The structure of graphite filaments, *Zeitschr. Kristall.* **111** (1958) 24–34
- 3.2 T. V. Hughes, C. R. Chambers: US Patent 405,480 (1889)
- 3.3 B. Maruyama, K. Alam: Carbon nanotubes and nanofibers in composite materials, *SAMPE J.* **38** (2002) 59–70
- 3.4 P. Schützenberger, L. Schützenberger: Sur quelques faits relatifs à l'histoire du carbone, *C. R. Acad. Sci. Paris* **111** (1890) 774–778
- 3.5 C. Pélabon, H. Pélabon: Sur une variété de carbone filamenteux, *C. R. Acad. Sci. (Paris)* **137** (1903) 706–708
- 3.6 R. T. K. Baker, P. S. Harris: The formation of filamentous carbon. In: *Chemistry and Physics of Carbon*, Vol. 14, ed. by P. L. Walker Jr., P. A. Thrower (Dekker, New York 1978) pp. 83–165
- 3.7 S. Iijima: Helical microtubules of graphite carbon, *Nature* **354** (1991) 56–58
- 3.8 S. Iijima, T. Ichihashi: Single-shell carbon nanotubes of 1-nm diameter, *Nature* **363** (1993) 603–605
- 3.9 D. S. Bethune, C. H. Kiang, M. S. de Vries, G. Gorman, R. Savoy, J. Vazquez, R. Bayers: Cobalt-catalysed growth of carbon nanotubes with single-atomic-layer walls, *Nature* **363** (1993) 605–607
- 3.10 J. Tersoff, R. S. Ruoff: Structural properties of a carbon–nanotube crystal, *Phys. Rev. Lett.* **73** (1994) 676–679
- 3.11 N. Wang, Z. K. Tang, G. D. Li, J. S. Chen: Single-walled 4 Å carbon nanotube arrays, *Nature* **408** (2000) 50–51
- 3.12 N. Hamada, S. I. Sawada, A. Oshiyama: New one-dimensional conductors, graphitemicrotubules, *Phys. Rev. Lett.* **68** (1992) 1579–1581
- 3.13 M. S. Dresselhaus, G. Dresselhaus, P. C. Eklund: *Science of Fullerenes and Carbon Nanotubes* (Academic, San Diego 1995)
- 3.14 M. Monthieux, B. W. Smith, B. Burteaux, A. Claye, J. Fisher, D. E. Luzzi: Sensitivity of single-wall nanotubes to chemical processing: An electron microscopy investigation, *Carbon* **39** (2001) 1261–1272
- 3.15 H. Allouche, M. Monthieux: Chemical vapor deposition of pyrolytic carbon onto carbon nanotubes II – Structure and texture, *Carbon* (2003) accepted
- 3.16 M. Audier, A. Oberlin, M. Oberlin, M. Coulon, L. Bonnetain: Morphology and crystalline order in catalytic carbons, *Carbon* **19** (1981) 217–224
- 3.17 Y. Saito: Nanoparticles and filled nanocapsules, *Carbon* **33** (1995) 979–988
- 3.18 P. J. F. Harris: *Carbon Nanotubes and Related Structures* (Cambridge Univ. Press, Cambridge 1999)
- 3.19 N. M. Rodriguez, A. Chambers, R. T. Baker: Catalytic engineering of carbon nanostructures, *Langmuir* **11** (1995) 3862–3866
- 3.20 H. W. Kroto, J. R. Heath, S. C. O'Brien, R. F. Curl, R. E. Smalley: C₆₀ Buckminsterfullerene, *Nature* **318** (1985) 162–163
- 3.21 W. Krätschmer, L. D. Lamb, K. Fostiropoulos, D. R. Huffman: Solid C₆₀: A new form of carbon, *Nature* **347** (1990) 354–358
- 3.22 T. Guo, P. Nikolaev, A. G. Rinzler, D. Tomaneck, D. T. Colbert, R. E. Smalley: Self-assembly of tubular fullerenes, *J. Phys. Chem.* **99** (1995) 10694–10697
- 3.23 T. Guo, P. Nikolaev, A. Thess, D. T. Colbert, R. E. Smalley: Catalytic growth of single-walled nanotubes by laser vaporisation, *Chem. Phys. Lett.* **243** (1995) 49–54
- 3.24 A. G. Rinzler, J. Liu, H. Dai, P. Nikolaev, C. B. Huffman, F. J. Rodriguez-Macias, P. J. Boul, A. H. Lu, D. Heymann, D. T. Colbert, R. S. Lee, J. E. Fischer, A. M. Rao, P. C. Eklund, R. E. Smalley: Large scale purification of single wall carbon nanotubes: Process, product and characterization, *Appl. Phys. A* **67** (1998) 29–37
- 3.25 A. Thess, R. Lee, P. Nikolaev, H. Dai, P. Petit, J. Robert, C. Xu, Y. H. Lee, S. G. Kim, D. T. Colbert, G. Scuseria, D. Tomaneck, J. E. Fischer, R. E. Smal-

- ley: Crystalline ropes of metallic carbon nanotubes, *Science* **273** (1996) 487–493
- 3.26 L. M. de la Chapelle, J. Gavillet, J. L. Cochon, M. Ory, S. Lefrant, A. Loiseau, D. Pigache: A continuous wave CO₂ laser reactor for nanotube synthesis, *Proc. Electronic Properties Novel Materials–XVI Int. Winterschool – AIP Conf. Proc.*, Melville 1999, ed. by H. Kuzmany, J. Fink, M. Mehring, S. Roth (Springer, Berlin, Heidelberg 1999) **486** 237–240
- 3.27 M. Yudasaka, T. Komatsu, T. Ichihashi, S. Iijima: Single wall carbon nanotube formation by laser ablation using double targets of carbon and metal, *Chem. Phys. Lett.* **278** (1997) 102–106
- 3.28 M. Castignolles, A. Foutel-Richard, A. Mavel, J. L. Cochon, D. Pigache, A. Loiseau, P. Bernier: Combined experimental and numerical study of the parameters controlling the C-SWNT synthesis via laser vaporization, *Proc. Electronic Properties of Novel Materials–XVI Int. Winterschool – AIP Conf. Proc.*, Melville 2002, ed. by H. Kuzmany, J. Fink, M. Mehring, S. Roth (Springer, Berlin, Heidelberg 2002) **633** 385–389
- 3.29 T. W. Ebbesen, P. M. Ajayan: Large-scale synthesis of carbon nanotubes, *Nature* **358** (1992) 220–221
- 3.30 D. Ugarte: Morphology and structure of graphitic soot particles generated in arc-discharge C₆₀ production, *Chem. Phys. Lett.* **198** (1992) 596–602
- 3.31 T. W. Ebbesen: Carbon nanotubes, *Ann. Rev. Mater. Sci.* **24** (1994) 235–264
- 3.32 T. Beltz, J. Find, D. Herein, N. Pfänder, T. Rühle, H. Werner, M. Wohlers, R. Schlögl: On the production of different carbon forms by electric arc graphite evaporation, *Ber. Bunsenges. Phys. Chem.* **101** (1997) 712–725
- 3.33 C. Journet, W. K. Maser, P. Bernier, A. Loiseau, L. M. de la Chapelle, S. Lefrant, P. Deniard, R. Lee, J. E. Fischer: Large-scale production of single-walled carbon nanotubes by the electric-arc technique, *Nature* **388** (1997) 756–758
- 3.34 K. Saïdane, M. Razafinimanana, H. Lange, M. Baltas, A. Gleizes, J. J. Gonzalez: Influence of the carbon arc current intensity on fullerene synthesis, *Proc. 24th Int. Conf. on Phenomena in Ionized Gases, Warsaw 1999*, ed. by P. Pisarczyk, T. Pisarczyk, J. Wotowski, 203–204
- 3.35 H. Allouche, M. Monthieux, M. Pacheco, M. Razafinimanana, H. Lange, A. Huczko, T. P. Teulet, A. Gleizes, T. Sogabe: Physical characteristics of the graphite-electrode electric-arc as parameters for the formation of single-wall carbon nanotubes, *Proc. Eurocarbon (Deutsche Keram. Ges., Berlin 2000)* 1053–1054
- 3.36 M. Razafinimanana, M. Pacheco, M. Monthieux, H. Allouche, H. Lange, A. Huczko, A. Gleizes: Spectroscopic study of an electric arc with Gd and Fe doped anodes for the carbon nanotube formation, *Proc. 25th Int. Conf. on Phenomena in Ionized Gases, Nagoya 2001*, ed. by E. Goto (Nagoya Univ., Nagoya 2001) *Extend. Abstr.* **3** 297–298
- 3.37 M. Razafinimanana, M. Pacheco, M. Monthieux, H. Allouche, H. Lange, A. Huczko, P. Teulet, A. Gleizes, C. Goze, P. Bernier, T. Sogabe: Influence of doped graphite electrode in electric arc for the formation of single wall carbon nanotubes, *Proc. 6th Eur. Conf. on Thermal Plasma Processes – Progress in Plasma Processing of Materials, New York 2000*, ed. by P. Fauchais (Begell House, New York 2001) 649–654
- 3.38 M. Pacheco, H. Allouche, M. Monthieux, A. Razafinimanana, A. Gleizes: Correlation between the plasma characteristics and the morphology and structure of the carbon phases synthesised by electric arc discharge, *Proc. 25th Biennial Conf. on Carbon, Lexington 2001 (Univ. of Kentucky, Lexington 2001)* *Extend. Abstr.(CD-Rom)*, Novel/14.1
- 3.39 M. Pacheco, M. Monthieux, M. Razafinimanana, L. Donadieu, H. Allouche, N. Caprais, A. Gleizes: New factors controlling the formation of single-wall carbon nanotubes by arc plasma, *Proc. Carbon 2002 Int. Conf., Beijing 2002 (Tsinghua Univ., Beijing 2002)* (CD-Rom/Oral/1014)
- 3.40 M. Monthieux, M. Pacheco, H. Allouche, M. Razafinimanana, N. Caprais, L. Donadieu, A. Gleizes: New data about the formation of SWNTs by the electric arc method, *Electronic Properties of Molecular Nanostructures, AIP Conf. Proc.*, Melville 2002, ed. by H. Kuzmany, J. Fink, M. Mehring, S. Roth (Springer, Berlin, Heidelberg 2002) 182–185
- 3.41 H. Lange, A. Huczko, M. Sioda, M. Pacheco, M. Razafinimanana, A. Gleizes: Influence of gadolinium on carbon arc plasma and formation of fullerenes and nanotubes, *Plasma Chem. Plasma Process* **22** (2002) 523–536
- 3.42 C. Journet: La production de nanotubes de carbone. Ph.D. Thesis (University of Montpellier II, Montpellier 1998)
- 3.43 T. Sogabe, T. Masuda, K. Kuroda, Y. Hirohaya, T. Hino, T. Ymashina: Preparation of B₄C-mixed graphite by pressureless sintering and its air oxidation behavior, *Carbon* **33** (1995) 1783–1788
- 3.44 M. Ishigami, J. Cumings, A. Zettl, S. Chen: A simple method for the continuous production of carbon nanotubes, *Chem. Phys. Lett.* **319** (2000) 457–459
- 3.45 Y. L. Hsin, K. C. Hwang, F. R. Chen, J. J. Kai: Production and in-situ metal filling of carbon nanotube in water, *Adv. Mater.* **13** (2001) 830–833
- 3.46 H. W. Zhu, X. S. Li, B. Jiang, C. L. Xu, C. L. Zhu, Y. F. Zhu, D. H. Wu, X. H. Chen: Formation of carbon nanotubes in water by the electric arc technique, *Chem. Phys. Lett.* **366** (2002) 664–669
- 3.47 W. K. Maser, P. Bernier, J. M. Lambert, O. Stephan, P. M. Ajayan, C. Colliex, V. Brotons, J. M. Planeix, B. Coq, P. Molinier, S. Lefrant: Elaboration and characterization of various carbon nanostructures, *Synth. Met.* **81** (1996) 243–250

- 3.48 J. Gavillet, A. Loiseau, J. Thibault, A. Maigné, O. Stéphan, P. Bernier: TEM study of the influence of the catalyst composition on the formation and growth of SWNT, Proc. Electronic Properties Novel Materials-XVI Int. Winterschool – AIP Conf. Proc., Melville 2002, ed. by H. Kuzmany, J. Fink, M. Mehring, S. Roth (Springer, Berlin, Heidelberg 2002) **633** 202–206
- 3.49 L. P. F. Chibante, A. Thess, J. M. Alford, M. D. Diener, R. E. Smalley: Solar generation of the fullerenes, *J. Phys. Chem.* **97** (1993) 8696–8700
- 3.50 C. L. Fields, J. R. Pitts, M. J. Hale, C. Bingham, A. Lewandowski, D. E. King: Formation of fullerenes in highly concentrated solar flux, *J. Phys. Chem.* **97** (1993) 8701–8702
- 3.51 P. Bernier, D. Laplaze, J. Auriol, L. Barbedette, G. Flamant, M. Lebrun, A. Brunelle, S. Della-Negra: Production of fullerenes from solar energy, *Synth. Met.* **70** (1995) 1455–1456
- 3.52 M. J. Heben, T. A. Bekkedhal, D. L. Schultz, K. M. Jones, A. C. Dillon, C. J. Curtis, C. Bingham, J. R. Pitts, A. Lewandowski, C. L. Fields: Production of single wall carbon nanotubes using concentrated sunlight, Proc. Symp. Recent Adv. Chem. Phys. Fullerenes Rel. Mater., Pennington 1996, ed. by K. M. Kadish, R. S. Ruoff (Electrochemical Society, Pennington 1996) INC **3** 803–811
- 3.53 D. Laplaze, P. Bernier, C. Journet, G. Vié, G. Flamant, E. Philippot, M. Lebrun: Evaporation of graphite using a solar furnace, Proc. 8th Int. Symp. Solar Concentrating Technol., Köln 1996, ed. by M. Becker, M. Balmer (C. F. Müller Verlag, Heidelberg 1997)
- 3.54 D. Laplaze, P. Bernier, W. K. Maser, G. Flamant, T. Guillard, A. Loiseau: Carbon nanotubes: The solar approach, *Carbon* **36** (1998) 685–688
- 3.55 T. Guillard, S. Cetout, L. Alvarez, J. L. Sauvajol, E. Anglaret, P. Bernier, G. Flamant, D. Laplaze: Production of carbon nanotubes by the solar route, *Eur. Phys. J.* **5** (1999) 251–256
- 3.56 G. Flamant, D. Luxembourg, C. Mas, D. Laplaze: Carbon nanotubes from solar energy; a chemical engineering approach of the scale up, Proc. Am. Inst. Chem. Eng. Ann. Meeting, Indianapolis 2002, in print
- 3.57 G. G. Tibbets, M. Endo, C. P. Beetz: Carbon fibers grown from the vapor phase: A novel material, *SAMPE J.* **22** (1989) 30
- 3.58 R. T. K. Baker: Catalytic growth of carbon filaments, *Carbon* **27** (1989) 315–323
- 3.59 R. T. K. Baker, P. S. Harris, R. B. Thomas, R. J. Waite: Formation of filamentous carbon from iron, cobalt, and chromium catalyzed decomposition of acetylene, *J. Catal.* **30** (1973) 86–95
- 3.60 T. Koyama, M. Endo, Y. Oyuma: Carbon fibers obtained by thermal decomposition of vaporized hydrocarbon, *Jap. J. Appl. Phys.* **11** (1972) 445–449
- 3.61 M. Endo, A. Oberlin, T. Koyama: High resolution electron microscopy of graphitizable carbon fiber prepared by benzene decomposition, *Jap. J. Appl. Phys.* **16** (1977) 1519–1523
- 3.62 N. M. Rodriguez: A review of catalytically grown carbon nanofibers, *J. Mater. Res.* **8** (1993) 3233–3250
- 3.63 W. R. Davis, R. J. Slawson, G. R. Rigby: An unusual form of carbon, *Nature* **171** (1953) 756
- 3.64 H. P. Boehm: Carbon from carbon monoxide disproportionation on nickel and iron catalysts; morphological studies and possible growth mechanisms, *Carbon* **11** (1973) 583–590
- 3.65 M. Audier, A. Oberlin, M. Coulon: Crystallographic orientations of catalytic particles in filamentous carbon; case of simple conical particles, *J. Cryst. Growth* **55** (1981) 546–549
- 3.66 M. Audier, M. Coulon: Kinetic and microscopic aspects of catalytic carbon growth, *Carbon* **23** (1985) 317–323
- 3.67 M. Audier, A. Oberlin, M. Coulon: Study of biconic microcrystals in the middle of carbon tubes obtained by catalytic disproportionation of CO, *J. Cryst. Growth* **57** (1981) 524–534
- 3.68 A. Thaib, G. A. Martin, P. Pinheiro, M. C. Schouler, P. Gadelle: Formation of carbon nanotubes from the carbon monoxide disproportionation reaction over $\text{Co/Al}_2\text{O}_3$ and Co/SiO_2 catalysts, *Catal. Lett.* **63** (1999) 135–141
- 3.69 P. Pinheiro, M. C. Schouler, P. Gadelle, M. Mermoux, E. Dooryhée: Effect of hydrogen on the orientation of carbon layers in deposits from the carbon monoxide disproportionation reaction over $\text{Co/Al}_2\text{O}_3$ catalysts, *Carbon* **38** (2000) 1469–1479
- 3.70 P. Pinheiro, P. Gadelle: Chemical state of a supported iron-cobalt catalyst during CO disproportionation. I. Thermodynamic study, *J. Phys. Chem. Solids* **62** (2001) 1015–1021
- 3.71 P. Pinheiro, P. Gadelle, C. Jeandey, J. L. Oddou: Chemical state of a supported iron-cobalt catalyst during CO disproportionation. II. Experimental study, *J. Phys. Chem. Solids* **62** (2001) 1023–1037
- 3.72 C. Laurent, E. Flahaut, A. Peigney, A. Rousset: Metal nanoparticles for the catalytic synthesis of carbon nanotubes, *New J. Chem.* **22** (1998) 1229–1237
- 3.73 A. Peigney, C. Laurent, F. Dobigeon, A. Rousset: Carbon nanotubes grown in situ by a novel catalytic method, *J. Mater. Res.* **12** (1997) 613–615
- 3.74 V. Ivanov, J. B. Nagy, P. Lambin, A. Lucas, X. B. Zhang, X. F. Zhang, D. Bernaerts, G. Van Tendeloo, S. Amelinckx, J. Van Landuyt: The study of nanotubules produced by catalytic method, *Chem. Phys. Lett.* **223** (1994) 329–335
- 3.75 V. Ivanov, A. Fonseca, J. B. Nagy, A. Lucas, P. Lambin, D. Bernaerts, X. B. Zhang: Catalytic production and purification of nanotubules having fullerene-scale diameters, *Carbon* **33** (1995) 1727–1738
- 3.76 K. Hernadi, A. Fonseca, J. B. Nagy, D. Bernaerts, A. Fudala, A. Lucas: Catalytic synthesis of carbon nanotubes using zeolite support, *Zeolites* **17** (1996) 416–423

- 3.77 H. Dai, A. G. Rinzler, P. Nikolaev, A. Thess, D. T. Colbert, R. E. Smalley: Single-wall nanotubes produced by metal-catalysed disproportionation of carbon monoxide, *Chem. Phys. Lett.* **260** (1996) 471–475
- 3.78 A. M. Cassel, J. A. Raymakers, J. Kong, H. Dai: Large scale CVD synthesis of single-walled carbon nanotubes, *J. Phys. Chem. B* **109** (1999) 6484–6492
- 3.79 B. Kitiyanan, W. E. Alvarez, J. H. Harwell, D. E. Resasco: Controlled production of single-wall carbon nanotubes by catalytic decomposition of CO on bimetallic Co–Mo catalysts, *Chem. Phys. Lett.* **317** (2000) 497–503
- 3.80 E. Flahaut: Synthèse par voie catalytique et caractérisation de composites nanotubes de carbone–metal–oxyde Poudres et matériaux denses. Ph.D. Thesis (Univers. Paul Sabatier, Toulouse 1999)
- 3.81 A. Govindaraj, E. Flahaut, C. Laurent, A. Peigney, A. Rousset, C. N. R. Rao: An investigation of carbon nanotubes obtained from the decomposition of methane over reduced $Mg_{1-x}M_xAl_2O_4$ spinel catalysts, *J. Mater. Res.* **14** (1999) 2567–2576
- 3.82 E. Flahaut, A. Peigney, C. Laurent, A. Rousset: Synthesis of single-walled carbon nanotube–Co–MgO composite powders and extraction of the nanotubes, *J. Mater. Chem.* **10** (2000) 249–252
- 3.83 J. Kong, A. M. Cassel, H. Dai: Chemical vapor deposition of methane for single-walled carbon nanotubes, *Chem. Phys. Lett.* **292** (1998) 567–574
- 3.84 R. Marangoni, P. Serp, R. Feurrer, Y. Kihn, P. Kalck, C. Vahlas: Carbon nanotubes produced by substrate free metalorganic chemical vapor deposition of iron catalyst and ethylene, *Carbon* **39** (2001) 443–449
- 3.85 R. Sen, A. Govindaraj, C. N. R. Rao: Carbon nanotubes by the metallocene route, *Chem. Phys. Lett.* **267** (1997) 276–280
- 3.86 Y. Y. Fan, H. M. Cheng, Y. L. Wei, G. Su, S. H. Shen: The influence of preparation parameters on the mass production of vapor grown carbon nanofibers, *Carbon* **38** (2000) 789–795
- 3.87 L. Ci, J. Wei, B. Wei, J. Liang, C. Xu, D. Wu: Carbon nanofibers and single-walled carbon nanotubes prepared by the floating catalyst method, *Carbon* **39** (2001) 329–335
- 3.88 O. A. Nerushev, M. Sveningsson, L. K. L. Falk, F. Rohmund: Carbon nanotube films obtained by thermal vapour deposition, *J. Mater. Chem.* **11** (2001) 1122–1132
- 3.89 F. Rohmund, L. K. L. Falk, F. E. B. Campbell: A simple method for the production of large arrays of aligned carbon nanotubes, *Chem. Phys. Lett.* **328** (2000) 369–373
- 3.90 G. G. Tibbets, C. A. Bernardo, D. W. Gorkiewicz, R. L. Alig: Role of sulfur in the production of carbon fibers in the vapor phase, *Carbon* **32** (1994) 569–576
- 3.91 W. Q. Han, P. Kholer-Riedlich, T. Seeger, F. Ernst, M. Ruhle, N. Grobert, W. K. Hsu, B. H. Chang, Y. Q. Zhu, H. W. Kroto, M. Terrones, H. Terrones: Aligned CN_x nanotubes by pyrolysis of ferrocene under NH_3 atmosphere, *Appl. Phys. Lett.* **77** (2000) 1807–1809
- 3.92 R. E. Smalley, J. H. Hafner, D. T. Colbert, K. Smith: Catalytic growth of single-wall carbon nanotubes from metal particles, US patent US19980601010903 (1998)
- 3.93 T. Kyotani, L. F. Tsai, A. Tomita: Preparation of ultrafine carbon tubes in nanochannels of an anodic aluminum oxide film, *Chem. Mater.* **8** (1996) 2109–2113
- 3.94 W. K. Hsu, J. P. Hare, M. Terrones, H. W. Kroto, D. R. M. Walton, P. J. F. Harris: Condensed-phase nanotubes, *Nature* **377** (1995) 687
- 3.95 W. S. Cho, E. Hamada, Y. Kondo, K. Takayanagi: Synthesis of carbon nanotubes from bulk polymer, *Appl. Phys. Lett.* **69** (1996) 278–279
- 3.96 Y. L. Li, Y. D. Yu, Y. Liang: A novel method for synthesis of carbon nanotubes: Low temperature solid pyrolysis, *J. Mater. Res.* **12** (1997) 1678–1680
- 3.97 S. Fan, M. Chapline, N. Franklin, T. Tomblar, A. M. Cassel, H. Dai: Self-oriented regular arrays of carbon nanotubes and their field emission properties, *Science* **283** (1999) 512–514
- 3.98 M. L. Terranova, S. Piccirillo, V. Sessa, P. Sbornicchia, M. Rossi, S. Botti, D. Manno: Growth of single-walled carbon nanotubes by a novel technique using nano-sized graphite as carbon source, *Chem. Phys. Lett.* **327** (2000) 284–290
- 3.99 R. L. Vander Wal, T. Ticich, V. E. Curtis: Diffusion flame synthesis of single-walled carbon nanotubes, *Chem. Phys. Lett.* **323** (2000) 217–223
- 3.100 Y. Y. Wei, G. Eres, V. I. Merkulov, D. H. Lowdens: Effect of film thickness on carbon nanotube growth by selective area chemical vapor deposition, *Appl. Phys. Lett.* **78** (2001) 1394–1396
- 3.101 W. Z. Li, S. S. Xie, L. X. Qian, B. H. Chang, B. S. Zou, W. Y. Zhou, R. A. Zha, G. Wang: Large scale synthesis of aligned carbon nanotubes, *Science* **274** (1996) 1701–1703
- 3.102 F. Zheng, L. Liang, Y. Gao, J. H. Sukamto, L. Aardahl: Carbon nanotubes synthesis using mesoporous silica templates, *Nanolett.* **2** (2002) 729–732
- 3.103 S. H. Jeong, O.-K. Lee, K. H. Lee, S. H. Oh, C. G. Park: Preparation of aligned carbon nanotubes with prescribed dimension: Template synthesis and sonication cutting approach, *Chem. Mater.* **14** (2002) 1859–1862
- 3.104 N. S. Kim, Y. T. Lee, J. Park, H. Ryu, H. J. Lee, S. Y. Choi, J. Choo: Dependence of vertically aligned growth of carbon nanotubes on catalyst, *J. Phys. Chem. B* **106** (2002) 9286–9290
- 3.105 C. J. Lee, D. W. Kim, T. J. Lee, Y. C. Choi, Y. S. Park, Y. H. Lee, W. B. Choi, N. S. Lee, G.-S. Park, J. M. Kim: Synthesis of aligned carbon nanotubes using thermal chemical vapor deposition, *Chem. Phys. Lett.* **312** (1999) 461–468
- 3.106 W. D. Zhang, Y. Wen, S. M. Liu, W. C. Tjui, G. Q. Xu, L. M. Gan: Synthesis of vertically aligned carbon

- nanotubes on metal deposited quartz plates, *Carbon* **40** (2002) 1981–1989
- 3.107 S. Huang, L. Dai, A. W. H. Mau: Controlled fabrication of large scale aligned carbon nanofiber/nanotube patterns by photolithography, *Adv. Mater.* **14** (2002) 1140–1143
- 3.108 R. Andrews, D. Jacques, A. M. Rao, F. Derbyshire, D. Qian, X. Fan, E. C. Dickey, J. Chen: Continuous production of aligned carbon nanotubes: A step closer to commercial realization, *Chem. Phys. Lett.* **303** (1999) 467–474
- 3.109 C. N. R. Rao, R. Sen, B. C. Satishkumar, A. Govindaraj: Large aligned carbon nanotubes bundles from ferrocene pyrolysis, *Chem. Commun.* **15** (1998) 1525–1526
- 3.110 X. Zhang, A. Cao, B. Wei, Y. Li, J. Wei, C. Xu, D. Wu: Rapid growth of well-aligned carbon nanotube arrays, *Chem. Phys. Lett.* **362** (2002) 285–290
- 3.111 X. Zhang, A. Cao, Y. Li, C. Xu, J. Liang, D. Wu, B. Wei: Self-organized arrays of carbon nanotube ropes, *Chem. Phys. Lett.* **351** (2002) 183–188
- 3.112 K. S. Choi, Y. S. Cho, S. Y. Hong, J. B. Park, D. J. Kim: Effects of ammonia on the alignment of carbon nanotubes in metal-assisted chemical vapor deposition, *J. Eur. Cer. Soc.* **21** (2001) 2095–2098
- 3.113 M. Endo, H. W. Kroto: Formation of carbon nanofibers, *J. Phys. Chem.* **96** (1992) 6941–6944
- 3.114 R. S. Wagner: VLS mechanisms of crystal growth. In: *Whisker Technology*, ed. by P. Levit A. (Wiley, New York 1970) pp. 47–72
- 3.115 Y. H. Lee, S. G. Kim, D. Tomanek: Catalytic growth of single-wall carbon nanotubes: An ab initio study, *Phys. Rev. Lett.* **78** (1997) 2393–2396
- 3.116 H. Dai: Carbon Nanotubes: Synthesis, integration, and properties, *Acc. Chem. Res.* **35** (2002) 1035–1044
- 3.117 Y. Saito, M. Okuda, N. Fujimoto, T. Yoshikawa, M. Tomita, T. Hayashi: Single-wall carbon nanotubes growing radially from Ni fine particles formed by arc evaporation, *Jpn. J. Appl. Phys.* **33** (1994) L526–L529
- 3.118 J. Bernholc, C. Brabec, M. Buongiorno Nardelli, A. Malti, C. Roland, B. J. Yakobson: Theory of growth and mechanical properties of nanotubes, *Appl. Phys. A* **67** (1998) 39–46
- 3.119 M. Pacheco: Synthèse des nanotubes de carbone par arc électrique. Ph.D. Thesis (Université Toulouse III, Toulouse 2003)
- 3.120 K. Méténier, S. Bonnamy, F. Béguin, C. Journet, P. Bernier, L. M. de la Chapelle, O. Chauvet, S. Lefrant: Coalescence of single walled nanotubes and formation of multi-walled carbon nanotubes under high temperature treatments, *Carbon* **40** (2002) 1765–1773
- 3.121 P. G. Collins, P. Avouris: Nanotubes for electronics, *Sci. Am.* **283** (2000) 38–45
- 3.122 Q.-H. Yang, P. X. Hou, S. Bai, M. Z. Wang, H. M. Cheng: Adsorption and capillarity of nitrogen in aggregated multi-walled carbon nanotubes, *Chem. Phys. Lett.* **345** (2001) 18–24
- 3.123 S. Inoue, N. Ichikuni, T. Suzuki, T. Uematsu, K. Kaneko: Capillary condensation of N₂ on multi-wall carbon nanotubes, *J. Phys. Chem.* **102** (1998) 4689–4692
- 3.124 M. Eswaramoorthy, R. Sen, C. N. R. Rao: A study of micropores in single-walled carbon nanotubes by the adsorption of gases and vapors, *Chem. Phys. Lett.* **304** (1999) 207–210
- 3.125 A. Peigney, Ch. Laurent, E. Flahaut, R. R. Bacsa, A. Rousset: Specific surface area of carbon nanotubes and bundles of carbon nanotubes, *Carbon* **39** (2001) 507–514
- 3.126 E. Frackowiak, S. Delpeux, K. Jurewicz, K. Szostak, D. Cazorla-Amoros, F. Béguin: Enhanced capacitance of carbon nanotubes through chemical activation, *Chem. Phys. Lett.* **336** (2002) 35–41
- 3.127 M. Muris, N. Dupont-Pavlosky, M. Bienfait, P. Zepfenfeld: Where are the molecules adsorbed on single-walled nanotubes?, *Surf. Sci.* **492** (2001) 67–74
- 3.128 A. Fujiwara, K. Ishii, H. Suematsu, H. Kataura, Y. Maniwa, S. Suzuki, Y. Achiba: Gas adsorption in the inside and outside of single-walled carbon nanotubes, *Chem. Phys. Lett.* **336** (2001) 205–211
- 3.129 C. M. Yang, H. Kanoh, K. Kaneko, M. Yudasaka, S. Iijima: Adsorption behaviors of HiPco single-walled carbon nanotubes aggregates for alcohol vapors, *J. Phys. Chem.* **106** (2002) 8994–8999
- 3.130 J. Zhao, A. Buldum, J. Han, J. P. Lu: Gas molecule adsorption in carbon nanotubes and nanotube bundles, *Nanotechnology* **13** (2002) 195–200
- 3.131 K. A. Williams, P. C. Eklund: Monte Carlo simulation of H₂ physisorption in finite diameter carbon nanotube ropes, *Chem. Phys. Lett.* **320** (2000) 352–358
- 3.132 A. Chambers, C. Park, R. T. K. Baker, N. Rodriguez: Hydrogen storage in graphite nanofibers, *J. Phys. Chem. B.* **102** (1998) 4253–4256
- 3.133 J. Hilding, E. A. Grulke, S. B. Sinnott, D. Qian, R. Andrews, M. Jagtoyen: Sorption of butane on carbon multiwall nanotubes at room temperature, *Langmuir* **17** (2001) 7540–7544
- 3.134 K. Masenelli-Varlot, E. McRae, N. Dupont-Pavlosky: Comparative adsorption of simple molecules on carbon nanotubes. Dependence of the adsorption properties on the nanotube morphology, *Appl. Surf. Sci.* **196** (2002) 209–215
- 3.135 D. J. Browning, M. L. Gerrard, J. B. Lakeman, I. M. Mellor, R. J. Mortimer, M. C. Turpin: Studies into the storage of hydrogen in carbon nanofibers: Proposal of a possible mechanism, *Nanolett.* **2** (2002) 201–205
- 3.136 F. H. Yang, R. T. Yang: Ab initio molecular orbital study of adsorption of atomic hydrogen on graphite: insight into hydrogen storage in carbon nanotubes, *Carbon* **40** (2002) 437–444
- 3.137 G. E. Froudakis: Why alkali-metal-doped carbon nanotubes possess high hydrogen uptake, *Nanolett.* **1** (2001) 531–533

- 3.138 H. Ulbricht, G. Moos, T. Hertel: Physisorption of molecular oxygen on single-wall carbon nanotube bundles and graphite, *Phys. Rev. B* **66** (2002) 075404-1-075404-7
- 3.139 H. Ulbricht, J. Kriebel, G. Moos, T. Hertel: Desorption kinetics and interaction of Xe with single-wall carbon nanotube bundles, *Chem. Phys. Lett.* **363** (2002) 252-260
- 3.140 R. Saito, G. Dresselhaus, M. S. Dresselhaus: *Physical Properties of Carbon Nanotubes* (Imperial College Press, London 1998)
- 3.141 A. Charlier, E. McRae, R. Heyd, M. F. Charlier, D. Moretti: Classification for double-walled carbon nanotubes, *Carbon* **37** (1999) 1779-1783
- 3.142 A. Charlier, E. McRae, R. Heyd, M. F. Charlier: Metal semi-conductor transitions under uniaxial stress for single- and double-walled carbon nanotubes, *J. Phys. Chem. Solids* **62** (2001) 439-444
- 3.143 H. Ajiki, T. Ando: Electronic states of carbon nanotubes, *J. Phys. Soc. Jap.* **62** (1993) 1255-1266
- 3.144 C. T. White, T. N. Todorov: Carbon nanotubes as long ballistic conductors, *Nature* **393** (1998) 240-242
- 3.145 S. Frank, P. Poncharal, Z. L. Wang, W. A. de Heer: Carbon nanotube quantum resistors, *Science* **280** (1998) 1744-1746
- 3.146 W. Liang, M. Bockrath, D. Bozovic, J. H. Hafner, M. Tinkham, H. Park: Fabry-Perot interference in a nanotube electron waveguide, *Nature* **411** (2001) 665-669
- 3.147 L. Langer, V. Bayot, E. Grivei, J.-P. Issi, J.-P. Heremans, C. H. Olk, L. Stockman, C. van Haesendonck, Y. Buynseraeder: Quantum transport in a multiwalled carbon nanotube, *Phys. Rev. Lett.* **76** (1996) 479-482
- 3.148 M. Bockrath, D. H. Cobden, J. Lu, A. G. Rinzler, R. E. Smalley, L. Balents, P. L. McEuen: Luttinger-liquid behaviour in carbon nanotubes, *Nature* **397** (1999) 598-601
- 3.149 K. Liu, S. Roth, G. S. Duesberg, G. T. Kim, D. Popa, K. Mukhopadhyay, R. Doome, J. B'Nagy: Antilocalization in multiwalled carbon nanotubes, *Phys. Rev. B* **61** (2000) 2375-2379
- 3.150 Y. A. Kasumov, R. Deblock, M. Kociak, B. Reulet, H. Bouchiat, I. I. Khodos, Y. B. Gorbatov, V. T. Volkov, C. Journet, M. Burghard: Supercurrents through single-walled carbon nanotubes, *Science* **284** (1999) 1508-1511
- 3.151 B. W. Alphenaar, K. Tsukagoshi, M. Wagner: Magnetoresistance of ferromagnetically contacted carbon nanotubes, *Phys. Eng.* **10** (2001) 499-504
- 3.152 P. M. Ajayan, M. Terrones, A. de la Guardia, V. Hue, N. Grobert, B. Q. Wei, H. Lezec, G. Ramanath, T. W. Ebbesen: Nanotubes in a flash - Ignition and reconstruction, *Science* **296** (2002) 705
- 3.153 S. Berber, Y. Kwon, D. Tomanek: Unusually high thermal conductivity of carbon nanotubes, *Phys. Rev. Lett.* **84** (2000) 4613-4616
- 3.154 S. N. Song, X. K. Wang, R. P. H. Chang, J. B. Ketterson: Electronic properties of graphite nanotubules from galvanomagnetic effects, *Phys. Rev. Lett.* **72** (1994) 697-700
- 3.155 M.-F. Yu, O. Lourie, M. J. Dyer, K. Moloni, T. F. Kelley, R. S. Ruoff: Strength and breaking mechanism of multiwalled carbon nanotubes under tensile load, *Science* **287** (2000) 637-640
- 3.156 D. A. Walters, L. M. Ericson, M. J. Casavant, J. Liu, D. T. Colbert, K. A. Smith, R. E. Smalley: Elastic strain of freely suspended single-wall carbon nanotube ropes, *Appl. Phys. Lett.* **74** (1999) 3803-3805
- 3.157 B. G. Demczyk, Y. M. Wang, J. Cumingd, M. Hetamn, W. Han, A. Zettl, R. O. Ritchie: Direct mechanical measurement of the tensile strength and elastic modulus of multiwalled carbon nanotubes, *Mater. Sci. Eng. A* **334** (2002) 173-178
- 3.158 R. P. Gao, Z. L. Wang, Z. G. Bai, W. A. De Heer, L. M. Dai, M. Gao: Nanomechanics of individual carbon nanotubes from pyrolytically grown arrays, *Phys. Rev. Lett.* **85** (2000) 622-625
- 3.159 M. M. J. Treacy, T. W. Ebbesen, J. M. Gibson: Exceptionally high Young's modulus observed for individual carbon nanotubes, *Nature* **381** (1996) 678-680
- 3.160 N. Yao, V. Lordie: Young's modulus of single-wall carbon nanotubes, *J. Appl. Phys.* **84** (1998) 1939-1943
- 3.161 O. Lourie, H. D. Wagner: Transmission electron microscopy observations of fracture of single-wall carbon nanotubes under axial tension, *Appl. Phys. Lett.* **73** (1998) 3527-3529
- 3.162 S. C. Tsang, Y. K. Chen, P. J. F. Harris, M. L. H. Green: A simple chemical method of opening and filling carbon nanotubes, *Nature* **372** (1994) 159-162
- 3.163 M. Montieux: Filling single-wall carbon nanotubes, *Carbon* **40** (2002) 1809-1823
- 3.164 W. K. Hsu, S. Y. Chu, E. Munoz-Picone, J. L. Boldu, Firth S., P. Franchi, B. P. Roberts, A. Shilder, H. Terrones, N. Grobert, Y. Q. Zhu, M. Terrones, M. E. McHenry, H. W. Kroto, D. R. M. Walton: Metallic behaviour of boron-containing carbon nanotubes, *Chem. Phys. Lett.* **323** (2000) 572-579
- 3.165 R. Czerw, M. Terrones, J. C. Charlier, X. Blasé, B. Foley, R. Kamalakaran, N. Grobert, H. Terrones, D. Tekleab, P. M. Ajayan, W. Blau, M. Rühle, D. L. Carroll: Identification of electron donor states, in N-doped carbon nanotubes, *Nanolett.* **1** (2001) 457-460
- 3.166 O. Stephan, P. M. Ajayan, C. Colliex, P. Redlich, J. M. Lambert, P. Bernier, P. Lefin: Doping graphitic and carbon nanotube structures with boron and nitrogen, *Science* **266** (1994) 1683-1685
- 3.167 A. Loiseau, F. Willaime, N. Demoncy, N. Schramchenko, G. Hug, C. Colliex, H. Pascard: Boron nitride nanotubes, *Carbon* **36** (1998) 743-752
- 3.168 C. C. Tang, L. M. de la Chapelle, P. Li, Y. M. Liu, H. Y. Dang, S. S. Fan: Catalytic growth of nanotube

- and nanobamboo structures of boron nitride, *Chem. Phys. Lett.* **342** (2001) 492–496
- 3.169 K. Suenaga, C. Colliex, N. Demoncey, A. Loiseau, H. Pascard, F. Willaime: Synthesis of nanoparticles and nanotubes with well separated layers of boron–nitride and carbon, *Science* **278** (1997) 653–655
- 3.170 D. Golberg, Y. Bando, L. Bourgeois, K. Kurashima, T. Sato: Large-scale synthesis and HRTEM analysis of single-walled B- and N-doped carbon nanotube bundles, *Carbon* **38** (2000) 2017–2027
- 3.171 B. Burteaux, A. Claye, B. W. Smith, M. Monthieux, D. E. Luzzi, J. E. Fischer: Abundance of encapsulated C₆₀ in single-wall carbon nanotubes, *Chem. Phys. Lett.* **310** (1999) 21–24
- 3.172 D. Ugarte, A. Châtelain, W. A. de Heer: Nanocapillarity and chemistry in carbon nanotubes, *Science* **274** (1996) 1897–1899
- 3.173 J. Cook, J. Sloan, M. L. H. Green: Opening and filling carbon nanotubes, *Fuller. Sci. Technol.* **5** (1997) 695–704
- 3.174 P. M. Ajayan, S. Iijima: Capillarity-induced filling of carbon nanotubes, *Nature* **361** (1993) 333–334
- 3.175 P. M. Ajayan, T. W. Ebbesen, T. Ichihashi, S. Iijima, K. Tanigaki, H. Hiura: Opening carbon nanotubes with oxygen and implications for filling, *Nature* **362** (1993) 522–525
- 3.176 S. Seraphin, D. Zhou, J. Jiao, J. C. Withers, R. Loufty: Yttrium carbide in nanotubes, *Nature* **362** (1993) 503
- 3.177 S. Seraphin, D. Zhou, J. Jiao, J. C. Withers, R. Loufty: Selective encapsulation of the carbides of yttrium and titanium into carbon nanoclusters, *Appl. Phys. Lett.* **63** (1993) 2073–2075
- 3.178 R. S. Ruoff, D. C. Lorents, B. Chan, R. Malhotra, S. Subramoney: Single-crystal metals encapsulated in carbon nanoparticles, *Science* **259** (1993) 346–348
- 3.179 A. Loiseau, H. Pascard: Synthesis of long carbon nanotubes filled with Se, S, Sb, and Ge by the arc method, *Chem. Phys. Lett.* **256** (1996) 246–252
- 3.180 N. Demoncey, O. Stephan, N. Brun, C. Colliex, A. Loiseau, H. Pascard: Filling carbon nanotubes with metals by the arc discharge method: The key role of sulfur, *Eur. Phys. J. B* **4** (1998) 147–157
- 3.181 C. H. Kiang, J. S. Choi, T. T. Tran, A. D. Bacher: Molecular nanowires of 1 nm diameter from capillary filling of single-walled carbon nanotubes, *J. Phys. Chem. B* **103** (1999) 7449–7551
- 3.182 Z. L. Zhang, B. Li, Z. J. Shi, Z. N. Gu, Z. Q. Xue, L. M. Peng: Filling of single-walled carbon nanotubes with silver, *J. Mater. Res.* **15** (2000) 2658–2661
- 3.183 A. Govindaraj, B. C. Satishkumar, M. Nath, C. N. R. Rao: Metal nanowires and intercalated metal layers in single-walled carbon nanotubes bundles, *Chem. Mater.* **12** (2000) 202–205
- 3.184 J. Mittal, M. Monthieux, H. Allouche: Synthesis of SWNT-based hybrid nanomaterials from photolysis-enhanced chemical processes, *Chem. Phys. Lett.* **339** (2001) 311–318
- 3.185 E. Dujardin, T. W. Ebbesen, H. Hiura, K. Tanigaki: Capillarity and wetting of carbon nanotubes, *Science* **265** (1994) 1850–1852
- 3.186 E. Flahaut, J. Sloan, K. S. Coleman, V. C. Williams, S. Friedrichs, N. Hanson, M. L. H. Green: 1D p-block halide crystals confined into single walled carbon nanotubes, *Proc. Mater. Res. Soc. Symp.* **633** (2001) A13.15.1–A13.15.6
- 3.187 J. Sloan, A. I. Kirkland, J. L. Hutchison, M. L. H. Green: Integral atomic layer architectures of 1D crystals inserted into single walled carbon nanotubes, *Chem. Commun.* (2002) 1319–1332
- 3.188 J. Sloan, M. C. Novotny, S. R. Bailey, G. Brown, C. Xu, V. C. Williams, S. Friedrichs, E. Flahaut, R. L. Calender, A. P. E. York, K. S. Coleman, M. L. H. Green, R. E. Dunin-Borkowski, J. L. Hutchison: Two layer 4 : 4 co-ordinated KI crystals grown within single walled carbon nanotubes, *Chem. Phys. Lett.* **329** (2000) 61–65
- 3.189 G. Brown, S. R. Bailey, J. Sloan, C. Xu, S. Friedrichs, E. Flahaut, K. S. Coleman, J. L. Hutchinson, R. E. Dunin-Borkowski, M. L. H. Green: Electron beam induced in situ clusterisation of 1D ZrCl₄ chains within single-walled carbon nanotubes, *Chem. Commun.* **9** (2001) 845–846
- 3.190 B. W. Smith, M. Monthieux, D. E. Luzzi: Encapsulated C₆₀ in carbon nanotubes, *Nature* **396** (1998) 323–324
- 3.191 B. W. Smith, D. E. Luzzi: Formation mechanism of fullerene peapods and coaxial tubes: A path to large scale synthesis, *Chem. Phys. Lett.* **321** (2000) 169–174
- 3.192 K. Hirahara, K. Suenaga, S. Bandow, H. Kato, T. Okazaki, H. Shinohara, S. Iijima: One-dimensional metallo-fullerene crystal generated inside single-walled carbon nanotubes, *Phys. Rev. Lett.* **85** (2000) 5384–5387
- 3.193 B. W. Smith, M. Monthieux, D. E. Luzzi: Carbon nanotube encapsulated fullerenes: A unique class of hybrid material, *Chem. Phys. Lett.* **315** (1999) 31–36
- 3.194 D. E. Luzzi, B. W. Smith: Carbon cage structures in single wall carbon nanotubes: A new class of materials, *Carbon* **38** (2000) 1751–1756
- 3.195 S. Bandow, M. Takisawa, K. Hirahara, M. Yudasaka, S. Iijima: Raman scattering study of double-wall carbon nanotubes derived from the chains of fullerenes in single-wall carbon nanotubes, *Chem. Phys. Lett.* **337** (2001) 48–54
- 3.196 B. W. Smith, D. E. Luzzi, Y. Achiba: Tumbling atoms and evidence for charge transfer in La₂@C₈₀@SWNT, *Chem. Phys. Lett.* **331** (2000) 137–142
- 3.197 K. Suenaga, M. Tence, C. Mory, C. Colliex, H. Kato, T. Okazaki, H. Shinohara, K. Hirahara, S. Bandow, S. Iijima: Element-selective single atom imaging, *Science* **290** (2000) 2280–2282
- 3.198 D. E. Luzzi, B. W. Smith, R. Russo, B. C. Satishkumar, F. Stercel, N. R. C. Nemes: Encapsulation of metallo-fullerenes and metalloenes in carbon nanotubes, *Proc. Electronic Properties of Novel Materials–XVI Int. Winterschool – AIP Conf. Proc., Melville 2001*, ed. by

- H. Kuzmany, J. Fink, M. Mehring, S. Roth (Springer, Berlin, Heidelberg 2001) **591** 622–626
- 3.199 G. H. Jeong, R. Hatakeyama, T. Hirata, K. Tohji, K. Motomiya, N. Sato, Y. Kawazoe: Structural deformation of single-walled carbon nanotubes and fullerene encapsulation due to magnetized plasma ion irradiation, *Appl. Phys. Lett.* **79** (2001) 4213–4215
- 3.200 Y. P. Sun, K. Fu, Y. Lin, W. Huang: Functionalized carbon nanotubes: Properties and applications, *Acc. Chem. Res.* **35** (2002) 1095–1104
- 3.201 J. Chen, M. A. Hamon, M. Hui, C. Yongsheng, A. M. Rao, P. C. Eklund, R. C. Haddon: Solution properties of single-walled carbon nanotubes, *Science* **282** (1998) 95–98
- 3.202 J. Chen, A. M. Rao, S. Lyuksyutov, M. E. Itkis, M. A. Hamon, H. Hu, R. W. Cohn, P. C. Eklund, D. T. Colbert, R. E. Smalley, R. C. Haddon: Dissolution of full-length single-walled carbon nanotubes, *J. Phys. Chem. B* **105** (2001) 2525–2528
- 3.203 F. Pompeo, D. E. Resasco: Water solubilization of single-walled carbon nanotubes by functionalization with glucosamine, *Nanolett.* **2** (2002) 369–373
- 3.204 Y. P. Sun, W. Huang, Y. Lin, K. Fu, A. Kitaygorodskiy, L. A. Riddle, Y. J. Yu, D. L. Carroll: Soluble dendron-functionalized carbon nanotubes: Preparation, characterization, and properties, *Chem. Mater.* **13** (2001) 2864–2869
- 3.205 K. Fu, W. Huang, Y. Lin, L. A. Riddle, D. L. Carroll, Y. P. Sun: Defunctionalization of functionalized carbon nanotubes, *Nanolett.* **1** (2001) 439–441
- 3.206 P. W. Chiu, G. S. Duesberg, U. Dettlaff-Weglikowska, S. Roth: Interconnection of carbon nanotubes by chemical functionalization, *Appl. Phys. Lett.* **80** (2002) 3811–3813
- 3.207 E. T. Mickelson, C. B. Huffman, A. G. Rinzier, R. E. Smalley, R. H. Hauge, J. L. Margrave: Fluorination of single-wall carbon nanotubes, *Chem. Phys. Lett.* **296** (1998) 188–194
- 3.208 V. N. Khabashesku, W. E. Billups, J. L. Margrave: Fluorination of single-wall carbon nanotubes and subsequent derivatization reactions, *Acc. Chem. Res.* **35** (2002) 1087–1095
- 3.209 P. J. Boul, J. Liu, E. T. Michelson, C. B. Huffman, L. M. Ericson, I. W. Chiang, K. A. Smith, D. T. Colbert, R. H. Hauge, J. L. Margrave, R. E. Smalley: Reversible side-wall functionalization of buckytubes, *Chem. Phys. Lett.* **310** (1999) 367–372
- 3.210 J. L. Bahr, J. Yang, D. V. Kosynkin, M. J. Bronikowski, R. E. Smalley, J. M. Tour: Functionalization of carbon nanotubes by electrochemical reduction of aryl diazonium salts: A bucky paper electrode, *J. Am. Chem. Soc.* **123** (2001) 6536–6542
- 3.211 M. Holzinger, O. Vostrowsky, A. Hirsch, F. Hennrich, M. Kappes, R. Weiss, F. Jellen: Sidewall functionalization of carbon nanotubes, *Angew. Chem. Int. Ed.* **40** (2001) 4002–4005
- 3.212 Y. Chen, R. C. Haddon, S. Fang, A. M. Rao, P. C. Eklund, W. H. Lee, E. C. Dickey, E. A. Grulke, J. C. Pendergrass, A. Chavan, B. E. Haley, R. E. Smalley: Chemical attachment of organic functional groups to single-walled carbon nanotube material, *J. Mater. Res.* **13** (1998) 2423–2431
- 3.213 C. Velasco-Santos, A. L. Martinez-Hernandez, M. Lozada-Cassou, A. Alvarez-Castillo, V. M. Castano: Chemical functionalization of carbon nanotubes through an organosilane, *Nanotechnology* **13** (2002) 495–498
- 3.214 A. Star, J. F. Stoddart, D. Steuerman, M. Diehl, A. Boukai, E. W. Wong, X. Yang, S. W. Chung, H. Choi, J. R. Heath: Preparation and properties of polymer-wrapped single-walled carbon nanotubes, *Angew. Chem. Int. Ed.* **41** (2002) 1721–1725
- 3.215 J. H. Hafner, C. L. Cheung, A. T. Wooley, C. M. Lieber: Structural and functional imaging with carbon nanotube AFM probes, *Progr. Biophys. Molec. Biol.* **77** (2001) 73–110
- 3.216 S. S. Wong, E. Joselevich, A. T. Woodley, C. L. Cheung, C. M. Lieber: Covalently functionalized nanotubes as nanometre-size probes in chemistry and biology, *Nature* **394** (1998) 52–55
- 3.217 C. L. Cheung, J. H. Hafner, C. M. Lieber: Carbon nanotube atomic force microscopy tips: Direct growth by chemical vapor deposition and application to high-resolution imaging, *Proc. Nat. Acad. Sci.* (2000) 973809–973813
- 3.218 W. A. de Heer, A. Châtelain, D. Ugarte: A carbon nanotube field-emission electron source, *Science* **270** (1995) 1179–1180
- 3.219 J. M. Bonard, J. P. Salvetat, T. Stockli, W. A. de Heer, L. Forro, A. Chatelain: Field emission from single-wall carbon nanotube films, *Appl. Phys. Lett.* **73** (1998) 918–920
- 3.220 W. Zhu, C. Bower, O. Zhou, G. Kochanski, S. Jin: Large current density from carbon nanotube field emitters, *Appl. Phys. Lett.* **75** (1999) 873–875
- 3.221 Y. Saito, R. Mizushima, T. Tanaka, K. Tohji, K. Uchida, M. Yumura, S. Uemura: Synthesis, structure, and field emission of carbon nanotubes, *Fuller. Sci. Technol.* **7** (1999) 653–664
- 3.222 J. Kong, N. R. Franklin, C. Zhou, M. G. Chapline, S. Peng, K. Cho, H. Dai: Nanotube molecular wire as chemical sensors, *Science* **287** (2000) 622–625
- 3.223 P. G. Collins, K. Bradley, M. Ishigami, A. Zettl: Extreme oxygen sensitivity of electronic properties of carbon nanotubes, *Science* **287** (2000) 1801–1804
- 3.224 H. Chang, J. D. Lee, S. M. Lee, Y. H. Lee: Adsorption of NH₃ and NO₂ molecules on carbon nanotubes, *Appl. Phys. Lett.* **79** (2001) 3863–3865
- 3.225 O. K. Varghese, P. D. Kichambre, D. Gong, K. G. Ong, E. C. Dickey, C. A. Grimes: Gas sensing characteristics of multi-wall carbon nanotubes, *Sens. Actuators B* **81** (2001) 32–41
- 3.226 K. G. Ong, K. Zeng, C. A. Grimes: A wireless, passive carbon nanotube-based gas sensor, *IEEE Sens. J.* **2** (2002) 82–88

- 3.227 J. Kong, M. G. Chapline, H. Dai: Functionalized carbon nanotubes for molecular hydrogen sensors, *Adv. Mater.* **13** (2001) 1384–1386
- 3.228 F. Rodriguez-Reinoso: The role of carbon materials in heterogeneous catalysis, *Carbon* **36** (1998) 159–175
- 3.229 E. Auer, A. Freund, J. Pietsch, T. Tacke: Carbon as support for industrial precious metal catalysts, *Appl. Catal. A* **173** (1998) 259–271
- 3.230 J. M. Planeix, N. Coustel, B. Coq, B. Botrons, P. S. Kumbhar, R. Dutartre, P. Geneste, P. Bernier, P. M. Ajayan: Application of carbon nanotubes as supports in heterogeneous catalysis, *J. Am. Chem. Soc.* **116** (1994) 7935–7936
- 3.231 B. Coq, J. M. Planeix, V. Brotons: Fullerene-based materials as new support media in heterogeneous catalysis by metals, *Appl. Catal. A* **173** (1998) 175–183
- 3.232 G. Mestl, N. I. Maksimova, N. Keller, V. V. Roddatis, R. Schlögl: Carbon nanofilaments in heterogeneous catalysis: An industrial application for new carbon materials?, *Angew. Chem. Int. Ed. Engl.* **40** (2001) 2066–2068
- 3.233 J. E. Fischer, A. T. Johnson: Electronic properties of carbon nanotubes, *Current Opinion Solid State Mater. Sci.* **4** (1999) 28–33
- 3.234 M. Menon, A. N. Andriotis, G. E. Froudakis: Curvature dependence of the metal catalyst atom interaction with carbon nanotubes walls, *Chem. Phys. Lett.* **320** (2000) 425–434
- 3.235 R. Giordano, Ph. Serp, Ph. Kalck, Y. Kihn, J. Schreiber, C. Marhic, J.-L. Duvail: Preparation of Rhodium supported on carbon nanotubes catalysts via surface mediated organometallic reaction, *Eur. J. Inorg. Chem.* (2003) 610–617
- 3.236 T. Kyotani, S. Nakazaki, W.-H. Xu, A. Tomita: Chemical modification of the inner walls of carbon nanotubes by HNO_3 oxidation, *Carbon* **39** (2001) 782–785
- 3.237 Z. J. Liu, Z. Y. Yuan, W. Zhou, L. M. Peng, Z. Xu: Co/carbon nanotubes monometallic system: The effects of oxidation by nitric acid, *Phys. Chem. Chem. Phys.* **3** (2001) 2518–2521
- 3.238 H.-B. Chen, J. D. Lin, Y. Cai, X. Y. Wang, J. Yi, J. Wang, G. Wei, Y. Z. Lin, D. W. Liao: Novel multi-walled nanotubes-supported and alkali-promoted Ru catalysts for ammonia synthesis under atmospheric pressure, *Appl. Surf. Sci.* **180** (2001) 328–335
- 3.239 Y. Zhang, H. B. Zhang, G. D. Lin, P. Chen, Y. Z. Yuan, K. R. Tsai: Preparation, characterization and catalytic hydroformylation properties of carbon nanotubes-supported Rh-phosphine catalyst, *Appl. Catal. A* **187** (1999) 213–224
- 3.240 M. S. Dresselhaus, K. A. Williams, P. C. Eklund: Hydrogen adsorption in carbon materials, *Mater. Res. Soc. Bull.* (November 1999) 45–50
- 3.241 H.-M. Cheng, Q.-H. Yang, C. Liu: Hydrogen storage in carbon nanotubes, *Carbon* **39** (2001) 1447–1454
- 3.242 G. G. Tibbetts, G. P. Meisner, C. H. Olk: Hydrogen storage capacity of carbon nanotubes, filaments, and vapor-grown fibers, *Carbon* **39** (2001) 2291–2301
- 3.243 F. L. Darkrim, P. Malbrunot, G. P. Tartaglia: Review of hydrogen storage adsorption in carbon nanotubes, *Int. J. Hydrogen Energy* **27** (2002) 193–202
- 3.244 C. Park, P. E. Anderson, C. D. Tan, R. Hidalgo, N. Rodriguez: Further studies of the interaction of hydrogen with graphite nanofibers, *J. Phys. Chem. B* **103** (1999) 10572–1058
- 3.245 C. C. Ahn, Y. Ye, B. V. Ratnakumar, C. Witham, R. C. Bowman, B. Fultz: Hydrogen adsorption measurements on graphite nanofibers, *Appl. Phys. Lett.* **73** (1998) 3378–3380
- 3.246 Q. Wang, J. K. Johnson: Computer simulations of hydrogen adsorption on graphite nanofibers, *J. Phys. Chem. B* **103** (1999) 277–281
- 3.247 M. Rzepka, P. Lamp, M. A. de la Casa-Lillo: Physisorption of hydrogen on microporous carbon and carbon nanotubes, *J. Phys. Chem. B* **102** (1998) 10894–10898
- 3.248 A. C. Dillon, K. M. Jones, T. A. Bekkedahl, C. H. Kiang, D. S. Bethune, M. J. Heben: Storage of hydrogen in single-walled carbon nanotubes, *Nature* **386** (1997) 377–379
- 3.249 Y. Ye, C. C. Ahn, C. Witham, R. C. Bowman, B. Fultz, J. Liu, A. G. Rinzler, D. Colbert, K. A. Smith, R. E. Smalley: Hydrogen adsorption and cohesive energy of single-walled carbon nanotubes, *Appl. Phys. Lett.* **74** (1999) 2307–2309
- 3.250 C. Liu, Y. Y. Fan, M. Liu, H. T. Cong, H. M. Cheng, M. S. Dresselhaus: Hydrogen storage in single-walled carbon nanotubes at room temperature, *Science* **286** (1999) 1127–1129
- 3.251 M. Hirscher, M. Becher, M. Haluska, U. Dettlaff-Weglikowska, A. Quintel, G. S. Duesberg, Y. M. Choi, P. Dwones, M. Hulman, S. Roth, I. Stepanek, P. Bernier: Hydrogen storage in sonicated carbon materials, *Appl. Phys. A* **72** (2001) 129–132
- 3.252 P. A. Gordon, R. B. Saeger: Molecular modeling of adsorptive energy storage: Hydrogen storage in single-walled carbon nanotubes, *Ind. Eng. Chem. Res.* **38** (1999) 4647–4655
- 3.253 P. Marinelli, R. Pellenq, J. Conard: H stocké dans les carbones un site légèrement métastable, *matériaux, Tours 2002 AF-14-020*
- 3.254 S. M. Lee, H. Y. Lee: Hydrogen storage in single-walled carbon nanotubes, *Appl. Phys. Lett.* **76** (2000) 2877–2879
- 3.255 S. M. Lee, K. S. Park, Y. C. Choi, Y. S. Park, J. M. Bok, D. J. Bae, K. S. Nahm, Y. G. Choi, C. S. Yu, N. Kim, T. Frauenheim, Y. H. Lee: Hydrogen adsorption in carbon nanotubes, *Synth. Met.* **113** (2000) 209–216
- 3.256 H. Cheng, G. P. Pez, A. C. Cooper: Mechanism of hydrogen sorption in single-walled carbon nanotubes, *J. Am. Chem. Soc.* **123** (2001) 5845–5846
- 3.257 A. Kusnetzova, D. B. Mawhinney, V. Naumenko, J. T. Yates, J. Liu, R. E. Smalley: Enhancement

- of adsorption inside of single-walled nanotubes: Opening the entry ports, *Chem. Phys. Lett.* **321** (2000) 292–296
- 3.258 G. E. Gadd, M. Blackford, S. Moricca, N. Webb, P. J. Evans, A. M. Smith, G. Jacobsen, S. Leung, A. Day, Q. Hua: The world's smallest gas cylinders?, *Science* **277** (1997) 933–936
- 3.259 Z. Mao, S. B. Sinnott: A computational study of molecular diffusion and dynamic flow through carbon nanotubes, *J. Phys. Chem. B* **104** (2000) 4618–4624
- 3.260 Z. Mao, S. B. Sinnott: Separation of organic molecular mixtures in carbon nanotubes and bundles: Molecular dynamics simulations, *J. Phys. Chem. B* **105** (2001) 6916–6924
- 3.261 C. Gu, G.-H. Gao, Y. X. Yu, T. Nitta: Simulation for separation of hydrogen and carbon monoxide by adsorption on single-walled carbon nanotubes, *Fluid Phase Equilibria* **194/197** (2002) 297–307
- 3.262 R. Q. Long, R. T. Yang: Carbon nanotubes as superior sorbent for dioxine removal, *J. Am. Chem. Soc.* **123** (2001) 2058–2059
- 3.263 Y. H. Li, S. Wang, A. Cao, D. Zhao, X. Zhang, C. Xu, Z. Luan, D. Ruan, J. Liang, D. Wu, B. Wei: Adsorption of fluoride from water by amorphous alumina supported on carbon nanotubes, *Chem. Phys. Lett.* **350** (2001) 412–416
- 3.264 Y. H. Li, S. Wang, J. Wei, X. Zhang, C. Xu, Z. Luan, D. Wu, B. Wei: Lead adsorption on carbon nanotubes, *Chem. Phys. Lett.* **357** (2002) 263–266
- 3.265 C. Park, E. S. Engel, A. Crowe, T. R. Gilbert, N. M. Rodriguez: Use of carbon nanofibers in the removal of organic solvents from water, *Langmuir* **16** (2000) 8050–8056
- 3.266 M. P. Mattson, R. C. Haddon, A. M. Rao: Molecular functionalization of carbon nanotubes and use as substrates for neuronal growth, *J. Molec. Neurosci.* **14** (2000) 175–182
- 3.267 J. J. Davis, M. L. H. Green, H. A. O. Hill, Y. C. Leung, P. J. Sadler, J. Sloan, A. V. Xavier, S. C. Tsang: The immobilization of proteins in carbon nanotubes, *Inorg. Chim. Acta* **272** (1998) 261–266
- 3.268 R. J. Chen, Y. Zhang, D. Wang, H. Dai: Noncovalent sidewall functionalization of single-walled carbon nanotubes for protein immobilization, *J. Am. Chem. Soc.* **123** (2001) 3838–3839
- 3.269 M. Shim, N. W. S. Kam, R. J. Chen, Y. Li, H. Dai: Functionalization of carbon nanotubes for biocompatibility and biomolecular recognition, *Nanolett.* **2** (2002) 285–288
- 3.270 C. Dwyer, M. Guthold, M. Falvo, S. Washburn, R. Superfine, D. Erie: DNA-functionalized single-walled carbon nanotubes, *Nanotechnology* **13** (2002) 601–604
- 3.271 H. Huang, S. Taylor, K. Fu, Y. Lin, D. Zhang, T. W. Hanks, A. M. Rao, Y. Sun: Attaching proteins to carbon nanotubes via diimide-activated amidation, *Nanolett.* **2** (2002) 311–314
- 3.272 C. V. Nguyen, L. Delzeit, A. M. Cassell, J. Li, J. Han, M. Meyyappan: Preparation of nucleic acid functionalized carbon nanotube arrays, *Nanolett.* **2** (2002) 1079–1081
- 3.273 B. R. Azamian, J. J. Davis, K. S. Coleman, C. B. Bagshaw, M. L. H. Green: Bioelectrochemical single-walled carbon nanotubes, *J. Am. Chem. Soc.* **124** (2002) 12664–12665
- 3.274 C. L. Xu, B. Q. Wei, R. Z. Ma, J. Liang, X. K. Ma, D. H. Wu: Fabrication of aluminum-carbon nanotube composites and their electrical properties, *Carbon* **37** (1999) 855–858
- 3.275 T. Kuzumaki, K. Miyazawa, H. Ichinose, K. Ito: Processing of carbon nanotube reinforced aluminum composite, *J. Mater. Res.* **13** (1998) 2445–2449
- 3.276 T. Kuzumaki, O. Ujiie, H. Ichinose, K. Ito: Mechanical characteristics and preparation of carbon nanotube fiber-reinforced Ti composite, *Adv. Eng. Mater.* **2** (2000) 416–418
- 3.277 S. R. Dong, J. P. Tu, X. B. Zhang: An investigation of the sliding wear behavior of Cu-matrix composite reinforced by carbon nanotubes, *Mater. Sci. Eng. A* **313** (2001) 83–87
- 3.278 Y. B. Li, Q. Ya, B. Q. Wei, J. Liang, D. H. Wu: Processing of a carbon nanotubes-Fe82P18 metallic glass composite, *J. Mater. Sci. Lett.* **17** (1998) 607–609
- 3.279 A. Peigney: Tougher ceramics with carbon nanotubes, *Nature Mater.* **2** (2003) 15–16
- 3.280 G. D. Zhan, J. D. Kuntz, J. Wan, A. K. Mukherjee: Single-wall carbon nanotubes as attractive toughening agents in alumina-based composites, *Nature Mater.* **2** (2003) 38–42
- 3.281 J. Sun, L. Gao, W. Li: Colloidal processing of carbon nanotube/alumina composites, *Chem. Mater.* **14** (2002) 5169–5172
- 3.282 V. G. Gavalas, R. Andrews, D. Bhattacharyya, L. G. Bachas: Carbon nanotube sol-gel composite materials, *Nanolett.* **1** (2001) 719–721
- 3.283 S. Rul, Ch. Laurent, A. Peigney, A. Rousset: Carbon nanotubes prepared in-situ in a cellular ceramic by the gelcasting-foam method, *J. Eur. Ceram. Soc.* **23** (2003) 1233–1241
- 3.284 R. Z. Ma, J. Wu, B. Q. Wei, J. Liang, D. H. Wu: Processing and properties of carbon nanotube/nano-SiC ceramic, *J. Mater. Sci.* **33** (1998) 5243–5246
- 3.285 C. Laurent, A. Peigney, O. Dumortier, A. Rousset: Carbon nanotubes-Fe-alumina nanocomposites. Part II: Microstructure and mechanical properties of the hot-pressed composites, *J. Eur. Ceram. Soc.* **18** (1998) 2005–2013
- 3.286 A. Peigney, C. Laurent, A. Rousset: Synthesis and characterization of alumina matrix nanocomposites containing carbon nanotubes, *Key Eng. Mater.* **132–136** (1997) 743–746
- 3.287 A. Peigney, C. Laurent, E. Flahaut, A. Rousset: Carbon nanotubes in novel ceramic matrix nanocomposites, *Ceram. Intern.* **26** (2000) 677–683

- 3.288 S. Rul: Synthèse de composites nanotubes de carbone-métal-oxyde. Ph.D. Thesis (Université Toulouse III, Toulouse 2002)
- 3.289 E. Flahaut, A. Peigney, C. Laurent, C. Marliere, F. Chastel, A. Rousset: Carbon nanotube-metal-oxide nanocomposites: Microstructure, electrical conductivity and mechanical properties, *Acta Mater.* **48** (2000) 3803–3812
- 3.290 R.R. Bacsa, C. Laurent, A. Peigney, W.S. Bacsa, T. Vaugien, A. Rousset: High specific surface area carbon nanotubes from catalytic chemical vapor deposition process, *Chem. Phys. Lett.* **323** (2000) 566–571
- 3.291 P. Coquay, A. Peigney, E. De Grave, R.E. Vandenberghe, C. Laurent: Carbon nanotubes by a CVD method. Part II: Formation of nanotubes from (Mg,Fe)O catalysts, *J. Phys. Chem. B* **106** (2002) 13199–13210
- 3.292 E. Flahaut, Ch. Laurent, A. Peigney: Double-walled carbon nanotubes in composite powders, *J. Nanosci. Nanotech.* **3** (2003) 151–158
- 3.293 A. Peigney, P. Coquay, E. Flahaut, R.E. Vandenberghe, E. De Grave, C. Laurent: A study of the formation of single- and double-walled carbon nanotubes by a CVD method, *J. Phys. Chem. B* **105** (2001) 9699–9710
- 3.294 R.W. Siegel, S.K. Chang, B.J. Ash, J. Stone, P.M. Ajayan, R.W. Doremus, L.S. Schadler: Mechanical behavior of polymer and ceramic matrix nanocomposites, *Scr. Mater.* **44** (2001) 2061–2064
- 3.295 A. Peigney, E. Flahaut, C. Laurent, F. Chastel, A. Rousset: Aligned carbon nanotubes in ceramic-matrix nanocomposites prepared by high-temperature extrusion, *Chem. Phys. Lett.* **352** (2002) 20–25
- 3.296 S.L. Huang, M.R. Koblischka, K. Fossheim, T.W. Ebbesen, T.H. Johansen: Microstructure and flux distribution in both pure and carbon-nanotube-embedded $\text{Bi}_2\text{Sr}_2\text{CaCu}_2\text{O}_{8+\delta}$ superconductors, *Physica C* **311** (1999) 172–186
- 3.297 L. L. Yowell: Thermal management in ceramics: Synthesis and characterization of a zirconia-carbon nanotube composite, *Proc Mater. Res. Soc. Symp.* **633** (2002) A17.4.1–A17.4.6
- 3.298 A. Weidenkaff, S.G. Ebbinghaus, T. Lippert: $\text{Ln}_{1-x}\text{A}_x\text{CoO}_3$ (Ln = Er, La; A = Ca, Sr)/carbon nanotube composite materials applied for rechargeable Zn/Air batteries, *Chem. Mater.* **14** (2002) 1797–1805
- 3.299 D.S. Lim, J.W. An, H.J. Lee: Effect of carbon nanotube addition on the tribological behavior of carbon/carbon composites, *Wear* **252** (2002) 512–517
- 3.300 R. Andrews, D. Jacques, A. M. Rao, T. Rantell, F. Derbyshire, Y. Chen, J. Chen, R. C. Haddon: Nanotube composite carbon fibers, *Appl. Phys. Lett.* **75** (1999) 1329–1331
- 3.301 P.M. Ajayan, O. Stephan, C. Colliex, D. Trauth: Aligned carbon nanotube arrays formed by cutting a polymer resin-nanotube composite, *Science* **265** (1994) 1212–14
- 3.302 R. Haggenueller, H.H. Gommans, A.G. Rinzler, J.E. Fischer, K.I. Winey: Aligned single-wall carbon nanotubes in composites by melt processing methods, *Chem. Phys. Lett.* **330** (2000) 219–225
- 3.303 L.S. Schadler, S.C. Giannaris, P.M. Ajayan: Load transfer in carbon nanotube epoxy composites, *Appl. Phys. Lett.* **73** (1998) 3842–3844
- 3.304 S.J.V. Frankland, A. Caglar, D.W. Brenner, M. Griebel: Molecular simulation of the influence of chemical cross-links on the shear strength of carbon nanotube-polymer interfaces, *J. Phys. Chem. B* **106** (2002) 3046–3048
- 3.305 H. D. Wagner: Nanotube-polymer adhesion: A mechanics approach, *Chem. Phys. Lett.* **361** (2002) 57–61
- 3.306 P.M. Ajayan, L.S. Schadler, C. Giannaris, A. Rubio: Single-walled carbon nanotube-polymer composites: Strength and weakness, *Adv. Mater.* **12** (2000) 750–753
- 3.307 X. Gong, J. Liu, S. Baskaran, R.D. Voise, J.S. Young: Surfactant-assisted processing of carbon nanotube/polymer composites, *Chem. Mater.* **12** (2000) 1049–1052
- 3.308 E.T. Thostenson, W.Z. Li, D.Z. Wang, Z.F. Ren, T.W. Chou: Carbon nanotube/carbon fiber hybrid multiscale composites, *J. Appl. Phys.* **91** (2002) 6034–6037
- 3.309 M.J. Biercuk, M.C. Llaguno, M. Radosavljevic, J.K. Hyun, A.T. Johnson, J.E. Fischer: Carbon nanotube composites for thermal management, *Appl. Phys. Lett.* **80** (2002) 2767–2769
- 3.310 S. Barrau, P. Demont, A. Peigney, C. Laurent, C. Lacabanne: DC and AC conductivity of carbon nanotube-Epoxy composites macromolecules, *Macromol.* **36** (2003) 5187–5194
- 3.311 J. Sandler, M.S.P. Shaffer, T. Prasse, W. Bauhofer, K. Schulte, A.H. Windle: Development of a dispersion process for carbon nanotubes in an epoxy matrix and the resulting electrical properties, *Polymer* **40** (1999) 5967–5971
- 3.312 Z. Jin, K.P. Pramoda, G. Xu, S.H. Goh: Dynamic mechanical behavior of melt-processed multi-walled carbon nanotube/poly(methyl methacrylate) composites, *Chem. Phys. Lett.* **337** (2001) 43–47
- 3.313 Z. Jin, K. P. Pramoda, S. H. Goh, G. Xu: Poly(vinylidene fluoride)-assisted melt-blending of multi-walled carbon nanotube/poly(methyl methacrylate) composites, *Mat. Res. Bull.* **37** (2002) 271–278
- 3.314 C.A. Cooper, D. Ravich, D. Lips, J. Mayer, H.D. Wagner: Distribution and alignment of carbon nanotubes and nanofibrils in a polymer matrix, *Compos. Sci. Technol.* **62** (2002) 1105–1112
- 3.315 J.M. Benoit, B. Corraze, S. Lefrant, W.J. Blau, P. Bernier, O. Chauvet: Transport properties of PMMA-carbon nanotubes composites, *Synth. Met.* **121** (2001) 1215–1216

- 3.316 J. M. Benoit, B. Corraze, O. Chauvet: Localization, Coulomb interactions, and electrical heating in single-wall carbon nanotubes/polymer composites, *Phys. Rev. B: Cond. Matter. Mater. Phys.* **65** (2002) 241405/1–241405/4
- 3.317 M. S. P. Shaffer, A. H. Windle: Fabrication and characterization of carbon nanotube/poly(vinyl alcohol) composites, *Adv. Mater.* **11** (1999) 937–941
- 3.318 L. Jin, C. Bower, O. Zhou: Alignment of carbon nanotubes in a polymer matrix by mechanical stretching, *Appl. Phys. Lett.* **73** (1998) 1197–1199
- 3.319 H. D. Wagner, O. Lourie, Y. Feldman, R. Tenne: Stress-induced fragmentation of multiwall carbon nanotubes in a polymer matrix, *Appl. Phys. Lett.* **72** (1998) 188–190
- 3.320 H. D. Wagner, O. Lourie, X. F. Zhou: Macrofragmentation and microfragmentation phenomena in composite materials, *Composites Part A* **30A** (1998) 59–66
- 3.321 J. R. Wood, Q. Zhao, H. D. Wagner: Orientation of carbon nanotubes in polymers and its detection by Raman spectroscopy, *Composites Part A* **32A** (2001) 391–399
- 3.322 Q. Zhao, J. R. Wood, H. D. Wagner: Using carbon nanotubes to detect polymer transitions, *J. Polym. Sci., Part B: Polym. Phys.* **39** (2001) 1492–1495
- 3.323 M. Cochet, W. K. Maser, A. M. Benito, M. A. Callejas, M. T. Martinez, J. M. Benoit, J. Schreiber, O. Chauvet: Synthesis of a new polyaniline/nanotube composite: In-situ polymerisation and charge transfer through site-selective interaction, *Chem. Commun.* **16** (2001) 1450–1451
- 3.324 D. Qian, E. C. Dickey, R. Andrews, T. Rantell: Load transfer and deformation mechanisms in carbon nanotube-polystyrene composites, *Appl. Phys. Lett.* **76** (2000) 2868–2870
- 3.325 C. Wei, D. Srivastava, K. Cho: Thermal expansion and diffusion coefficients of carbon nanotube-polymer composites, Los Alamos Nat. Lab., Preprint Archive, Condensed Matter (archiv:cond-mat/0203349) (2002) 1–11
- 3.326 C. Pirlot, I. Willems, A. Fonseca, J. B. Nagy, J. Delhalle: Preparation and characterization of carbon nanotube/polyacrylonitrile composites, *Adv. Eng. Mater.* **4** (2002) 109–114
- 3.327 L. Cao, H. Chen, M. Wang, J. Sun, X. Zhang, F. Kong: Photoconductivity study of modified carbon nanotube/oxotitanium phthalocyanine composites, *J. Phys. Chem. B* **106** (2002) 8971–8975
- 3.328 I. Musa, M. Baxendale, G. A. J. Amaratunga, W. Eccleston: Properties of regular poly(3-octylthiophene)/multi-wall carbon nanotube composites, *Synth. Met.* **102** (1999) 1250
- 3.329 E. Kymakis, I. Alexandou, G. A. J. Amaratunga: Single-walled carbon nanotube-polymer composites: Electrical, optical and structural investigation, *Synth. Met.* **127** (2002) 59–62
- 3.330 K. Yoshino, H. Kajii, H. Araki, T. Sonoda, H. Take, S. Lee: Electrical and optical properties of conducting polymer-fullerene and conducting polymer-carbon nanotube composites, *Fuller. Sci. Technol.* **7** (1999) 695–711
- 3.331 S. A. Curran, P. M. Ajayan, W. J. Blau, D. L. Carroll, J. N. Coleman, A. B. Dalton, A. P. Davey, A. Drury, B. McCarthy, S. Maier, A. Strevens: A composite from poly(m-phenylenevinylene-co-2,5-dioctoxy-p-phenylenevinylene) and carbon nanotubes. A novel material for molecular optoelectronics, *Adv. Mater.* **10** (1998) 1091–1093
- 3.332 P. Fournet, D. F. O'Brien, J. N. Coleman, H. H. Horhold, W. J. Blau: A carbon nanotube composite as an electron transport layer for M3EH-PPV based light-emitting diodes, *Synth. Met.* **121** (2001) 1683–1684
- 3.333 H. S. Woo, R. Czerw, S. Webster, D. L. Carroll, J. Ballato, A. E. Strevens, D. O'Brien, W. J. Blau: Hole blocking in carbon nanotube-polymer composite organic light-emitting diodes based on poly(m-phenylene vinylene-co-2,5-dioctoxy-p-phenylene vinylene), *Appl. Phys. Lett.* **77** (2000) 1393–1395
- 3.334 H. S. Woo, R. Czerw, S. Webster, D. L. Carroll, J. W. Park, J. H. Lee: Organic light emitting diodes fabricated with single wall carbon nanotubes dispersed in a hole conducting buffer: The role of carbon nanotubes in a hole conducting polymer, *Synth. Met.* **116** (2001) 369–372
- 3.335 H. Ago, K. Petritsch, M. S. P. Shaffer, A. H. Windle, R. H. Friend: Composites of carbon nanotubes and conjugated polymers for photovoltaic devices, *Adv. Mater.* **11** (1999) 1281–1285
- 3.336 B. Vigolo, A. Pénicaud, C. Coulon, C. Sauder, R. Pailler, C. Journet, P. Bernier, P. Poulin: Macroscopic fibers and ribbons of oriented carbon nanotubes, *Science* **290** (2000) 1331–1334
- 3.337 B. Vigolo, P. Poulin, M. Lucas, P. Launois, P. Bernier: Improved structure and properties of single-wall carbon nanotube spun fibers, *Appl. Phys. Lett.* **11** (2002) 1210–1212
- 3.338 P. Poulin, B. Vigolo, P. Launois: Films and fibers of oriented single wall nanotubes, *Carbon* **40** (2002) 1741–1749
- 3.339 K. Jiang, Q. Li, S. Fan: Spinning continuous carbon nanotube yarn, *Nature* **419** (2002) 801
- 3.340 P. Lambin, A. Fonseca, J. P. Vigneron, J. B'Nagy, A. A. Lucas: Structural and electronic properties of bent carbon nanotubes, *Chem. Phys. Lett.* **245** (1995) 85–89
- 3.341 L. Chico, V. H. Crespi, L. X. Benedict, S. G. Louie, M. L. Cohen: Pure carbon nanoscale devices: Nanotube heterojunctions, *Phys. Rev. Lett.* **76** (1996) 971–974
- 3.342 Z. Yao, H. W. C. Postma, L. Balents, C. Dekker: Carbon nanotube intramolecular junctions, *Nature* **402** (1999) 273–276

- 3.343 S. J. Tans, A. R. M. Verschueren, C. Dekker: Room temperature transistor based on single carbon nanotube, *Nature* **393** (1998) 49–52
- 3.344 R. Martel, T. Schmidt, H. R. Shea, T. Hertel, P. Avouris: Single and multi-wall carbon nanotube field effect transistors, *Appl. Phys. Lett.* **73** (1998) 2447–2449
- 3.345 V. Derycke, R. Martel, J. Appenzeller, P. Avouris: Carbon nanotube inter- and intramolecular logic gates, *Nanolett.* **1** (2001) 453–456
- 3.346 P. Kim, C. M. Lieber: Nanotube nanotweezers, *Science* **286** (1999) 2148–2150
- 3.347 P. G. Collins, M. S. Arnold, P. Avouris: Engineering carbon nanotubes using electrical breakdown, *Science* **292** (2001) 706–709
- 3.348 R. H. Baughman, C. Changxing, A. A. Zakhidov, Z. Iqbal, J. N. Barisci, G. M. Spinks, G. G. Wallace, A. Mazzoldi, D. de Rossi, A. G. Rinzler, O. Jaschinski S. Roth, M. Kertesz: Carbon nanotubes actuators, *Science* **284** (1999) 1340–1344
- 3.349 Y. Gao, Y. Bando: Carbon nanothermometer containing gallium, *Nature* **415** (2002) 599
- 3.350 C. Niu, E. K. Sichel, R. Hoch, D. Moy, H. Tennent: High power electro-chemical capacitors based on carbon nanotube electrodes, *Appl. Phys. Lett.* **70** (1997) 1480–1482
- 3.351 E. Frackowiak, F. Béguin: Electrochemical storage of energy in carbon nanotubes and nanostructured carbons, *Carbon* **40** (2002) 1775–1787
- 3.352 E. Frackowiak, K. Jurewicz, K. Szostak, S. Delpeux, F. Béguin: Nanotubular materials as electrodes for supercapacitors, *Fuel Process. Technol.* **77** (2002) 213–219